

Design of A Novel Biologically Inspired Robot Fish With Low Cost

by

Xinyu Jian

Submitted to the Department of Mechanical Engineering
in partial fulfillment of the requirements for the degree of

Master of Engineering in Mechanical Engineering

at the

MEMORIAL UNIVERSITY OF NEWFOUNDLAND

Convocation Date: October 20 2022

© Memorial University of Newfoundland 2022. All rights reserved.

Author
Department of Mechanical Engineering
August 9, 2022

Certified by
Ting Zou
Assistant Professor
Thesis Supervisor

Accepted by
N/A
Chairman, Department Committee on Graduate Theses

Design of A Novel Biologically Inspired Robot Fish With Low Cost

by

Xinyu Jian

Submitted to the Department of Mechanical Engineering
on August 9, 2022, in partial fulfillment of the
requirements for the degree of
Master of Engineering in Mechanical Engineering

Abstract

Being a novel form of underwater vehicle, the robot fish has the advantages of good maneuverability, quick response, high propulsion efficiency, and low noise. It is widely used in marine biological observation, marine water quality monitoring, submarine pipeline inspection, and exploration. It is one of the hot research topics in the marine field. Compared to the robot fish propulsion mechanism using rigid components, which has problems of no adaptability to underwater motion, and low motion efficiency and inability to imitate the fish body to perform flexible swings, the soft robot fish has higher swimming efficiency, and is the focus of this project.

In this work, the design of a novel soft robot fish, with focus on actuation system design, is proposed. The actuation system is based on the motor-driven bevel gear mechanism, which has the advantages of realizing rapid speed regulation, two-way drive, and adjustment range in a small space. One advantage of our design is its straightforward assembly and relatively simple fabrication, which can be completed mainly using 3D printing technology. Three different designs are proposed, based on a comprehensive comparison in terms of efficiency, reliability, and fabrication cost, one design is chosen to be fabricated and tested. The test focuses on the relationship between the swing amplitude, frequency, and swimming speed of the tail. The experiment is mainly divided into two parts: the test of driving the tail of the propulsion mechanism; and the robot fish underwater movement. The test results show that the design achieves the expected motion goal and is engineering feasible, which provides a new solution for the design of the robot fish.

Key Words: robot fish, propulsion mechanism, software, swimming experiment

Thesis Supervisor: Ting Zou
Title: Assistant Professor

Acknowledgments

I am really grateful to my supervisor Dr. Zou for her meticulous guidance and selfless support. Each of my academic achievement wins her sincere encouragement. Over the past years, she not only guides me in the academic field, but also helps me a lot in my daily life when I am in need. Without her help, I couldn't have fitted in the new environment overseas quickly and smoothly. Additionally, my thanks also go to my friends under the guidance of Dr. Zou. Frequent communication with them have made me know more that I didn't know in the past. Their help and support always make me feel that I am not alone. Besides, I would like to thank the university and the department since I have been equipped with the tools for doing research and given generous help when I encountered difficulties. My life spent here is rather meaningful and worthy of being remembered deeply. I will keep what I learn here in my heart and take it to the future of my life. In addition, I want to thank for my parent's and fiancée's great support in my life.

Contents

1	Introduction	11
1.1	Thesis Overview	11
1.2	Literature Review	12
1.2.1	Fish Locomotion Types Overview	13
1.2.2	Kinematics	20
1.2.3	Dynamics	22
1.3	Case Study	26
1.3.1	UC-IKA	26
1.3.2	SoFi	29
2	Robot Fish Mechanism Design	31
2.1	Design Philosophy	31
2.2	Design Considerations	36
2.2.1	Actuation System	36
2.2.2	Materials	41
2.2.3	Overall Design	42
2.3	Mechanical Design	44
2.3.1	Head	46
2.3.2	Body	49
2.3.3	Actuator	50
2.3.4	Tail	52
2.3.5	Fins	57
2.3.6	COM and COB	57

2.3.7	Watertight Design	60
2.4	Electronics	63
2.5	Software	66
2.5.1	Development Environment	66
2.5.2	Motor Angle Calculation	68
2.5.3	Controller	70
3	Prototyping	72
3.1	3D Printed Parts	72
3.2	Silicone Molding	74
3.3	Assembly	76
4	Prototype Experiment	79
4.1	Experiment Set-up	79
4.2	Test Results	80
4.2.1	Tail Experiment	80
4.2.2	Static Experiment	83
4.2.3	Dynamic Experiment	84
5	Conclusions	89
5.1	Result Analysis	89
5.2	Future Work	90
A	Mechanics	93
A.1	Preliminary Actuator Designs	93
A.1.1	The First Version	93
A.1.2	The Second Version	95
A.2	Gear Parameters	96
A.3	Calculate the COB in SolidWorks	97
A.4	Prototyping Parts	98
B	Electronics	100

C Software	101
C.1 Motor Control Function	101
C.2 Dual Loop PID Controller	103

List of Figures

1-1	Number of Publications on Robot Fish Each Year	14
1-2	Number of Citations on Robot Fish Each Year	14
1-3	Morphological features of fish	15
1-4	Fish swimming with (a) BCF mode, and (b) MPF mode, where the thrust generation is highlighted in shaded areas	16
1-5	Top View of Carangiform Fish	20
1-6	Swing Illustration[1]	23
1-7	UC-IKA Design [2]	28
1-8	The Structure of SoFi [3]	30
2-1	Robot Fish Design Process	33
2-2	Overall Design Layers	35
2-3	Shape Design of our Carangiform Robot Fish	43
2-4	Inside Layout of our Robot Fish	45
2-5	Head SolidWorks Model	47
2-6	Details in the Head Loft Design	48
2-7	Baffle inside the Head SolidWorks Model	48
2-8	The Body SolidWorks Model	49
2-9	The CAD Model of the Actuator	50
2-10	The Exploded View of the Actuator CAD Model	51
2-11	Bevel Gears	52
2-12	The Tail CAD Model	53
2-13	The Schematic Diagram of Caudal Fin	54

2-14	The Swim Schematic Diagram	56
2-15	The Tail Swing Range	56
2-16	The Fins of Robot Fish	58
2-17	Bevel Gears	59
2-18	COM and COB	61
2-19	Body - Head Connection Schematic Diagram	62
2-20	Body - Tail Connection Schematic Diagram	63
2-21	The Circuit of Robot Fish	64
2-22	The Project Logical Schematic Diagram	67
2-23	The Encoder Schematic Diagram	69
2-24	The Schematic Diagram of the Dual-loop PID Controller	71
3-1	The 3D Printer Anet ET4	73
3-2	Two Support Structures	74
3-3	All Parts of Robot Fish	75
3-4	The Mold of Making Tail	75
3-5	Procedures While Making the Tail	76
3-6	Robot Fish Parts	77
3-7	Procedures to Assemble the Robot Fish	78
3-8	Final Assembly	78
4-1	Water Tank	79
4-2	Experiment Electronics	80
4-3	Tail Maximal Angle	81
4-4	Motor Response curve (30°)	82
4-5	Tail Swings Between $[-40^\circ, 40^\circ]$	82
4-6	Tail Swings Between $[-60^\circ, 10^\circ]$	83
4-7	Continuously Change Variables	83
4-8	Straight Line Experiment (swing amplitude 30° , frequency 4 Hz)	85
4-9	Speed Under Different Swing Amplitudes and Frequencies	85
4-10	Straight Line Experiment (swing amplitude 30°)	86

4-11 Steering Experiment (Offset Angle 10°)	87
4-12 Steering Experiment (Offset Angle 20°)	88
4-13 Steering Experiment (Offset Angle 30°)	88
A-1 The First Version Actuator	94
A-2 The Second Version Actuator	96
A-3 Fill Tail Surface	98

List of Tables

1.1	Different Locomotions Comparison	21
2.1	Different Motor Drive Types	37
2.2	Actuation Systems Comparison	41
4.1	Steering Experiment Test Sets and Result	86
A.1	Spur Gears Parameters	96
A.2	Standard Parts	98
A.3	3D Printed Parts	99
B.1	Hardware Purchase Link	100

Chapter 1

Introduction¹

More than 70% of the surface of our planet is covered by water, dominated by fish. With millions of years' evolution, fish can exhibit astonishing performance and energy harvesting ability. For example, the rainbow trout extracts energy from the oncoming vertices, and even dead trout fish can be propelled upstream [4]. Fish also demonstrates extraordinary propulsion efficiencies, superior acceleration, and excellent maneuverability [5]. Therefore, learning the morphology and swimming behaviors of fish, and implementing those principles into the design of robot fish opens a new door for the next generation underwater vehicles [6].

1.1 Thesis Overview

There are many robot fish prototypes since the first robot fish was created in 1994 [7]. However, most of them are mechanically complicated with a high material cost, from thousands dollars to tens of thousands. Is it possible to build a robot fish that has simple structure, results in a low cost, such as hundreds of dollars, and keeps somewhat dynamic performance?

This thesis proposes a new actuator design for bio-inspired soft robot fish with a low cost: the motor drives the bevel gear to make the PVC layer swing; the PVC

¹Material from: ‘Xinyu Jian and Ting Zou, *A Review of Locomotion, Control, and Implementation of Robot Fish*, Journal of Intelligent & Robotic Systems, under revision, submitted on 10 June, 2022.’

layer and the soft tail are poured together; driven by the PVC layer, the soft tail swings. What's more, the whole fish mechanical structure, circuit, and control system are designed for this actuation mechanism. In addition, this thesis selects suitable materials and hardware to make the soft tail and whole fish. By properly designing the software, the prototype can realize the control of the soft tail swing. Finally, the water tank experiment was carried out. The parts cost, including electronics parts and 3D printed parts, is around four hundred dollars. This thesis is based on the conventional format style. The structure of this thesis is as follows:

The first chapter introduces the research background and the work of this thesis. It introduces the knowledge of fish biology required for the research of the robot fish, such as the swimming mechanisms, kinematics, and dynamics of swimming patterns; current research on the robot fish is reviewed, and two representative designs are selected for case studies.

The second chapter expounds on the design concept and engineering thinking of the robot fish, describes the mechanical structure of each part in detail, and introduces the circuit, software architecture, key code, and controller of the whole system.

The third chapter introduces the materials, equipment, technology, and process of making the prototype.

The fourth chapter conducts a tail swing experiment, underwater static experiment, straight swimming, and turning experiment. Experiments show that the control system can make the tail swing under different amplitudes and frequencies. The robot fish prototype can swim underwater forward and turn, which verifies the effectiveness of this design.

The fifth chapter summarizes the research content and lists the follow-up research work.

1.2 Literature Review

Nowadays, bionics has emerged at the historic moment, providing many ideas for the design of new forms of underwater vehicles. Inspired by biological systems, through

learning, imitating, copying and recreating their structure, function, working principle and control mechanism, the existing underwater robots can be improved, and brand new forms of underwater vehicles—biologically inspired robotic underwater vehicles, or in short, robot fish—has appeared [7, 8, 9].

Suggested by its name, a robot fish is the outcome inspired by the morphology of its bionic counterparts, aiming at achieving similar shape and swimming locomotion. In the past years, the idea of robot fish has attracted continuously increasing attentions academically and publicly. Prompted by both scientific and commercial needs, we have witnessed a boom in the development of robot fish. Since the first robot fish—RoboTuna was built in 1994 [7], the idea of bio-inspired robot fish has gradually become a hot spot [1]. It imitates the shape and movement pattern of biological fish to achieve high-efficient and fast movement [10]. The development of robot fish is the outcome of robust combination of comprehensive research realms, such as bionics, mechanics, electronics, automatic control, and material science. Compared to the classic rigid-form underwater robots, e.g., the widely used AUV (Autonomous Underwater Vehicle), the robot fish has the advantages of advanced maneuverability, high propulsion efficiency, and low noise [11]. Underwater robots using traditional propellers will produce lateral eddy currents during propeller rotation, which increases energy consumption, reduces propulsion efficiency, and is noisy [12]. Imitating the swimming propulsion mode of fish, the development of high-efficiency, low-noise, flexible and mobile robot fish for underwater operations in complex environments has become the goal pursued by researchers [13, 14]. As shown in Figs. 1-1 and 1-2, the related research is attracting more and more attention².

1.2.1 Fish Locomotion Types Overview

The robot fish is promoted by imitating the swimming mode of fish, with its classification divided according to that of fish swimming. Thus, being familiar with the types of fish swimming is significant to grasp the big picture of robot fish. Fish or cetaceans commonly use tail-wagging as the main propulsion method, supplemented

²Data is provided by Web of Science

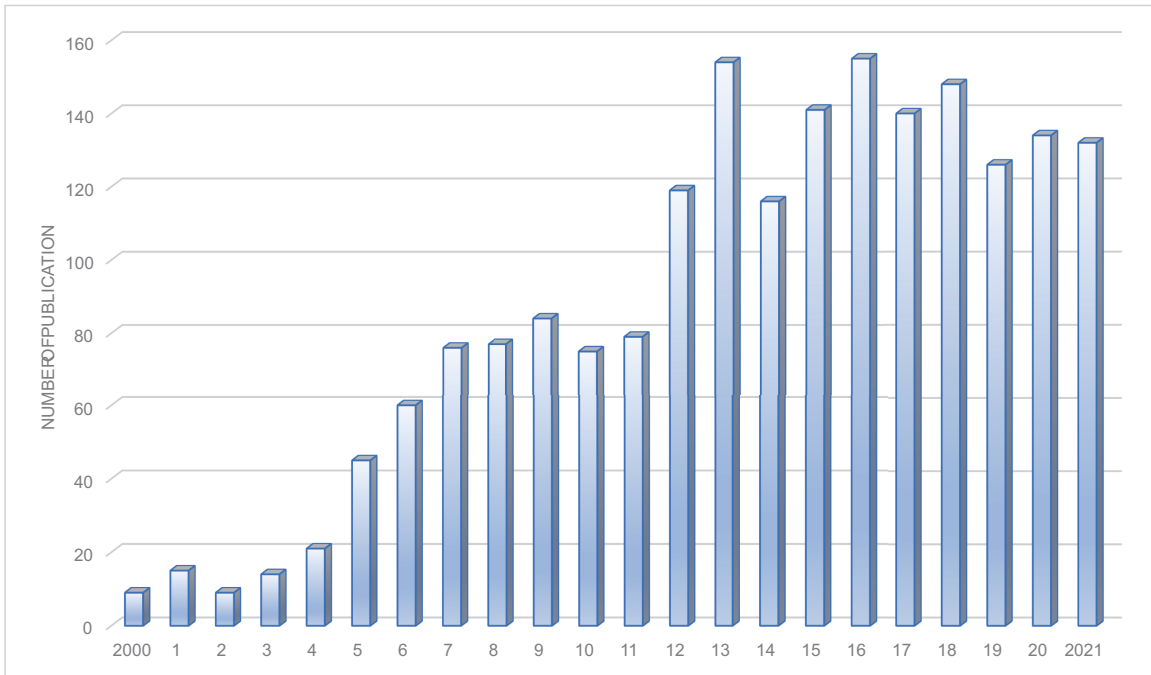


Figure 1-1: Number of Publications on Robot Fish Each Year

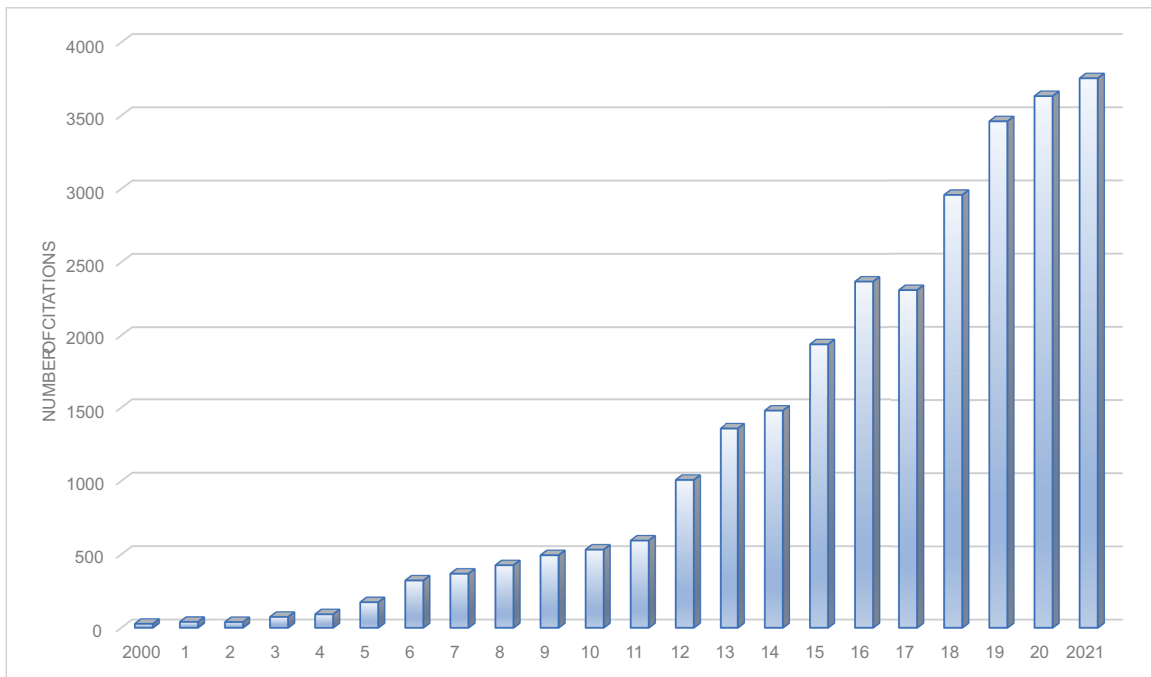


Figure 1-2: Number of Citations on Robot Fish Each Year

by other fins, such as pelvic fins and anal fins, as auxiliary sources of thrust or to control the direction of travel. Figure 1-3 shows the commonly-adopted terminologies on the description of fish morphology [15].

The fish swimming types classification scheme and nomenclature are originally proposed by Breder [16]. Lindsey [17] and Webb [18] concluded the above classification into two modes according to the different body parts used by propulsion: body and/or caudal fin propulsion (BCF) mode, and media and/or paired fin propulsion (MPF) mode [19]. The BCF mode waves a certain part of the body and the tail fin to form a backward propulsion wave. Around 85% fish use this method of propulsion [20]. BCF mode can achieve continuous, fast and efficient swimming. The dorsal, anal, pectoral, and pelvic fins of most fishes are only used to assist in propulsion and adjust posture; on the other hand, the MPF mode fish, which accounts for about 15% of the total fish population [20], use these fins as their main propulsion components. In spite of owning good stability and high mobility, the MPF mode is accompanied by slow swimming speed [21].

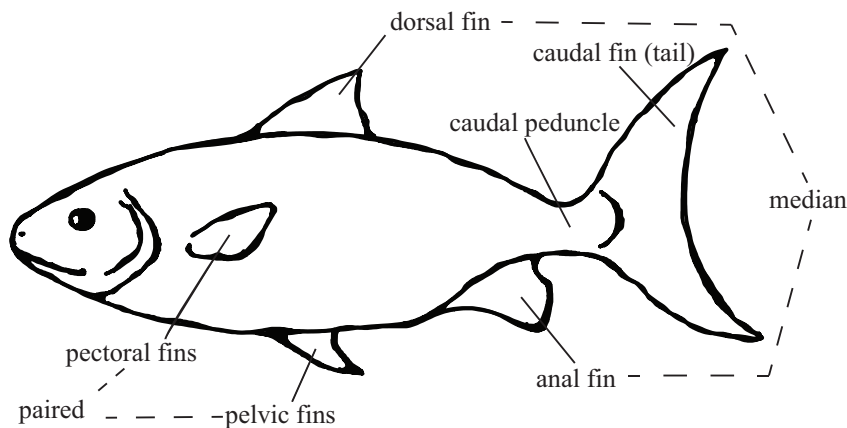


Figure 1-3: Morphological features of fish

Furthermore, both BCF and MPF modes can be divided into two movement types: undulatory or oscillatory. In undulatory motions, the propulsive structure, e.g., tail, shows the passage of a wave along the main axis. On the other hand, there is no wave feature on the propulsive structure in oscillatory motions. Instead, the propulsive

structure, e.g., tail, swivels on its base [19]. However, undulatory movements can evolve into oscillatory movements by increasing the undulation wavelength. In addition, fish swimming can also be divided into smaller segments based on the propulsor. A detailed classification on fish swimming modes is illustrated in Fig. 1-4 [17].

In the following subsections, each segment is explained in detail with specific examples.

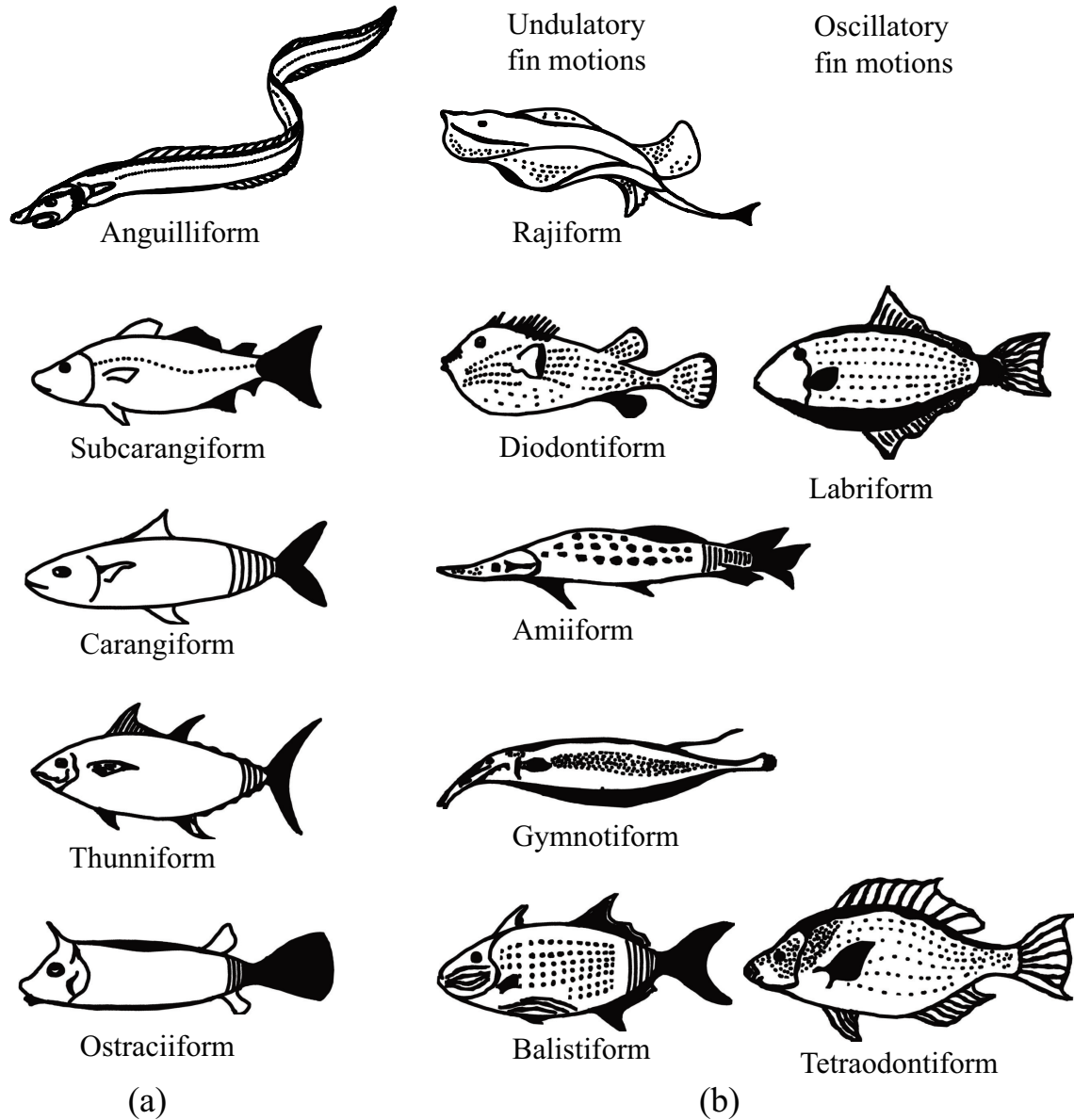


Figure 1-4: Fish swimming with (a) BCF mode, and (b) MPF mode, where the thrust generation is highlighted in shaded areas

BCF Swimming Mode

Categorization of the BCF mode can be determined in standards such as five forms by different wavelength, propulsive wave amplitude envelop, and thrust generation methods [19, 22], as shown in Fig. 1-4(a). It is noteworthy that there is no clear boundary between undulatory and oscillatory in the BCF mode. From anguilliform to ostraciiform, the movement type is transitioned from undulatory motion to oscillatory motion.

1. Anguilliform mode: eel being a typical example adopting this form. An apparent feature for anguilliform lies in the large amplitude of the fish body bend undulations. During the anguilliform swimming, at the minimum one complete wavelength can be passed along the fish body, leading to negligible yaw moment and tendency to recoil. Due to this feature, one distinguished characteristic of anguilliform swimmers, such as eel and lamprey, is that, they can move backward by reversing the direction of the propulsive wave. As a result, this mode allows high maneuverability, accompanied with low swimming speed [23].
2. Sub-carangiform mode: half of the fish body being involved in the undulations, leading to improved swimming speed. As a result, sub-carangiform fish is typically faster than anguilliform, with the price of decreased maneuverability.
3. Carangiform mode: including trout, herring, etc. One apparent feature is that the body part involved in the undulation is significant—about one-third of the posterior body length. As the most common form, it demonstrates faster speed, and suffers lower maneuverability.
4. Thunniform mode: typically seen in tuna, cetaceans, etc. It is significantly interesting by showcasing the optimal efficiency among all types of swimming modes. In thunniform mode, the caudal fin contributes more than 90% to the propulsive forces, leaving the rest produced by the added mass effect due to the lateral undulations near the peduncle; meanwhile, thrust can be generated during lift [24]. Fish adopting this swimming mode is distinguished by the

ability to maintain high cruising speed for a long period of time, namely, the scombridae, including the tunas, mackerels and bonitos. This is achieved by minimizing the pressure drag due to the slender, streamlined fish body during forward motion, while reducing induced drag by lift generation thanks to the relatively stiff, crescent moon shaped caudal fin.

5. Ostraciiform mode: both the fish body and caudal fin are relatively stiff. For ostraciiform swimmers, the stiff caudal fins oscillate like a pendulum to create high speed locomotion, while compared to their thunniform counterparts, which have relative soft body, the rest of the fish body remains rigid. Besides, ostraciiform swimmers have lower hydrodynamic efficiency than the thunniform swimmers [25].

MPF Swimming Mode

Compared to the BCF, the MPF mode, on the other side, performs an undulatory locomotion accompanied by low speeds and improved maneuverability. In spite of the wide applications in nature, the MPF is less investigated partially due to its complexity. The MPF mode encompasses diodontiform, gymnotiform, amiiform and balistiform locomotion, as classified in [19].

1. Rajiform: as a combination of undulation and oscillation, the rajiform has inherent advantages of high maneuverability. Significantly large pectoral fins—the lateral expansion of the fish body—are used, which may lead to two different types of locomotion, namely the undulatory or oscillatory locomotion [19]. With an increased undulation amplitude from the anterior body to its posterior counterpart, a wave is generated in undulation mode. The oscillatory mode, on the other hand, depends on the fast-flapping fins with larger amplitude to produce a wave, similar to the wings of a flying bird.
2. Diodontiforms: with vertical and undulatory pectoral fins, the undulation is possibly formed of two different wavelengths simultaneously at each instant: along up-down and flapping. The vertical component of forces produced by

the pectoral fins will provide up-down motions; at the same time, the pectoral fins will also create flapping motion accompanied with labriform mode. Consequently, though slow, diodontiform swimmers showcase precise manoeuvrability provided by the combination of these two modes, the blowfish being a typical example belonging to this category.

3. Gymnotiforms: using anal fin for undulation, instead of dorsal fin being used in amiiforms to achieve the similar locomotion. The South American electric fish is a typical paradigm adopting gymnotiform mode. A distinctive feature of gymnotiform is that it does not possess dorsal and caudal fins, or at least significantly small caudal fins, but having elongated anal fins. Due to this feature, in terms of reversing the rapid undulation direction of anal fins with short wavelength, fish with gymnotiforms can perform both backward and forward swimming [17].
4. Amiiforms: using the long dorsal fin to undulate for propulsion. The dorsal fin of amiiforms can see up to seven waves passing on it during undulation, with various range of undulation amplitude. The *Gymnarchus niloticus*—a freshwater fish in Africa—is a typical paradigm adopting amiiform for its swimming locomotion.
5. Balistiforms: defined for those swimming modes in which the dorsal and anal fins undulate simultaneously to create the propulsion. The undulation of the dorsal and anal fins creates a set of half-sized waves that can be seen on the fins. During undulation, both fins work together in an evolutionarily optimal way to efficiently produce horizontal forces to propel the fish forward.

MPF locomotion is normally composed of Tetraodontiform and Labriform, mainly in terms of the type of fins used and oscillatory mode [19].

1. Tetraodontiforms: puffer fish being a typical tetraodontiform swimmer. The propulsion mainly depends on the side-to-side flapping motion of dorsal and

anal fins, which is similar to balistiforms. It is noteworthy that, both dorsal and anal fins flap in the same way as the caudal fins for ostraciiform.

2. Labriforms: angelfish being a representative in this category. While swimming, the narrow pectoral fins of angelfishes are able to provide both types of oscillatory motions: flapping and rowing. Another example is the bird wrasse, whose pectoral fins are also dominated by flapping motion [26].

Based on the discussion above, a comparison on different fish locomotion types and their corresponding characteristics is summarized in Table 1.1.

1.2.2 Kinematics

For robot fish, as the basis for the design of the mechanical structure, motion parameters, and the control system, establishing an mathematical model to accurately describe the fish motion characteristics is crucial. Hence, being one of the key issues—a steady-state kinematic model—needs to be solved in the robot fish study.

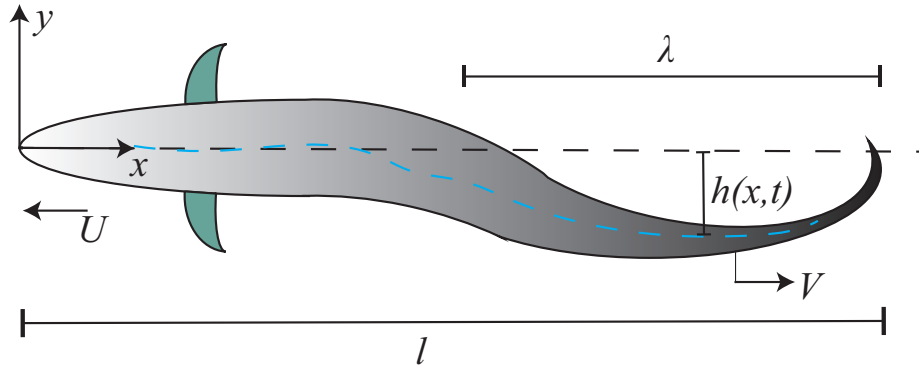


Figure 1-5: Top View of Carangiform Fish

Taking the Carangiform as an example, as shown in Figure 1-5, a top view of a Carangiform fish shows the parameters and variables to describe the kinematics of the fish. The origin of the body-fixed reference system \mathcal{F} is fixed at the forefront of the fish body, with x axis aligned with the forward-backward direction. Having full length l , the body is swimming forward at an average speed of U along the negative direction of the x -axis. The blue dashed line is the centerline of the fish body, and its

Table 1.1: Different Locomotions Comparison

Locomotion	Example	Features	Maneuverability	Speed
BCF	Anguilliform	Hyper-redundancy and full body undulation	High	Low
	Subcarangiform	Undulation of posterior half of the robot	Medium	Medium
	Carangiform	Undulation of posterior one third portion of the robot	Low	High
	Thunniform	Undulation of peduncle and caudal fin	Lowest	Highest
	Ostraciiform	Stiff body with pendulum-like oscillation of caudal fin	High	Low
MPF undulatory	Rajiform	Large flexible triangular shaped pectoral fins	Medium	Low
	Balistiform	Oscillating narrow based pectoral fins	Low	Low
	Gymnotiform	Hyper-redundancy of undulating anal fin	High	Medium
	Diodontiform	Broad undulating pectoral fin	High	High
	Amiiform	Long dorsal fin	Low	High
	Tetraodontiform	use dorsal and anal fins for propulsion		
MPF Osillatory	Labriform	have oscillatory and narrower pectoral fins		

lateral offset relative to the median plane $h(x, t)$ propagates to the back of the body at wave speed V and wavelength λ along the positive x-axis direction. For uniform linear swimming, the centerline of the fish body always stays on the x - y plane, with its amplitude becoming larger from beginning to end. The specific waveform can be observed by the high-speed shooting of fish swimming, post-processing images and fitting. Videler[20] proposed a model that fits the fish's lateral movement h_f with six Fourier coefficients a_j, b_j :

$$h_f(x, t) \approx \sum_{j=1,3,5} [a_j(x) \cos(2j\pi t/T) + b_j(x) \sin(2j\pi t/T)] \quad (1.1)$$

where T is the motion period. It is noteworthy that the first Fourier frequency has more significant influence on the amplitude and phase than the third and fifth Fourier frequency.

Barrett[27] takes the first Fourier frequency and simplifies it into a sine traveling wave with an amplitude envelope (Envelope):

$$h_f(x, t) \approx (c_1x + c_2x^2) \sin(\omega t - kx) \quad (1.2)$$

where ω is the frequency of fish tail swing, $k = \frac{\omega}{V} = \frac{2\pi}{\lambda}$ is the wave number, and the constants c_1, c_2 define the amplitude envelope. Barrett assumed that the head movement of the fish was negligible. This model and its similar variants are widely used in theoretical research on fish swimming.

1.2.3 Dynamics

The theoretical research on the wave-like swimming performance of the fish body can be divided into two aspects: the kinematics describing the swimming movement of the fish body, and the dynamics of the force on the body in swimming.

According to the selected main forces, the current wave propulsion theory can be divided into two categories: resistive force theory and reactive force theory. Having experienced a rapid development, the reaction force theory is relatively complete and

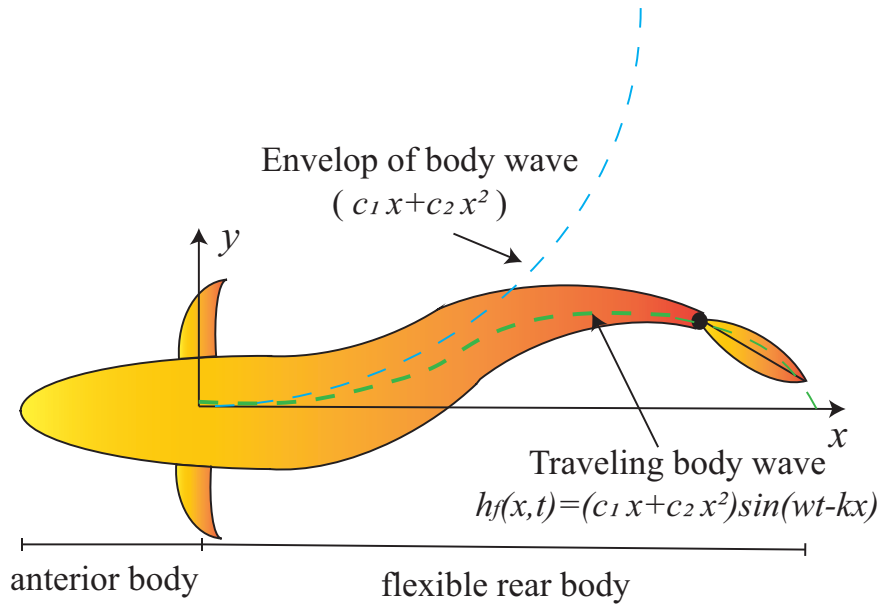


Figure 1-6: Swing Illustration[1]

has been used in actual calculations, mainly including Elongated Body Theory (EBT), Wave Plate Theory, and Actuator Disc Theory.

Resistive Force Theory

The quantitative analysis of hydrodynamics on aquatic animal swimming began in 1950, when Geoffrey Taylor was the first to analyze the flow of slender bodies of microorganisms and worms. The theory focuses on using viscous forces to establish the resistance theory to investigate the dynamics of the propulsion mechanism by analyzing the static balance of the interaction between the fluid and the body, while taking into account the constraints of thermodynamics and kinematics [28]. The theory of resistance can well explain the motion laws of tiny aquatic animals; however, since it ignores the inertial forces of fluid motion, it is only applicable when the Reynolds number is less than one during the tiny aquatic animals' swimming.

Elongated Body Theory

The elongated body theory illustrates that the dynamics of fish swimming belongs to the motion problem under high Reynolds numbers (hereinafter referred to as Re). In 1960s, Lighthill [29] proposed a theory that investigated the effect of the fluid flow outside the thin boundary layer on the fish body. The theory makes inertial effects dominate and justifies the use of the inviscid fluid models. Lighthill's theory has the following premises or assumptions:

1. The fish body is laterally symmetrical and slender;
2. The surface slope of the fish body is small;
3. The cross-sectional area of the front and rear ends of the fish body is zero;
4. Compared with forward movement, the lateral disturbance caused by movement is smaller, namely: $|\partial h/\partial x| \ll 1$, $|\partial h/\partial t| \ll U$.

The y -component of the cross-sectional velocity of the fish body observed by the moving water slice is approximately equal to the material derivative of the lateral displacement $h(x, t)$, as

$$w(x, t) = \frac{\partial h}{\partial t} + U \frac{\partial h}{\partial x} = Dh \quad (1.3)$$

where the material derivative $D = \frac{\partial}{\partial t} + U \frac{\partial}{\partial x}$.

The added mass $m(x)$ of the cross-section per unit length at x is:

$$m(x) = \frac{1}{4} \beta \pi b(x)^2 \rho_f \quad (1.4)$$

Among them, β is a geometrically dependent constant, which is about 1 in value; $b(x)$ is the length of the fish body x along the x axis; ρ_f is the density of the liquid.

The lateral force L_y exerted by the fish body on the water slice can be expressed

as the satellite derivative of $m(x)w(x, t)$, as

$$\begin{aligned}
L_y &= D(m(x)w(x, t)) \\
&= \left(\frac{\partial}{\partial t} + U \frac{\partial}{\partial x} \right) \left[m(x) \left(\frac{\partial h}{\partial t} + U \frac{\partial h}{\partial x} \right) \right] \\
&= m(x) \frac{\partial^2 h}{\partial t^2} + 2Um(x) \frac{\partial \partial h}{\partial t \partial x} + U \frac{\partial m(x)}{\partial x} \frac{\partial h}{\partial t} \\
&\quad + U^2 \frac{\partial m(x)}{\partial x} \frac{\partial h}{\partial x} + U^2 m(x) \frac{\partial^2 h}{\partial x^2}
\end{aligned} \tag{1.5}$$

The above formula describes the dynamics of a slender fish-like body moving in a flow field. If the shedding of the vortex only occurs in the contracted part of the fish-like body, then L_y can further simplify to the following form [30]:

$$\begin{aligned}
L_y &= mD^2h = m \left(\frac{\partial}{\partial t} + U \frac{\partial}{\partial x} \right)^2 h \\
&= m \frac{\partial^2 h}{\partial t^2} + 2Um \frac{\partial \partial h}{\partial t \partial x} + U^2 m \frac{\partial^2 h}{\partial x^2}
\end{aligned} \tag{1.6}$$

The dimensional analysis yields that $m \frac{\partial^2 h}{\partial t^2}$ dominates [31], thus we have:

$$L_y \sim m \frac{\partial^2 h}{\partial t^2} \tag{1.7}$$

Wave Plate Theory

In 1960, Wu [32] applied potential flow theory and linear boundary layer conditions to study the propulsion performance of flexible two-dimensional wave plates, and proposed the “two-dimensional wave plate theory”. Since then, Tong et al. have extended the two-dimensional wave plate model to three-dimensional conditions, based on the linear unsteady potential flow theory of small wave surfaces, studied wave plates of arbitrary planar shape and aspect ratio, and established the three-dimensional wave plate theory [33]. The theory uses the vortex ring panel method in the potential flow theory to solve in both the time domain and the frequency domain. The three-dimensional unsteady linear solution given by the semi-analytical and semi-numerical method confirms the qualitative law revealed by the slender body theory.

Actuator Disk Theory

Researchers also refer to the actuator disk theory—an effort to apply the momentum principle into fluid dynamics—to study the dynamic behaviors of robot fish. Its basic principle is to simplify the propulsion mechanism acting on the fluid into an ideal device—an “actuator disk”. When the fluid flows through the actuator disk, the surrounding pressure increases, and the thrust generated by the fluid on it is calculated by integrating the pressure increase on the surface of the entire actuator plate [34]. The main advantage of actuating disk theory is that it does not need to obtain the detailed dynamic characteristics of the propulsion mechanism. On the other hand, it suffers from the difficulty so as to fully satisfy the assumptions of energy and the existence of shedding vortices.

1.3 Case Study

A successful bionic robot fish is the outcome of robust integration of multiple realms of study in robotics and biology, including dynamic modeling, control, electronics, mechanics, fish biology, and so on [35]. With the boom of biomimetic robotics, biologically inspired robot fish has attracted more and more attention, with several paradigms of robot fish emerging. In this section, we will investigate the process of robot fish design and fabrication by means of a case study of two state-of-the-art robot fish: one being rigid robot fish, the other being the soft one.

1.3.1 UC-IKA

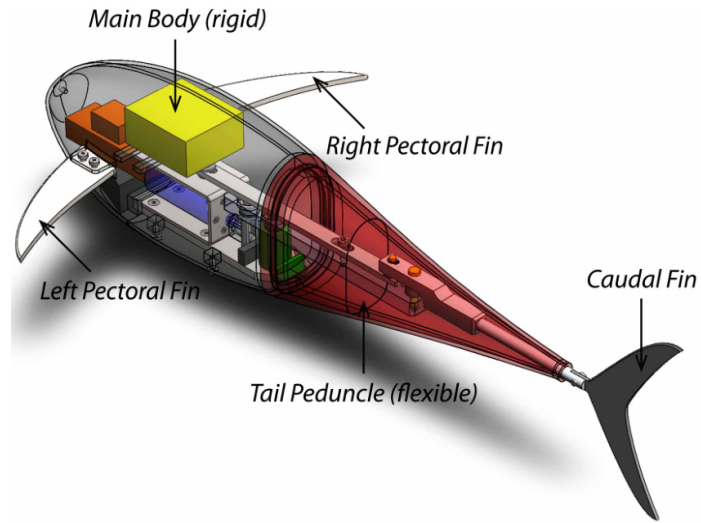
In an effort to implement the design principles into the robot fish design, the UC-IKA 1, as illustrated in Fig. 1-7(a), attracts researchers’ attention [36, 2]. The UC-IKA 1 is chosen here as it is a typical paradigm in the development of rigid robot fish, due to its straightforward design, robustness, reliability, and impressive good shape. The design objective of UC-IKA 1 is to mimic the undulatory swimming locomotion of tuna. As shown in Fig. 1-7(a), two main parts are included into the robot, namely,

the main body and the fish tail. The rigid main body, and the caudal fin—also rigid—are connected by a flexible tail peduncle. The peduncle is able to drive the caudal fin under undulation movement through an actuation mechanism inside. The mechanism is designed to transmit the output of the DC motor, which is installed in the main body, to the caudal fin.

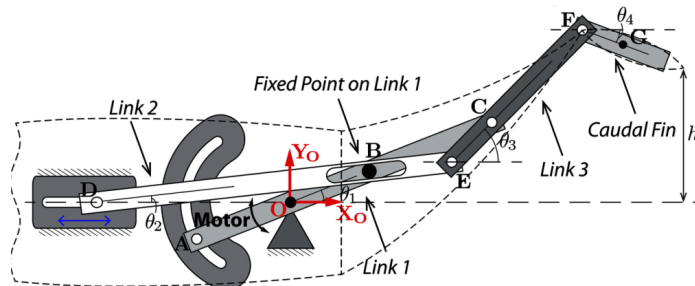
As a rigid and waterproof part, the main body is primarily designed to hold stationary components of a robot fish, including the microcontroller, batteries, and the DC motor. The pectoral fins, which are rigid as well, are fixed to the main body to provide additional stability. The tail, on the other hand, is not 100% rigid. It contains a tail peduncle, which is soft and flexible, and a rigid caudal fin. The tail peduncle connects the main body with the caudal fin, with an undulation actuation mechanism installed inside. Thanks to its sophisticated design, the actuation mechanism can transfer the output torque of the DC motor to the undulation of the caudal fin effectively.

Though much room exists ahead of researchers to match the real swimming location of tuna [37], the UC-IKA 1 has made remarkable achievements by virtue of its sophisticated actuation mechanism in its tail, as highlighted in Fig. 1-7(b). The tail fin is composed of a set of bars and joints, to be connected together, to form an oscillatory motion. When the fish stays still, rod AB overlaps with the center reference line. By rotating AB w.r.t. frame OX_oY_o using a motor attached at point O by only 14 degrees, a heave of 17 mm at point C and 56 mm at point F will be reached, in terms of the four bar linkage system.

This mechanism has a set of distinguished features. One being low number of DC motors used—the whole mechanism is actuated by only one motor. Thanks to this compact feature, it is easy to install the motor at, or close to the center of mass of the robot, resulting in low peduncle weight and low system moment of inertia. This will ease the control of the system. The mechanism also showcases improved capability to match the swimming locomotion of tuna cruising. For example, instead of providing undulations more close to the carangiform mode like mackerel, the UC-IKA 1 has a much closer agreement with tuna swimming, compared to some other



(a) UC-IKA Design: with a length of 65 cm and a weight of 4 kg



(b) the link mechanism of the tail peduncle

Figure 1-7: UC-IKA Design [2]

counterparts. The tail of UC-IKA 1 simulates the tuna caudal fin motion by limiting the undulation of the peduncle part close to the rigid body, since in nature, only the body part very close to the caudal fin takes part in their lift-based propulsion. While for carangiform swimmers, almost one-third of the fish body participates in undulation locomotion. Therefore, UC-IKA 1 not only improves mimicking the locomotion of tuna swimming, but also lowers energy dissipation. In addition to relatively simple mechanism assembly, it is also noteworthy that the third link is passively controlled, further leading to less DOFs to be controlled for the whole system.

The system allows quite satisfactory motion for tuna-like undulations underwater. According to the test results, a cruising speed of 0.29 m/s and 78% efficiency have been achieved. It is noteworthy that these satisfactory results are obtained without system optimization on the actuation mechanism. Therefore, upon optimization, improved performance will be anticipated for both swimming speed and efficiency. UC-IKA 2, an improved version, achieved an efficiency of 89% with the ability to make multiple gaits of locomotion [38].

1.3.2 SoFi

Being one of the most successful soft robot fish, the idea of SoFi (Soft Robot Fish)—a hydraulically driven soft robot fish—was initiated in 2014 [39]. Through three generations of improvement [39, 40, 3], SoFi has proven to be a flagship paradigm in the development of soft robot fish [3]. It is 18.5 feet long, weighs 3 pounds, and can dive to a maximum depth of 60 feet, and can work underwater for 40 minutes on a single charge, taking photos and videos through a fisheye lens. One distinguished feature for SoFi is the hydraulic power system. The hydraulic system creatively introduces the close water circulation system in the body. In terms of cyclically moving the water in the circulation system using a specifically designed water pump, the tail fin, which contains two symmetric chambers, with an elastic thin plate in between, can behave cyclic undulation motions under the water forces. The closed water circulation system in the body makes the tail bend and deform to complete the swimming. Thanks to the hydraulic power system, SoFi is able to swim in deeper water for long periods.

The outer shell of the SoFi is made of 3D printing, such as the head that holds the electronic parts, while the rear body is mostly made of silicone and soft plastic. The idea of soft robot fish opens a brand new window for the design of biologically inspired underwater vehicles, as it offers totally different approaches compared to the traditional rigid underwater vehicles with some apparent advantages. For example, SoFi has showcased significantly improved control levels due to its soft body compared to rigid underwater drones. Another advantage is no fear of collisions by virtue of a soft body. Relying on the structure of a fish-like tail, SoFi can swim straight in the ocean, turn around, and even float up or down in the ocean.

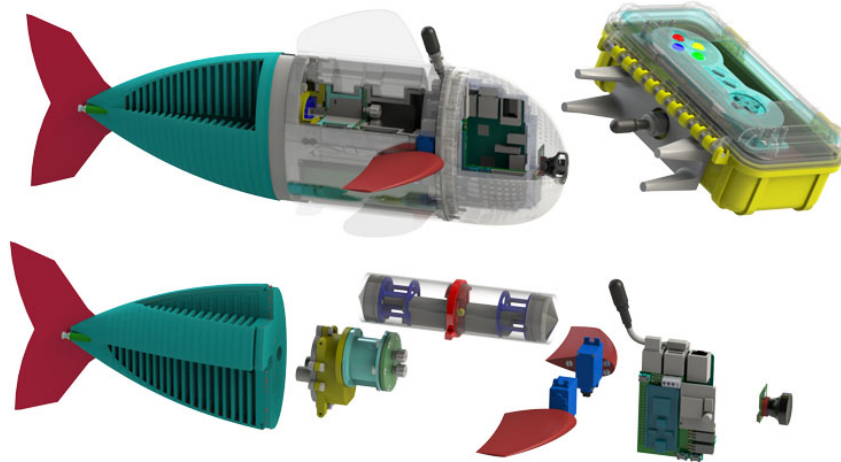


Figure 1-8: The Structure of SoFi [3]

In efforts to upgrade SoFi, researchers further replaced the radio with a waterproof controller and a special acoustic communication system they developed. By doing this, not only can sound waves travel farther, but the energy requirement is also lower. A special acoustic communication system can be used to change the speed and direction of SoFi's movement.

Chapter 2

Robot Fish Mechanism Design

Biological fish swim smoothly through the coordinated movement of the body and the tail; at the same time, the traveling wave motion is used to transfer energy from the back of the body to the tail, so that the caudal fin interacts with the water to generate thrust. The oscillating propulsion method of the caudal fin is the most efficient propulsion mode, propulsion mode, with high hydrodynamic efficiency and suitability for swimming for a long time and long distances. As a result, fish adopting the oscillating propulsion mode always behaves fast swimming in the ocean. Hence, the first priority of bio-inspired robot fish is to mimic this swimming morphology, including the shape.

In this chapter, the methodology we used to build a robot fish is firstly introduced. Afterwards, the general design idea of a robot fish is presented. Following that, the design of mechanism, electronics, and software for our robot fish are illustrated in details.

2.1 Design Philosophy

This research aims at testing engineering feasibility of a soft actuator, and proposing a novel design of a soft robot fish with relatively low cost.

There are several principles to follow when designing the mechanical structure:

1. Low cost. For example, we print gears using plastic 3D printing materials

rather than metal 3D printing materials. Although the plastic's strength is not as strong as the metal, its cost is much lower than the latter.

2. Easy to implement using common laboratory facilities and materials. For example, the 3D printer, the silicone gel.
3. Ockham's Razor Principle: entities should not be multiplied beyond necessity [41]. For example, other than the actuator system, nothing else is necessary to be placed in the robot fish body. We can remove the battery and control board for the first prototype, reducing the complexity.

The research method of robot fish is to analyze according to the structure and principle of biological fish, imitate according to its structure and principle, and design the actuator mechanism and fish body that meet the performance requirements. The design process of this thesis is as Fig. 2-1 shows.

First, a general research idea or direction is determined. Secondly, the size and swimming mechanism of the target fish are analyzed as needed. The shape and structure of the robot fish can be determined by the predefined key parameters from the target fish. According to the actual needs, the parameters irrelevant to the requirements are removed, and the key parameters are retained to obtain a simplified model.

Thirdly, according to the obtained key parameters, an implementable scheme is designed. The key parameters refer to the design requirements and design goals. According to the design requirements, find a practical and specific design scheme. Specifically, draw a design draft and then build 3D CAD (Three Dimensional Computer-Aided Design) models using software, such as SolidWorks. Here are several reminders when building CAD model:

1. Make fillet as much as you can to make the edge smooth.
2. Always simulate the assembling process in SolidWorks to check assembling issues. Otherwise, it might happen that physical parts cannot be assembled together, causing a waste of time and money.

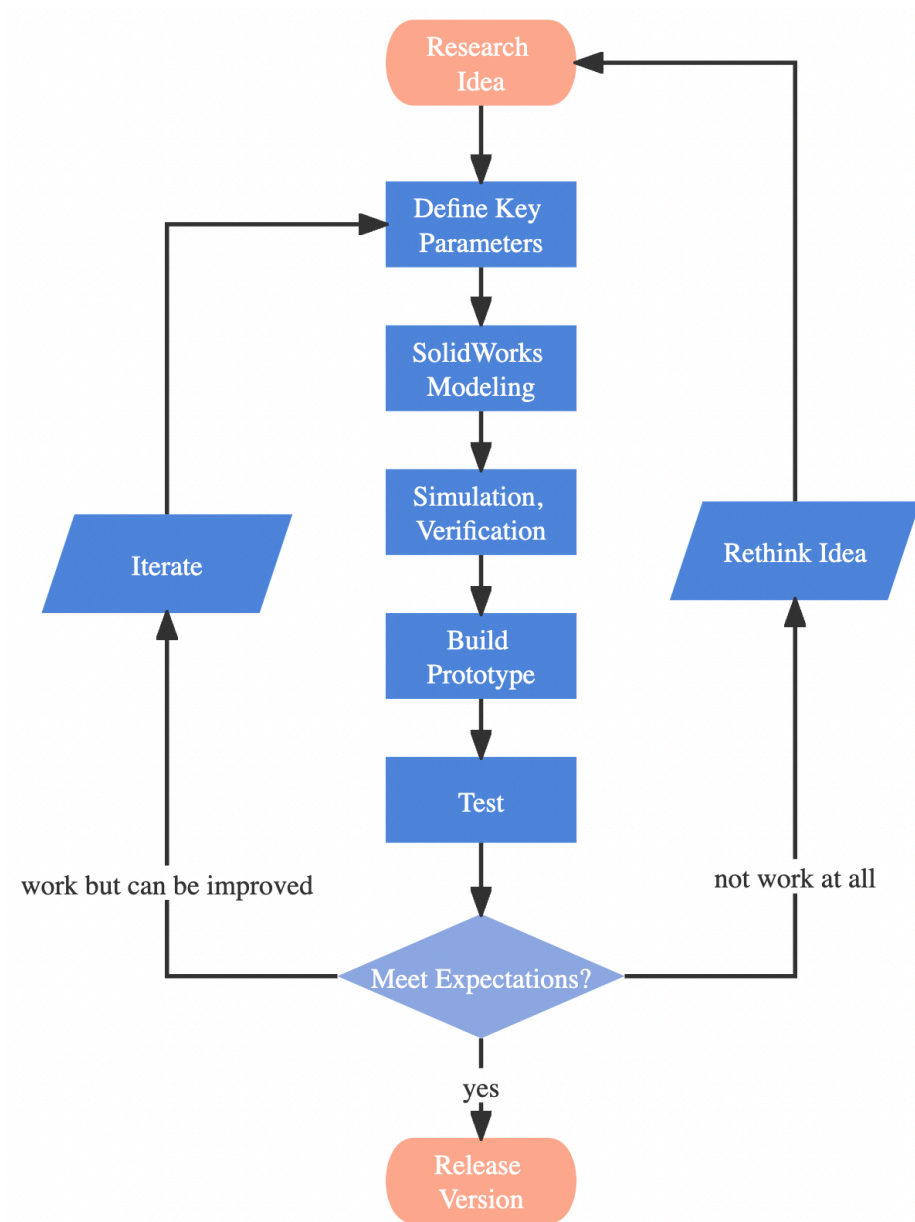


Figure 2-1: Robot Fish Design Process

Then, we might carry out a simulation to verify feasibility. If the solution is feasible, the next step can be prepared to make a physical model.

Finally, according to the designed scheme, a physical model is produced. The prototype needs to be tested to confirm whether it meets the requirements. Here are two situations:

1. The prototype can't produce the desired movement at all. This means our idea is not physically possible. So we need to rethink ideas and do it all over again.
2. The prototype demonstrates the desired movement to some degree, but it does not fully meet the requirements. In this case, we need to find out the reasons, modify the design scheme or key parameters, and verify the modified scheme through simulation and experiments. Continue the iterations until the requirements are met.

After iterations, a robot fish that meets the requirements is finally designed.

Both hardware and software are included in the architecture of a robot fish. Being the dominant system of hardware, the mechanical structure is equivalent to the “trunk” and “muscles” of a robot fish, along with the execution mechanism, while the control system, being the core of the entire system, is like the “brain” of a robot fish. The system design acts as a bridge to connect the conceptual design to reality: it not only realizes the engineering design into a practical robot, but also deals with many factors such as stability, durability, and so on. Generally, the mechanical structure of a robot fish includes two parts, namely the fish body and tail fin. The fish body is normally simplified as a rigid body for the installation of drivers, control systems, and sensors. According to the basic functions, the architecture of a robot fish can be divided into four layers, namely, the perception layer, the decision layer, the information exchange layer, and the execution layer.

1. Execution Layer: The robotic fish receives commands from the decision-making layer and performs corresponding actions.
2. Decision-making Layer: The most basic performance of a robot fish is to be able to autonomously navigate, track, operate and avoid obstacles. The robot fish

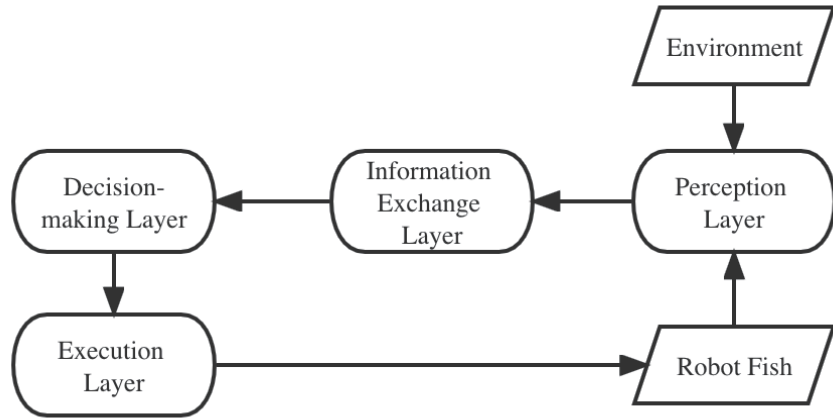


Figure 2-2: Overall Design Layers

obtains information resources through the perception layer, while the decision-making layer makes the judgment of various information and instructions according to the input signal and the unique control strategy of different tasks, generates corresponding control instructions, and completes the specified task.

3. Information Exchange Layer: Using the information exchange layer, the system transmits control commands to the robotic fish through the wireless communication module. At the same time, the sensor information collected by the camera and the internal execution state information of the robotic fish can also be fed back to the decision-making layer.
4. Perception Layer: In the perception layer, the robot fish obtains real-time external environment information, self-information, and target information, including the system resources, power performance, navigation information, the surrounding environment, as well as the perception and understanding of the target. It is difficult to provide complete information resources with a single sensor. Therefore, in the design of the robotic fish, various types of sensors are used to obtain information about the surrounding environment and the robot's motion. The fusion and filtering processing enhance the accuracy and reliability of the robot fish's perception of the outside world and its own information.

2.2 Design Considerations

Three main aspects are normally considered in the design of a robot fish: actuator design, material selection, and overall layout, which are summarized as follows. Actuator and material are the very two most important research topics since they lay the foundation of the robot fish performance. The overall layout includes everything else, such as communication, perception, and control. Before building a robot fish prototype, these three parts should be carefully inspected and combined to maximize the potential of your design.

2.2.1 Actuation System

Being a core part of the mechanism design, the actuation system aims at recreating the fish caudal movement, such as forward and backward moving and turning, in terms of using hardware. The design of the caudal fin swing system is the most important part of the robot fish. Therefore, a robust driving system design is the first priority, which can not only obtain high propulsion efficiency and good maneuverability, but also have the characteristics of small size, lightweight, large torque, and good controllability.

A close look at the existing robot fish designs reveals that mainly three types of actuators have been adopted: motor, hydraulic and pneumatic actuator, and smart material actuator.

Motor

The motor is the most commonly used actuation for robot fish. Through its rotational motion, the motor mainly drives the joints of the robot fish to move. The robot fish using motor as the actuation has the advantages of simplified structure, high reliability, and large torque, which in turn, makes it more suitable for imitating the biological fish type with fast swimming speed and outstanding maneuverability. The commonly used drive types of the motor include the servo motor drive, the steering gear drive, and the DC motor drive. An overview of the application and examples w.r.t. each motor drive type are listed in Table 2.1.

Table 2.1: Different Motor Drive Types

Drive Type	Usage	Example
Servo Motor	accurate control of positioning and movement	RoboTuna [42], RoboPike [43], SPC [44]
Steering Gear	accurate control of positioning and movement	PPF series [45]
DC Motor	auxiliary drive for special parts	TU Delft Robot Fish [46], iSplash [47]

There are two ways to apply motors in robot fish, according to the position of the motors.

- Joints could be actuated directly by motor. For example, RoboTuna [42] uses the transmission mechanism of pulleys and ropes to transmit the rotation of the six motors to the eight connecting rods to realize the reciprocating swing of the body. Lachat et al. designed a small robot fish, BoxyBot, by imitating the boxfish, actuated by three DC motors. Two motors were used to actuate pectoral fins, with the third one used to swing the tail fin, resulting in a maximum speed 0.37m/s [48].
- Joints are actuated indirectly by motors via the transmission mechanism. For example, six brushless servomotors were used in RoboTuna to control the corresponding tail joints angle through wires. RoboPike [43], the successor of RoboTuna, also applied a motor-wire actuation system. In [49], researchers proposed the mechanism of a pair of two motor-driven pectoral fins on both sides of the robot fish, leading to improved the maneuverability.

Hydraulic and Pneumatic Actuator

Rigid materials make the robot fish body stiff. Thus, with rigid materials, it is challenging to accurately simulate the soft body of the fish when it swims. Hence, an important research and development direction for the current robot fish is to use the

flexible material as the fish body, and the hydraulic device as the drive. By designing the cavity using flexible material, the spine structure of a real fish can be effectively simulated as that of a soft robot fish can be continuously deformed, with theoretically infinite degrees of freedom [50].

Equipped with high power density, hydraulic and pneumatic actuators can efficiently simulate the linear driving characteristics of fish muscles [51, 52, 53]. Festo developed a bionic robotic manta ray in 2007, using a high-power hydraulic propulsion system to control the movement of the pectoral fin with flapping wings[54]. Festo also constructed a pneumatically actuated carangiform robot fish with a flexible posterior body [55]. These robots demonstrated the feasibility of achieving completely fish-like movement through hydraulic and pneumatic actuators. The Draper Laboratory used four hydraulic cylinders to provide sufficient propulsion power in Vorticity Control Unmanned Undersea Vehicle (VCUUV) [56]. Marchese et al. designed a pneumatic-driven soft robot fish in 2014 [57], which can swim fast and continuously with a maximum speed 15 cm/s. In spite of the aforementioned achievements, the hydraulic and pneumatic actuation systems typically take up considerable space and are difficult to control. In order to solve this issue, researchers at MIT proposed a soft fluidic circulatory actuator using gear pump [39, 51, 40, 3], which is compact and efficient.

Smart Material Actuator

With the continuous research on materials and processes, new robot fishes made of smart materials have gradually emerged. Smart material actuators have inherent advantages of smaller size, lighter weight, and less noise, enabling robot fish made of the more flexible lightweight when moving, and have improved controllability underwater[58, 59]. Smart material can achieve complex movements without additional auxiliary devices [60]. Generally, there are mainly three types of smart material actuators for underwater robot fish: shape memory alloys(SMA), ionic polymer metal composites (IPMC) [61], and piezoelectric material [62].

Shape memory alloys are a class of alloy materials with a shape memory effect.

This is a specific effect that the deformed shape of the material will return to its original shape not by removing the applied external forces, but only by rising the temperature to a certain value, with properties that seem to retain a memory of the original shape [63].

Rossi et al. used the deformation of SMA to simulate the red muscles of fish, which can continuously change the curvature of the body [64]. Chen et al. attached the passive plastic fiber to the IPMC beam to make a caudal fin-driven robot fish [65]. Heo et al. designed a biomimetic fish robot actuated by piezoceramic actuators, which generates limited bending that is amplified and converted into a large tail swing via the transmission mechanism [66]. Seoul National University has developed a turtle-like swimming robot fish [67]. It uses a smart soft composite (SSC) structure composed of SMA wire, ABS, and PDMS to make pectoral and caudal fin drivers. The shell is made of 3D printed ABS, while the head is formed by PDMS pouring. By doing this, MPF mode is achieved. Nevertheless, smart materials are hard to be used in practice due to their control complexity, slow reaction, and small payload. Therefore, they are used in small or micro robot fish. C. Rossi et al. designed a flexible robot fish using SMA drives in 2011 [68, 64], showing the potential of using SMA rather than motor and gears. Wang and others developed a small flexible robot fish [69]. The robot fish embeds shape memory alloy wire into an elastic substrate to make an SMA driver, which drives the tail fin to swing and advance. In 2009, the team also developed a pectoral fin-tail fin hybrid mode of propulsion devilfish[70], whose driver is made of SMA cable embedded in the PVC film, with a maximum swimming speed of 57 mm/s. The University of Science and Technology of China [71] made a bionic robotic eel with SMA drives. The robot fish consists of three drive joints connected in series, using wave propulsion. In addition, in 2002, Northeastern University [72] developed another type of robotic eel with an SMA drive, which swims with its tail fin swinging. New York University and others developed a modeling framework in 2010 to study the free motion of a robot fish driven by an IPMC caudal fin [73], and evaluated the motion parameters through bending force and vibration measurements by means of reduction of the deformation modeling based on modal analysis. In

addition, MSU [65], HEU [74], VT [75] also did great job towards this direction. The robot fish is driven by a gearless mechanism, using the deformation of SMA to simulate the movement of the red muscle of the fish body, achieving continuous body bending. It is noteworthy that the maximum bending deformation of the tail fin can reach 72° . On the other hand, the thrust obtained is small, and the linear swimming speed is low.

Hybrid Actuation System

In addition, different actuation methods could be integrated to combine the advantages. In other words, the motor could be used together with other actuation methods. For instance, a DC motor was used in the vorticity control unmanned undersea vehicle (VCUUV) to drive the piston pump of hydraulic cylinders, resulting in stable, steady swimming speeds up to 1.2 m/s and turning rates up to 75 deg/s [76]. The great potential of the combination with motor and hydraulic actuators is demonstrated by the VCUUV, which can react faster and control precisely. Liao et al. developed a robot fish with a composite propulsion mechanism using dual swing tail fins and jet propulsion mechanisms as the propulsion system [77]. The tail fin swings in the opposite direction to offset the lateral disturbance caused by the swing of the single tail fin, while the injection system further improves its thrust. According to the experimental results, the composite propulsion mechanism exhibits higher controllability and maneuverability than the single tail fin swing mechanism, and the injection system generates high instantaneous acceleration. Aubin et al. created a robot fish powered by battery fluid, with the “Robot blood” as an electrolyte of zinc iodide [78]. During the discharge process, the zinc will be oxidized, releasing both electrons and soluble zinc ions; meanwhile, an electrons flow is created. The electric current generated by the movement of the electrons powers the microcontroller and the pump of the artificial circulation system. The electrolyte is used as hydraulic oil to make a hydraulic device to drive the fins to swing. Although the robot fish is significantly slow to respond, this idea has shed light on using novel approaches in solving soft robot fish driving problems in the future.

Table 2.2: Actuation Systems Comparison

Actuation	Pros	Cons	Example
Motor Actuated Fish	easy to design the mechanical propulsion structure can simplify the control task	must use at least one motor motor has limitations	RoboPike [43]
Hydraulic and Pneumatic Actuator	high power density efficiently simulate the linear driving characteristics of fish muscles	typically take large space difficult to control	SoFi [3]
Smart Material Actuator	can achieve more flexible and complex movements without additional auxiliary devices the robot fish made by smart material could be smaller, lighter, and quieter	hard to be used in practice due to their control complexity, slow reaction, and small payload	ZJU soft robot [79]
Hybrid Actuation	combine the advantages of the above three types	hard to design and control	VCUUV [56]

2.2.2 Materials

Typically, the materials used are determined by the structure of the robot fish. For robot fishes with discrete structures, rigid materials are used, while for continuous fish bodies, soft materials are used.

Rigid Material

In spite of the boom in the development of soft robots in recent years, the majority of robots on the market follows the classical rigid and discrete form, which is mainly composed of the assembly of multiple small rigid systems by means of linkages, gears, cables, pulleys, to name a few. The complicated assembly of multiple rigid parts is accomplished by significantly increased complex transmission of actuation power and high number of DOFs to control. Current state-of-the-art rigid biologically inspired underwater robots also have complex mechanisms. For example, in order to replicate the fish-like undulations, robot fish with rigid materials is designed as manipulator-like mechanism, driven directly by actuators, or indirectly using transmissions.

Soft Material

The past few years have witnessed an impressive growth in soft robots, the compliant grippers [80] and OctArm [81] being some typical paradigms. Thanks to the success of some soft robots, the soft robot fish has experienced significant development by implementing a similar idea. The design of soft robot fish follows a totally different principle from that of its rigid counterpart, i.e., by replicating the undulations of

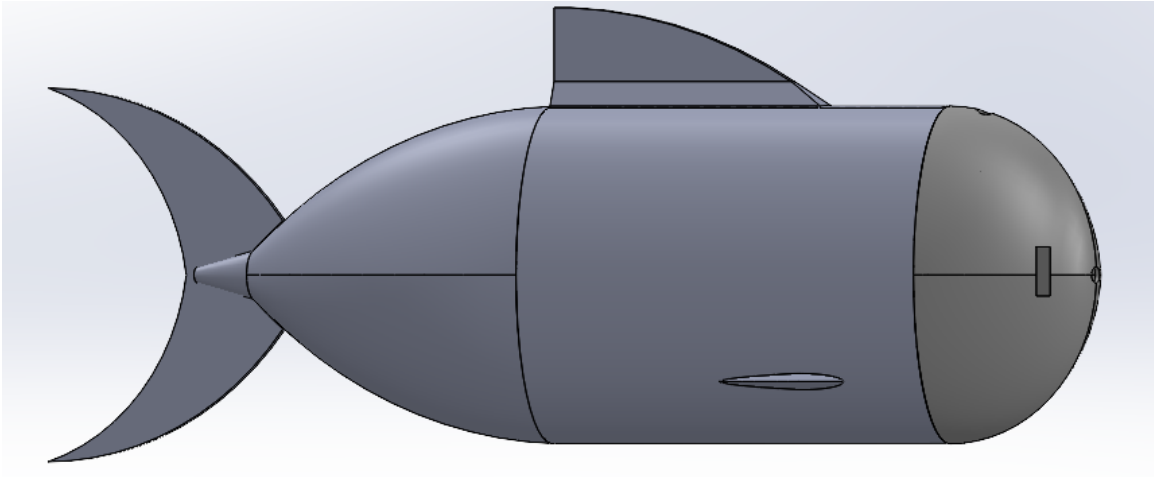
biological fish in a straightforward approach. Since in nature, a live fish achieves the swimming locomotion by the movement of its soft and flexible body, soft robot fish replicates this mechanism by directly applying an excitation on the soft robot body. One distinguished advantage of soft robot fish lies in its less complex but robust mechanism—only a flexible body and an excitation source are included.

Within the framework of dynamic analysis of mechanical structures, the vibration modes of a structure are determined by its geometry, material and excitation source, e.g., forces or torques being applied. It inspires researchers to design a mechanical structure in which the desired body motions are in compliant with the dominant vibration modes to reduce the number of actuations, in further, to reduce mechanism complexity. Therefore, for robot fish design, the dominant vibration mode of the robot fish body can match the flexible body motions of its biological counterparts under relatively simple actuations. Normally heterogeneous soft materials are used, whose dynamic responses are in agreement with the desired flexible body motions. The soft body also endows advantages of improved protection from the environment by encapsulating the mechanism and electrical components inside the continuous soft body.

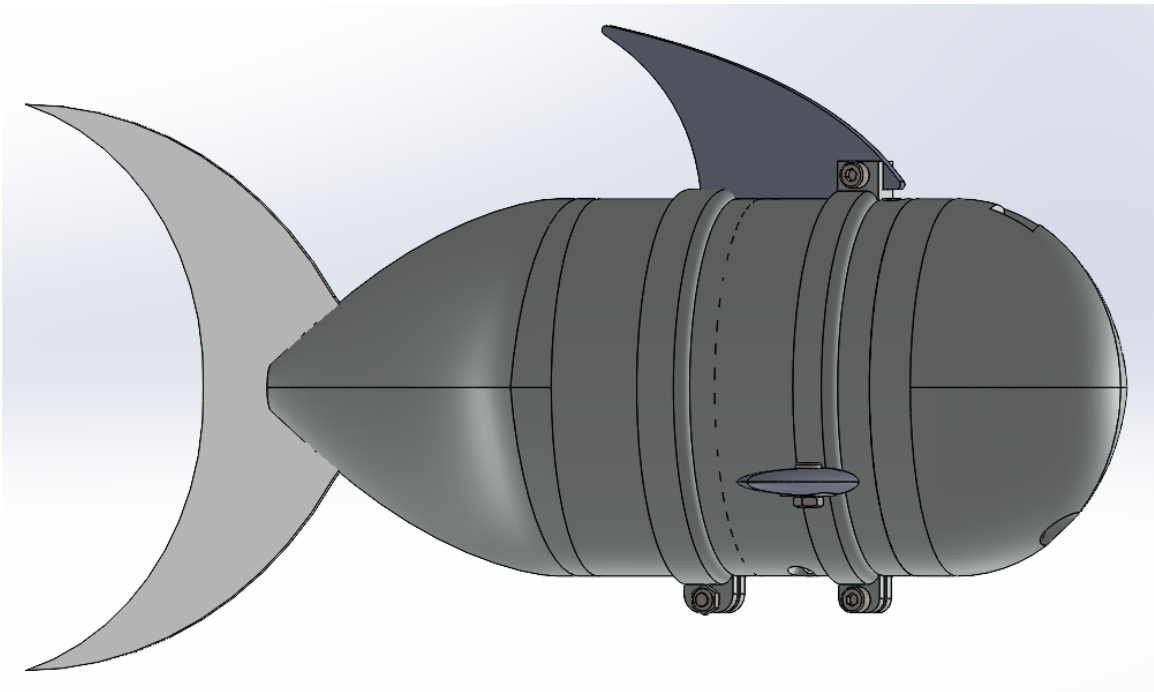
2.2.3 Overall Design

The carangiform is picked as the overall shape of our robot fish, mainly because its body-tail ratio makes the mechanical arrangement easier. As Fig. 2-3 shows, both the first and second designs are carangiform. For the former, the dimension is $746 \times 266 \times 264(L \times H \times W, mm)$, designed to accommodate everything inside, such as the battery and control board. Note that the dimension here is referred to as the longest normal Euclidean distance between any two points along Cartesian axes. However, during the process of iteration, we found that the size was so big that it exceeds the printing size limitation of the 3D printers. In addition, the main focus of this thesis is on the design and validation of the feasibility of the soft tail actuator mechanism. According to the aforementioned Ockham's Razor principle in the section Design Philosophy, we should simply remove the redundant parts, such as the battery

and control board. Thus, version 2, also the prototype version, is proposed. The dimension is $274 \times 136 \times 100(L \times H \times W, mm)$. It only contains the necessary actuator system, specifically, motor, gear box, and electric speed controller(ESC). The size is suitable to print the parts using 3D printers we have. And fewer parts make the inside space arrangement easier. Thus, a cable is needed to provide the fish power and control signal.



(a) Robot Fish Shape Design Version 1



(b) Robot Fish Shape Design Version 2

Figure 2-3: Shape Design of our Carangiform Robot Fish

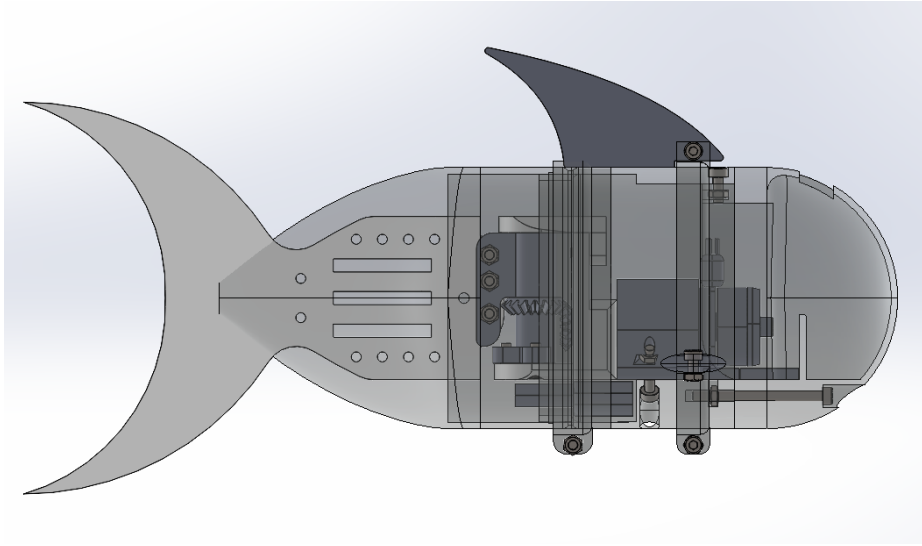
As illustrated in Fig. 2-3, the robot fish is composed of three parts: head, body, and tail. The shape of the head is important since it will determine the resistance to a large degree. The body is the core part of the robot fish, with most hardware inside, being the source of power for the robot fish. The tail is the source of propulsion to make fish swim forward or turn. Sometimes, there is also the fourth part: skin. It can reduce resistance, and isolate the water environment. Again, using Ockham's Razor principle, since we can make the 3D-printed head and body smooth and watertight, where the skin isn't needed.

In addition, inside the robot fish, there is mainly electric speed controller(ESC), DC brushless motor, gear box, transmission mechanism, and clump weight blocks. The actuation part uses a DC brushless motor as the driving component, which is also the most commonly used method in robot fish, as we discussed in Chapter 1. The motor's output shaft is in circular motion, which is not in line with the way the fish swim forward through the tail and fins. The circular motion needs to be converted into reciprocating motion through the gear transmission mechanism, so that the tail can be driven to swing back and forth like a fish, thus making the fish swims forward. In addition, in order to keep the robot fish balanced in the water, through 3D CAD simulations and multiple experiments, clump weight blocks with appropriate weights are placed at appropriate positions so that the robot fish can be stably suspended in the water.

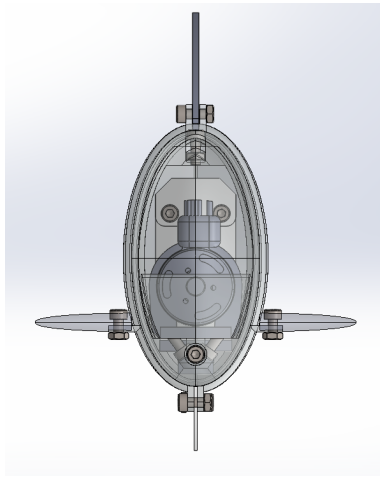
2.3 Mechanical Design

The design process of the robot fish and the overall mechanical structure of the robot fish are described above.

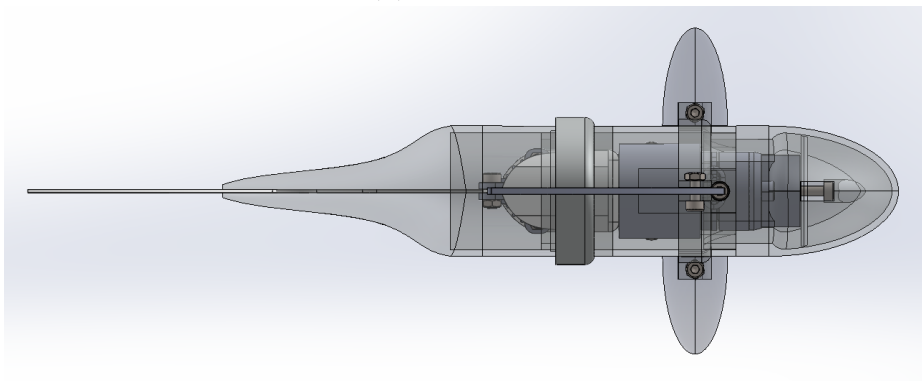
This section introduces the detailed design process of each part. The SolidWorks model of robot fish is uploaded to GitHub [82]. The mechanism and shape design process of the robot fish is complex. Many parameters are coupled together and need to be carefully considered. To focus on our goal, we ignore some minor parameters, which is conducive to abstracting a simple and reasonable model. The elaboration



(a) Side View



(b) Front View



(c) Top View

Figure 2-4: Inside Layout of our Robot Fish

of the mechanical design part is divided into seven parts: head, body, actuator, tail, fins, the center of mass(COM) and center of buoyancy(COB), and watertight design. Each section analyzes the key factors affecting the design and explains the SolidWorks model. In order to keep robot fish stable, the head, body, and tail need to ensure the balance between the left and right, and at the same time, the head, body, and tail coordinate to achieve the balance between the front and the rear with the help of clump weight blocks.

2.3.1 Head

The main goals of design the robot fish head are:

1. First, to look like a real fish head in appearance and to have a streamlined shape to minimize the friction.
2. Second, in terms of internal space, the inner cavity of the head is used to place modules that cannot touch water, such as wires, ESCs, etc. It should ensure sufficient space for extra weighting blocks.

Therefore, in the design process of the fish head, the key issues that should be considered include:

1. Effectiveness and convenience of sealing. The head needs to be used to place other modules, so the interface needs to be reserved. In addition, the interface needs to be sealed. Effectiveness means to ensure that the robot fish is completely watertight during the underwater movement; convenience means that it is relatively simple to assemble and disassemble while ensuring effectiveness.
2. The underwater balance of the head part, i.e., the center of mass(COM) and the center of buoyancy(COB). This will be discussed in detail in Section [2.3.6](#).

Regarding the shape of the head, fish with different shapes have different head characteristics. The overall shape of the head are designed according to the actual shape of the carp fish head. In addition, since our robot fish is tethered, the hole for

cables should be reserved. Fig. 2-5 shows the three views and the isotmetric view of the head.

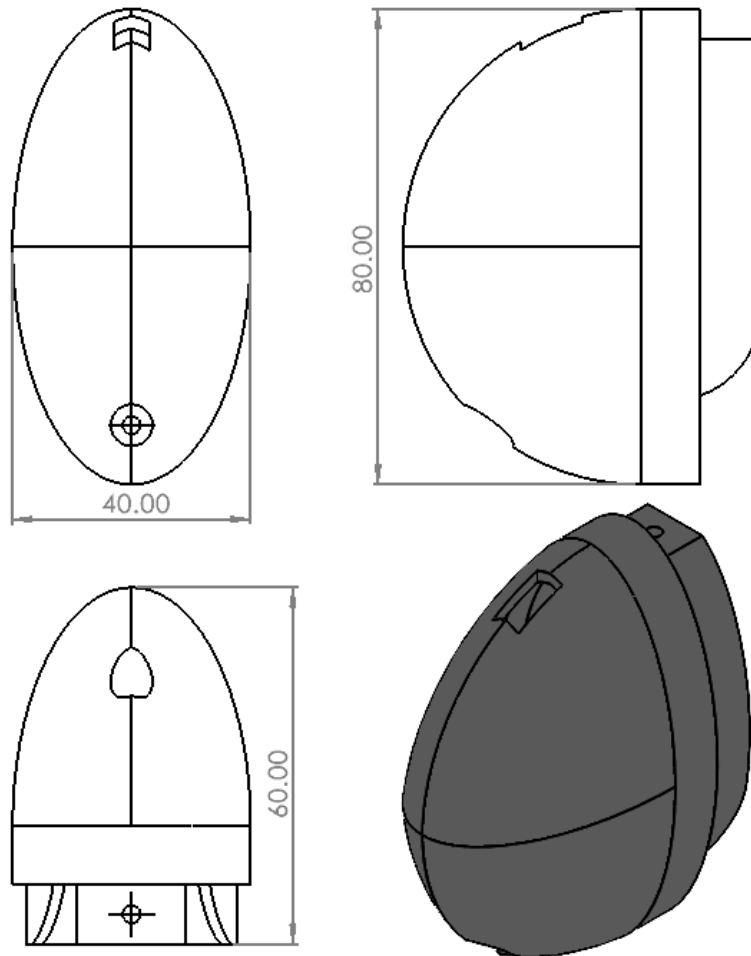


Figure 2-5: Head SolidWorks Model

The most important operation when building the head SolidWorks model is the loft. It's hard to make the whole head through the loft, so we make $\frac{1}{4}$ portion of the head via loft, then mirror it twice to get the whole head. There are two profiles and two guide curves. First, we draw three sketches, and one point as Fig. 2-6 (a) shows. Then build a lofted boss feature in SolidWorks, select the left point and right sketch as profiles, and select the top sketch and bottom sketch as guide curves. Now we will get the lofted boss as Fig. 2-6 (b) shows. Then mirror this loft twice to get the whole head, make the solid head a shell, and add other features. Open the head SolidWorks

model to inspect the loft feature.

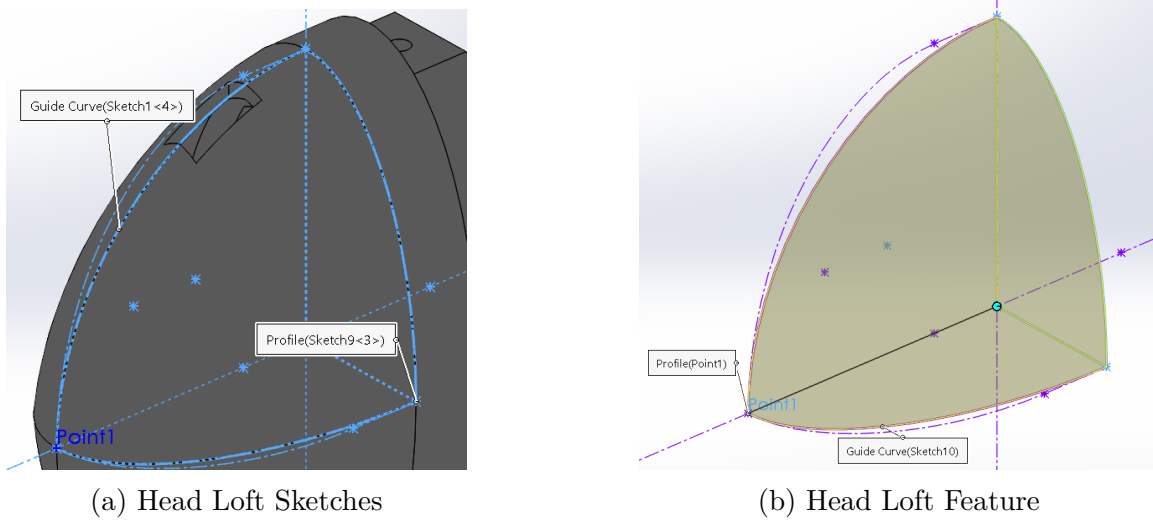


Figure 2-6: Details in the Head Loft Design

Inside the head, there is a baffle, as the blue area in Fig. 2-7 demonstrates. Two reasons for this baffle: one is that it can store the wires and avoid wires tangling with the motor; another is that it can prevent water from spreading if there is water leakage at the cable hole.

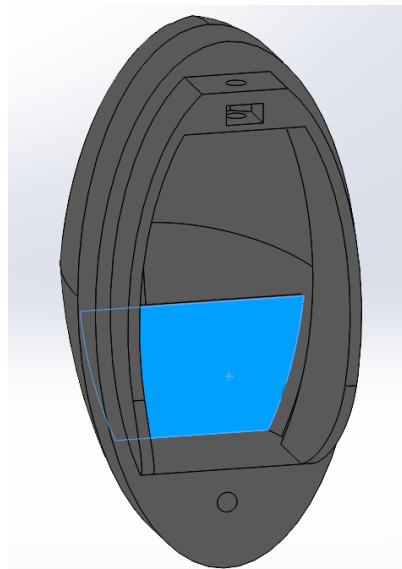


Figure 2-7: Baffle inside the Head SolidWorks Model

The head will be 3D printed using the Polylactic Acid (PLA) material.

2.3.2 Body

The body is like a bridge, which connects the head and tail. It also mounts the motor, electric speed controller(ESC), gears, and clump weight blocks. Three views and an isotmetric view of the body are shown in Fig. 2-8. There are several screw holes and nut holes whose position should be carefully calculated. Otherwise, the assembly would be difficult. The body is extruded from a 2mm thick ellipse ring whose outer ellipse has a 20mm semi-minor axis and a 40mm semi-major axis. On the right side, a smaller ellipse ring is for a better connection with the silicon rubber tail. See Chapter 3 for details.

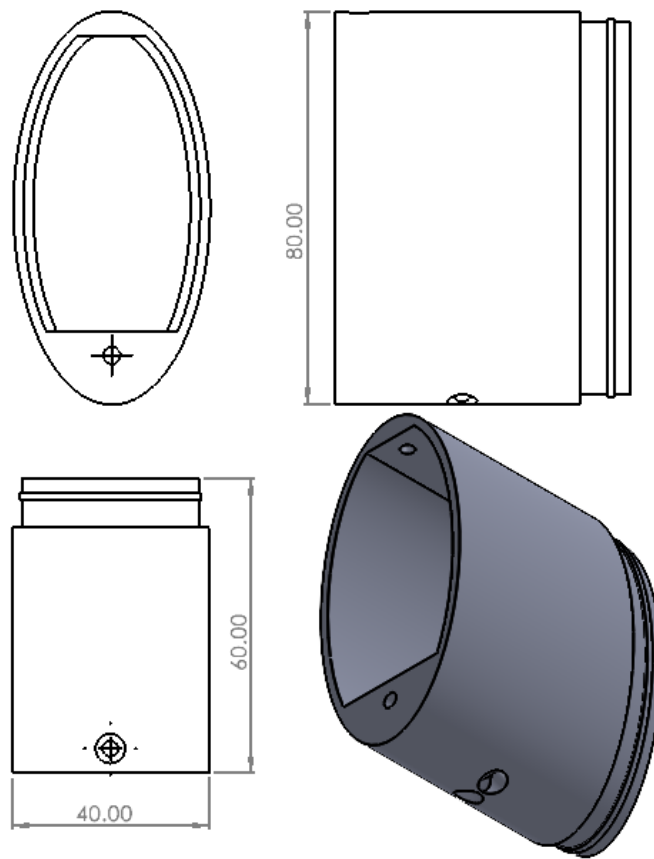


Figure 2-8: The Body SolidWorks Model

The body will be 3D printed using Polylactic Acid (PLA) material.

2.3.3 Actuator

The actuator is the source of the power. Figure 2-9 is the assembled actuator. Before this design version, there were two other designs. One is based on a slider-crank mechanism and worm gear; another uses bevel gear and sector gear. Refer to Appendix A.1 for details.

As demonstrated in Fig. 2-10, it is composed of the DC brushless motor, bevel gears, transmission mechanism, bearings, 3D printed stations, etc. The motor is positioned in a claw, and the claw will be connected to the body using two M3×16mm screws. In this way, the whole actuator is fixed to the body. The station to mount gears has as many fillets as possible, which will save materials, save space, and reduce the risk of cutting fingers.

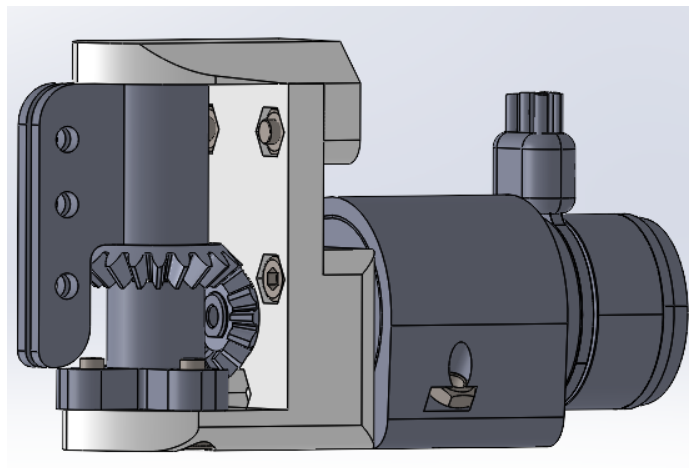


Figure 2-9: The CAD Model of the Actuator

The actuator works this way:

1. First, the motor outputs power.
2. Secondly, the high speed and low torque of the motor are changed to low speed and high torque through the planetary gear reduction mechanism, which is integrated with the motor.
3. Thirdly, the bevel gears convert the circular motion into reciprocating swing motion.

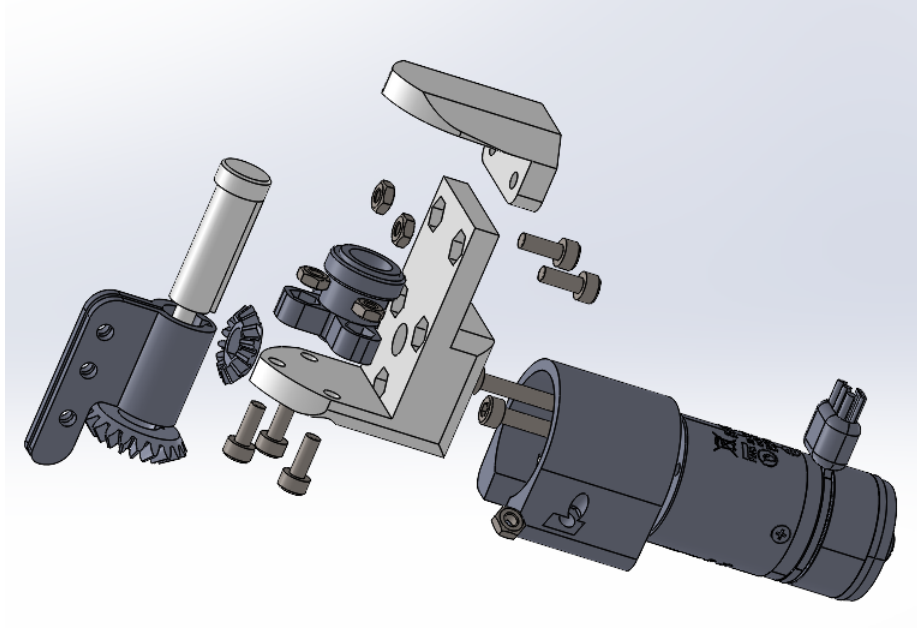
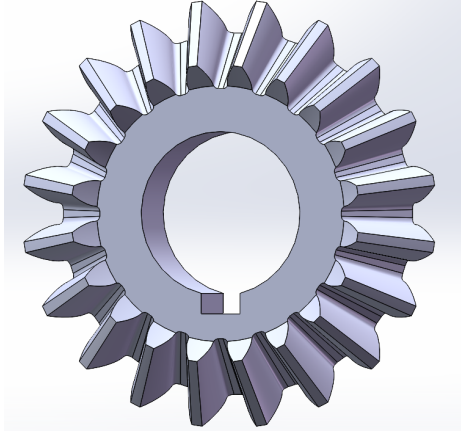


Figure 2-10: The Exploded View of the Actuator CAD Model

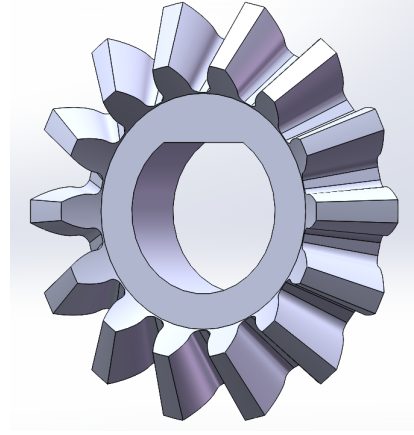
4. Finally, the swing of the rod claw drives the center constraint layer to produce the reciprocating swings we need to drive the robot fish to swim forward. The center constraint layer is poured with a silicone rubber tail.

Bevel gears are conical gears that transmit motion between two intersecting shafts. Bevel gears are used to transmit rotary motion between two intersecting axes, and the angle of intersection can be arbitrary, but most of them are 90° . We use 90° for easy positioning. According to its tooth line shape and direction, it can be divided into straight bevel gears, helical bevel gears, zero-degree bevel gears, and curvilinear bevel gears. As Fig. 2-11 shows, two spur bevel gears are used here. Spur bevel gears are easy to build CAD models and print via a 3D printer. Its pitch bevel tooth line is radially straight, and each tooth line passes through the pitch cone tip. The direction of its gear teeth is along the direction of the conical generatrix and gradually shrinks proportionally from the big end of the gear frustum to the small end. Finally, the space intersects at the intersection of the axes of the two-phase meshing gears.

One gear is in the vertical position and is placed on the motor shaft; the other one is in the horizontal position and is placed on the rotational rod. Their parameters are listed in Table A.1.



(a) Horizontal Gear



(b) Vertical Gear

Figure 2-11: Bevel Gears

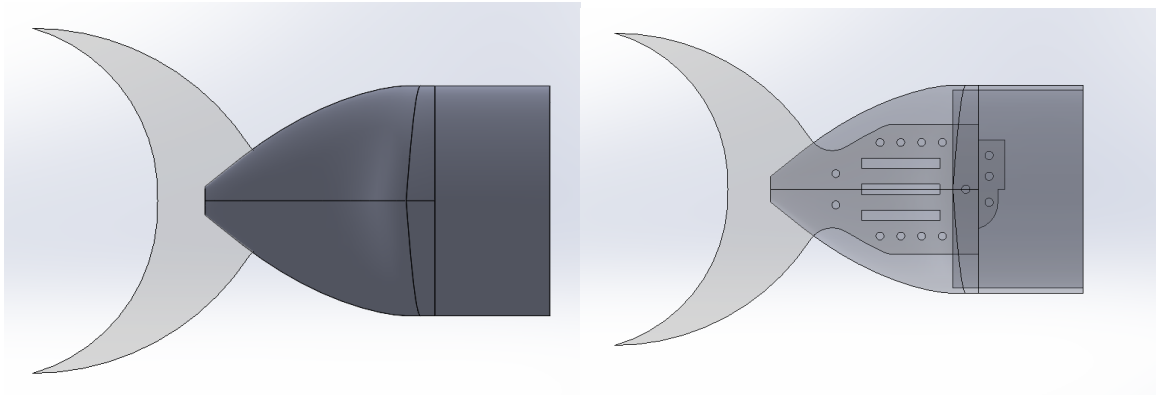
The material used for the 3D printing gear is nylon, which can withstand a temperature range of 175°C , and pressures up to 48MPa , and has high wear resistance.

2.3.4 Tail

The tail consists of two parts, as shown in Fig. 2-12: tail made of soft material, and bendable central constraining layer. The central constraining layer is connected with the actuator. The torque output by the motor is transmitted to the central constraining layer, which is a structure similar to a cantilever. The central constraining layer bends, causing the soft tail to bend and swing. On the right side of the soft tail, there is a cylindrical film. This part is used to be connected with the body to seal the water. In addition, this structure leaves a length allowance for bending. More details can be found in Chapter 3.

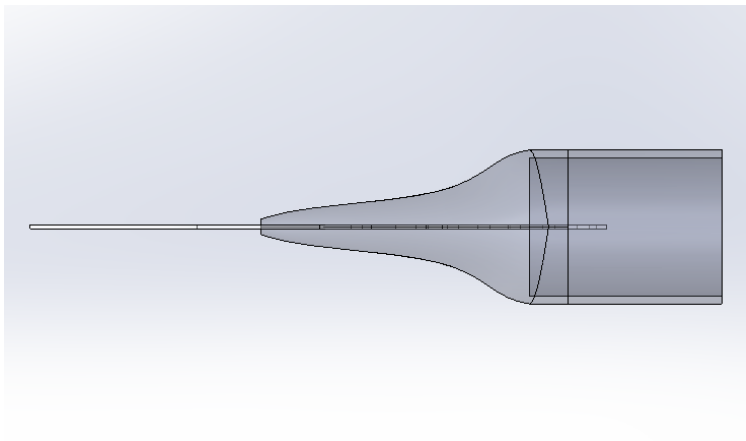
The caudal fin is the key structure that provides power, and its swing is the main source of forwarding power for the robot fish. Note that 90% of the fish's propulsion comes from the swing of its caudal fin [83]. The crescent-shaped tail fin is selected, and its propulsion force and propulsion efficiency depend on the following shape parameters and kinematic parameters:

1. The aspect ratio $R = d^2/S$, where d is the height of the caudal fin, and S is the area of the caudal fin. Within a certain range, the larger the aspect ratio,

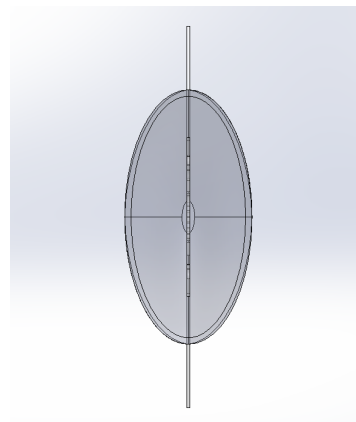


(a) Tail(Non-Transparent) Side View

(b) Tail Side View



(c) Tail Top View



(d) Tail Front View

Figure 2-12: The Tail CAD Model

the greater the propulsion efficiency and propulsion force of the fish, because the larger aspect ratio makes the tail fin less drag per unit of lift or thrust. The aspect ratio of tuna is between 4.5 and 7.2, while that of Carangidae fish is smaller. Our robot fish has aspect ratio $R = \frac{(120mm)^2}{3177mm^2} = 4.53$ as shown in Fig. 2-13. On the one hand, this aspect ratio can have a large thrust of the tuna crescent tail. On the other hand, it can ensure similar controllability as the Carangidae fish.

2. Stiffness of the caudal fin. The greater the stiffness, the greater the ability to generate thrust with less loss of efficiency. Therefore, we use Polyvinyl chloride (PVC) material to make the central constraining layer.
3. The oscillation frequency and amplitude of the caudal fin. This will be described in detail later.

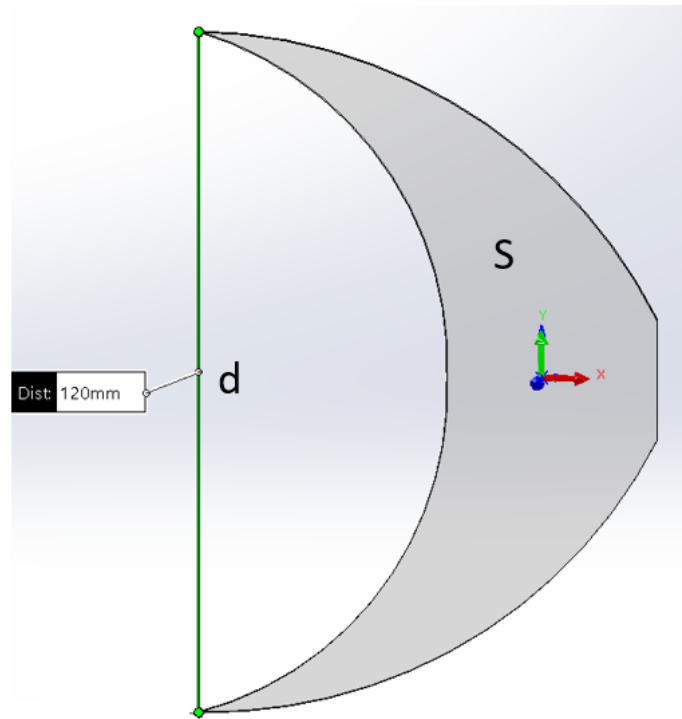


Figure 2-13: The Schematic Diagram of Caudal Fin

When the robot fish swims, how does it move forward or turn? We briefly introduce it through the following schematic diagram Fig. 2-14. Position a is the neutral

position, and initially it is in the horizontal position as Fig. 2-14 (a) shows. If the tail moves back and forth evenly between position b and c , due to the symmetrical movement, the displacement from a to b equals the displacement from a to c . The swing speed of the tail from a to b also equals the swing speed from a to c . Thus, the forces are the same. According to the basic physical law:

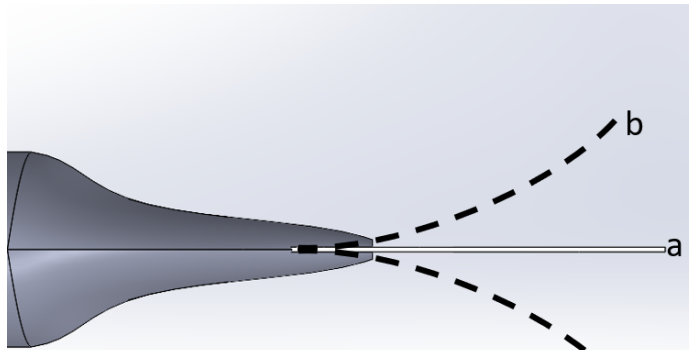
$$W = F \cdot d$$

where W is the work, F is the force, d is the displacement. the work of water on the tail from a to b equals that from a to c . In other words, the lateral forces cancel each other out, resulting in only a forward reaction force. Hence, only a forward reaction force is generated, and the robot fish will move forward in a straight line.

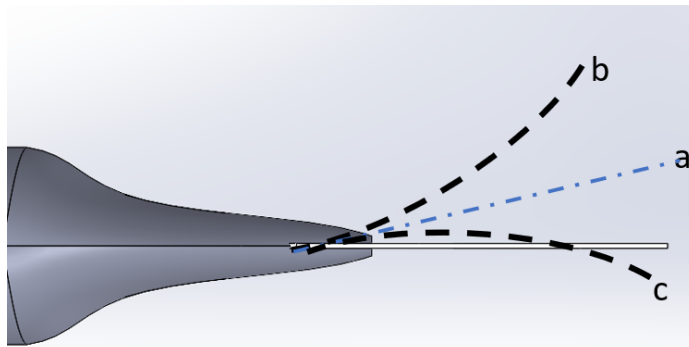
If the displacement from a to b is greater than the displacement from a to c , then the movement is asymmetric, the lateral force is unbalanced and cannot be counteracted. The fish is reacted forward and to the side c . In other words, we can regard that the neutral plane has an offset, shown in Fig. 2-14 (b). On the contrary, if the displacement from a to b is less than the displacement from a to c , the robot fish will move forward to side b .

How to control the tail to move in the direction we desire? To achieve this, we need to know the exact position of the tail. This is related to the selection of motors. We chose a motor with a photoelectric encoder. the encoder is a kind of position sensor. This encoder divides the 360 degrees into 8192 pieces, and it can sense which position the motor is in. In other words, the absolute value of the angle coordinates can be read directly, and there is no accumulated error. In addition, the location information is not lost after power is removed. However, the encoder is placed on the motor rotor, and the motor has a planetary gear reduction mechanism, which introduces a 36 : 1 reduction ratio. This will cause a problem: the position we get from the encoder is not the accurate position of the motor output shaft, i.e., the tail position. This will be discussed in detail in Section 2.5.

The tail swing range is $[-65^\circ, 65^\circ]$ as Fig. 2-15 shows.



(a) Initial Neutral Position



(b) Deviated Neutral Position

Figure 2-14: The Swim Schematic Diagram

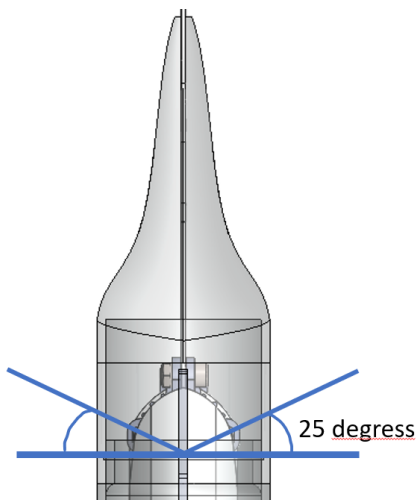


Figure 2-15: The Tail Swing Range

2.3.5 Fins

The fins of robot fish are designed to be easy to assemble and disassemble. It is because multiple trials are needed to find the suitable fin size. As Fig. 2-16 shows, one dorsal fin and two pectoral fins are attached to a body-shape ring, connected via screws and nuts.

To start with, let's inspect what the function of fins for the biological fish is. When the biological fish swims, the caudal fin swings left and right to push the fish forward. When the fish is not moving, the pectoral fins open to both sides of the fish. When the fish moves forward, it swings back and forth. When the fish turns, one side of the pectoral fin swings. The dorsal fins are used for balance. The dorsal fin keeps the fish on its side; without it, the fish would roll over. There are also some fish with a longer body; the dorsal fin can play a role in providing power, such as hairtail, moray eel, seahorse and so on.

Therefore, fins are necessary since the oscillating tail reduces the fish's stability. Without fins, the oscillating angle of the robot fish head around the yaw axis will be large, and the head will swing heavily. As a result, the robot fish is slowed down, and its gesture is unstable. For simplicity, we keep the pectoral fins static. The cross-section of pectoral fins is based on the NACA0010 foil. The CAD model of the pectoral fins uses the lofted feature in SolidWorks.

2.3.6 COM and COB

As we all know, no matter how you swing, the "tumbler" will never fall down. The lower the center of mass(COM) of an object, the more stable it is. That is, an object that is light above and heavy below is more stable. The COM is the center of the weight/gravity of the object. Therefore, when placing the internal items of the robot fish, put them at the bottom, and at the same time, ensure the balance of the left and right weights. And the COM of the whole robot fish is preferably located in the center of the body. Fig. 2-4 shows the inner parts arrangement. It can be observed that most of the internal parts are placed on the center line and lower section.

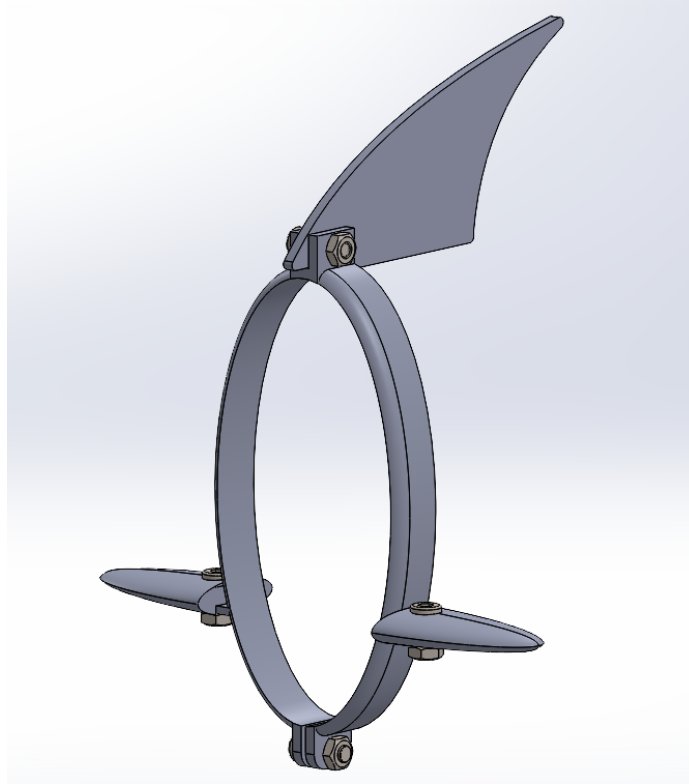


Figure 2-16: The Fins of Robot Fish

An object submerged in water will rotate to align the COM below the center of buoyancy(COB). The COB is the center of gravity of the fluid volume displaced.

Meanwhile, the robot fish stability can be affected due to the COB and COM, which are analyzed below.

Let's consider stable equilibrium first. Consider a submerged body in equilibrium whose COM is located right below the COB as Fig. 2-17 (a) shows. If the body is tilted slightly in any direction, the buoyant force B and the gravity G always produce a restoring moment M trying to return the body to its original position as Fig. 2-17 (b) shows. However, if one of the COM or COB is not on the centerline as Fig. 2-17 (c) shows, there is moment M anyway. Hence the fish body will rotate and stay tilted. This is the front view, and the same analysis applies to the side view. The longer the distance (arm) between the COB and COM, the more force is needed for the body to roll or pitch, making it more stable. In other words, the mass should be placed as low as possible in the object.

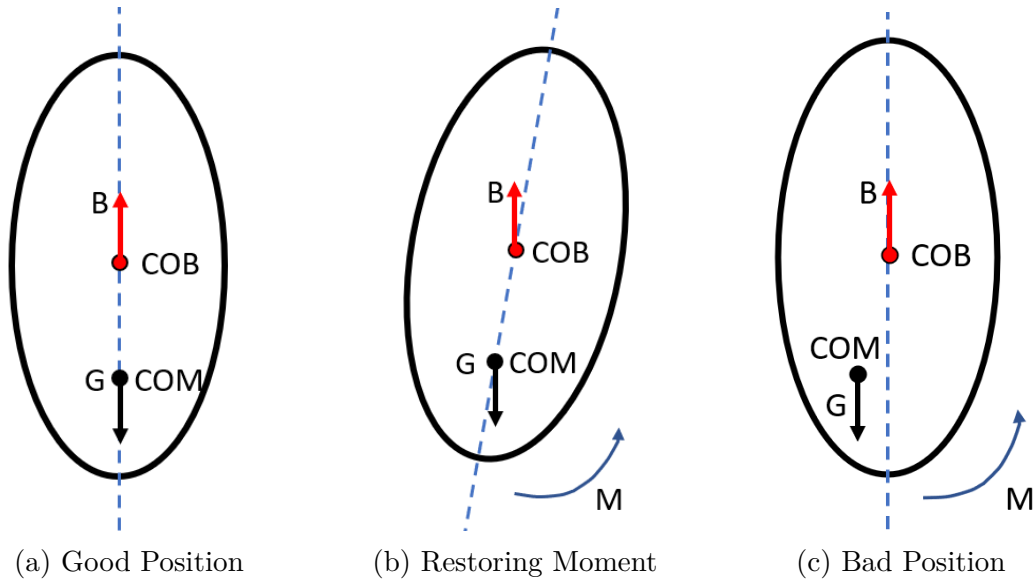


Figure 2-17: Bevel Gears

On the other hand, if COM is above COB, any disturbance from the equilibrium position will create a destroying moment which will turn the body away from its original position. The body is unstable in this case. When the COM and COB coincide, the body will always assume the same position in which it is placed, and hence it is in neutral equilibrium.

From the analysis above, we can conclude that the COM should be located right below the COB, and the distance between the COB and COM should be as long as possible.

The next step is to calculate the COM and COB. After we get the COM and COB, check if they meet the requirement above, and modify the model accordingly. Repeat the process until the result is optimal.

Calculate the COM:

Calculating the COM is relatively straightforward.

1. Design an initial robot fish model, make sure each part is symmetric about the central plane, and place inner parts as low as possible.
2. Print parts using a 3D printer.
3. Weight each part's mass using a scale.

4. Override each part model's mass in "SolidWorks - Evaluate - Mass Properties".
5. Show the Center of Mass in the robot fish assembly. You may check the mass of robot fish and COM's precise coordinate in "SolidWorks - Evaluate - Mass Properties".

Calculate the COB:

Calculating the COB is a little bit tricky. We need to use the "Offset Surfaces" feature in SolidWorks, and manipulate dozens of outer surfaces to form a whole fish body. The detailed operations are described in Appendix [A.3](#). The idea is that we build a solid fish body using the outer surfaces, and set the material to water. Then the mass of this solid is the buoyancy of the robot fish, and the COM of this solid is the COB of the robot fish.

Now we have COM and COB. Put this generated solid and the robot fish assembly together; we can check COM and COB very intuitively. As Fig. [2-18](#) shows, the yellow one is the COB, and the blue one is the COM. If the COM is not aligned with COB, we need to adjust the number of clump weight blocks and their positions in the robot fish assembly.

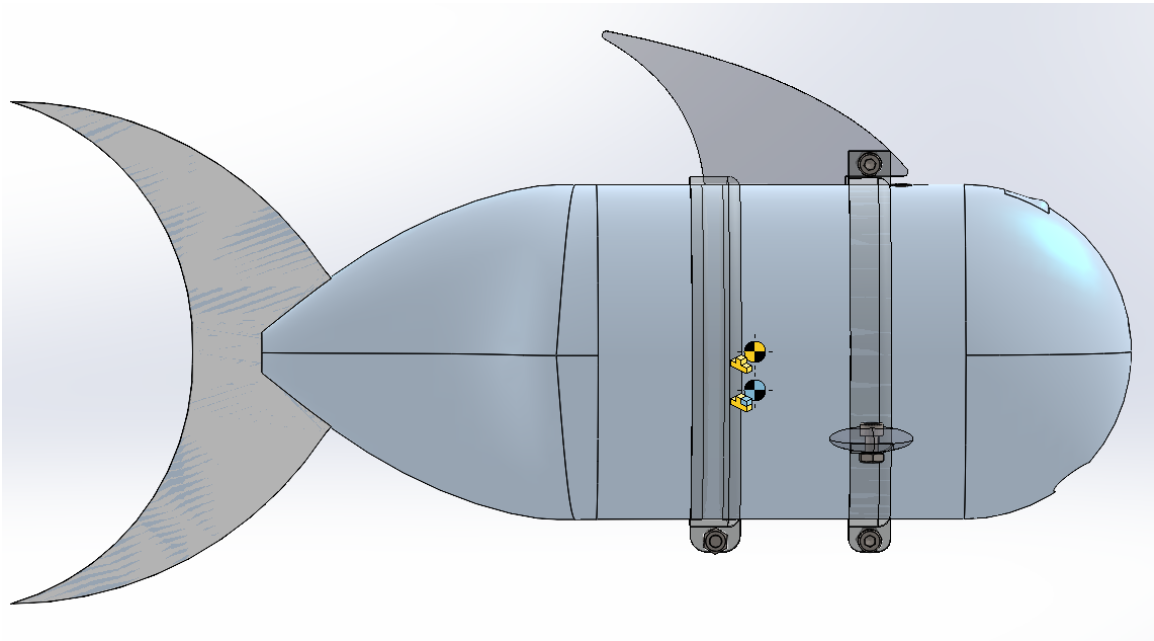
The clump weight block is a $18 \times 11 \times 3.5$ steel cuboid, whose mass is 5 grams. The clump weight blocks are placed as low as possible, which can be found in Fig. [2-4](#).

In this way, we can make sure that when the fish is in a static state in the water, it will neither dump to both sides nor lean forward or backward. When the fish is in a dynamic state, it will not tip over left and right, allowing a certain angle of shaking.

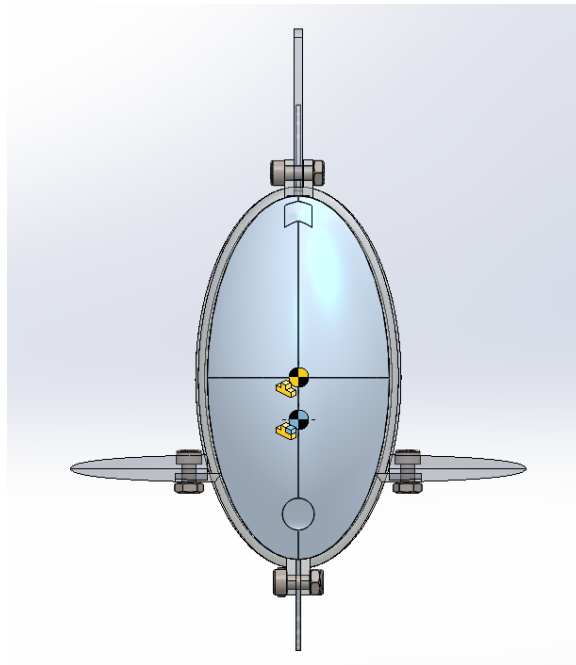
2.3.7 Watertight Design

Body - Head Connection

The body and head are connected using screws and nuts. As Fig. [2-19](#) shows, there is a 2mm thick silicone gasket between screw and nut. After the screw is tightened, the screw cap and screw hole will squeeze the silicone gasket to make the silicone



(a) Side View



(b) Front View

Figure 2-18: COM and COB

gasket watertight. Silicone gasket is also applied in other screw-nut connection if it is exposed to the water. There is a 2mm thick silicone seal ring between the head and body. It works like the silicone gasket. Both the silicone gasket and silicone seal ring are self-made.

As Fig. 2-7 shows, there is a extruded boss on the head. This is designed for watertight consideration. The extruded boss can make the connection between head and body tighter, and the nut hole on the top of the extruded boss can make the screw connection between head and body easier. In addition, it can help to position the silicone seal ring.

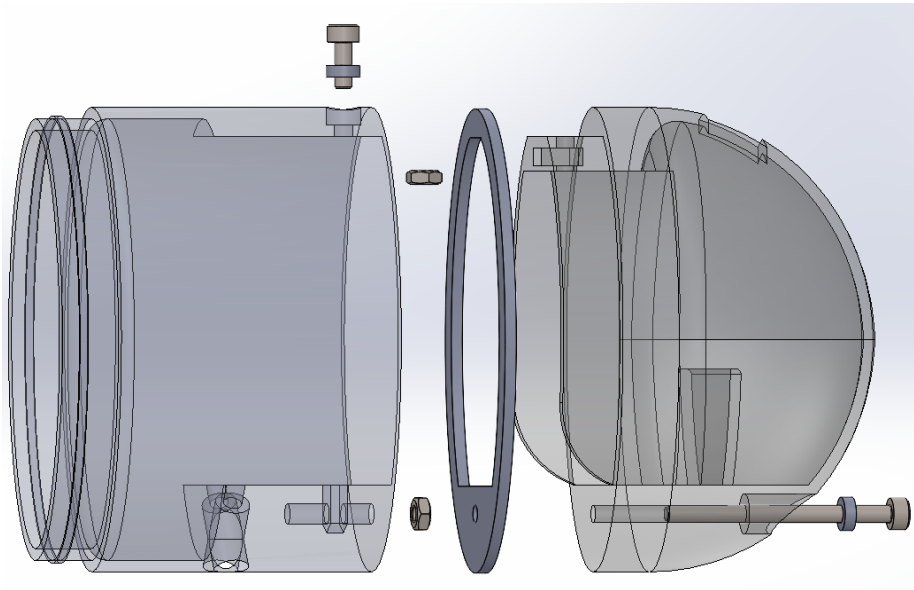


Figure 2-19: Body - Head Connection Schematic Diagram

Both silicone gasket and silicone seal ring can be made using a 3D printed mold. See Chapter 3 for details.

Other than self-made gadgets, waterproof tape, and silicone glue are also helpful.

Body - Tail Connection

The body and tail are connected via a pressure ring as shown in Fig. 2-20. The membrane part of the tail and the narrow mouth part of the body is squeezed together with a pressure ring. The pressure ring can be adjusted by tightening or loosening

the screw and nut. Thanks to the ductility of silicone rubber, this connection is watertight.

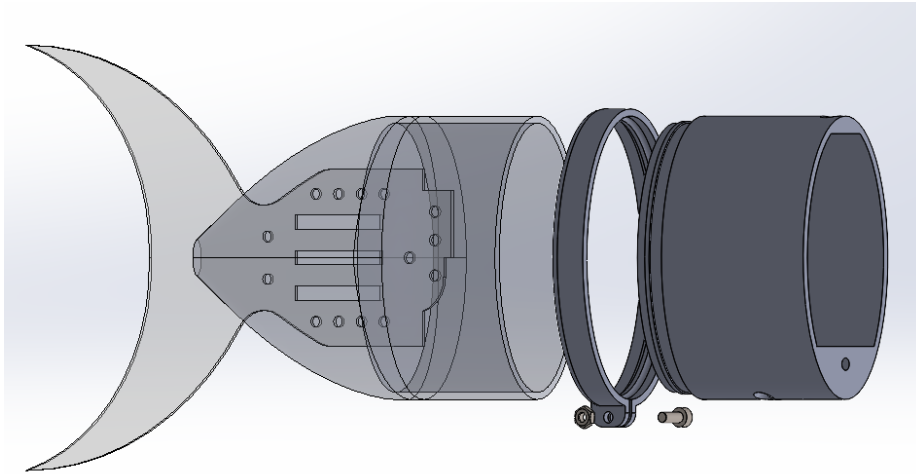


Figure 2-20: Body - Tail Connection Schematic Diagram

2.4 Electronics

The electronics are constructed following our tethered robot fish design. As Fig. 2-21 shows, there are two parts of the circuit: one is in the robot fish, and another is off the robot fish. Two parts are connected using a 4-meter cable. The workflow is as follows:

1. Turn on the power source.
2. After hearing a beep from the control board, turn on the remote controller, and put two three-position switches on the top to the upper position.
3. Adjust the tail to the central position using the right column joystick.
4. Switch the top-left three-position switch into the middle position.
5. Control the tail swing amplitude using the right column joystick, control the tail swing frequency using the right row joystick.
6. Control the tail offset to the central position using the left row joystick.

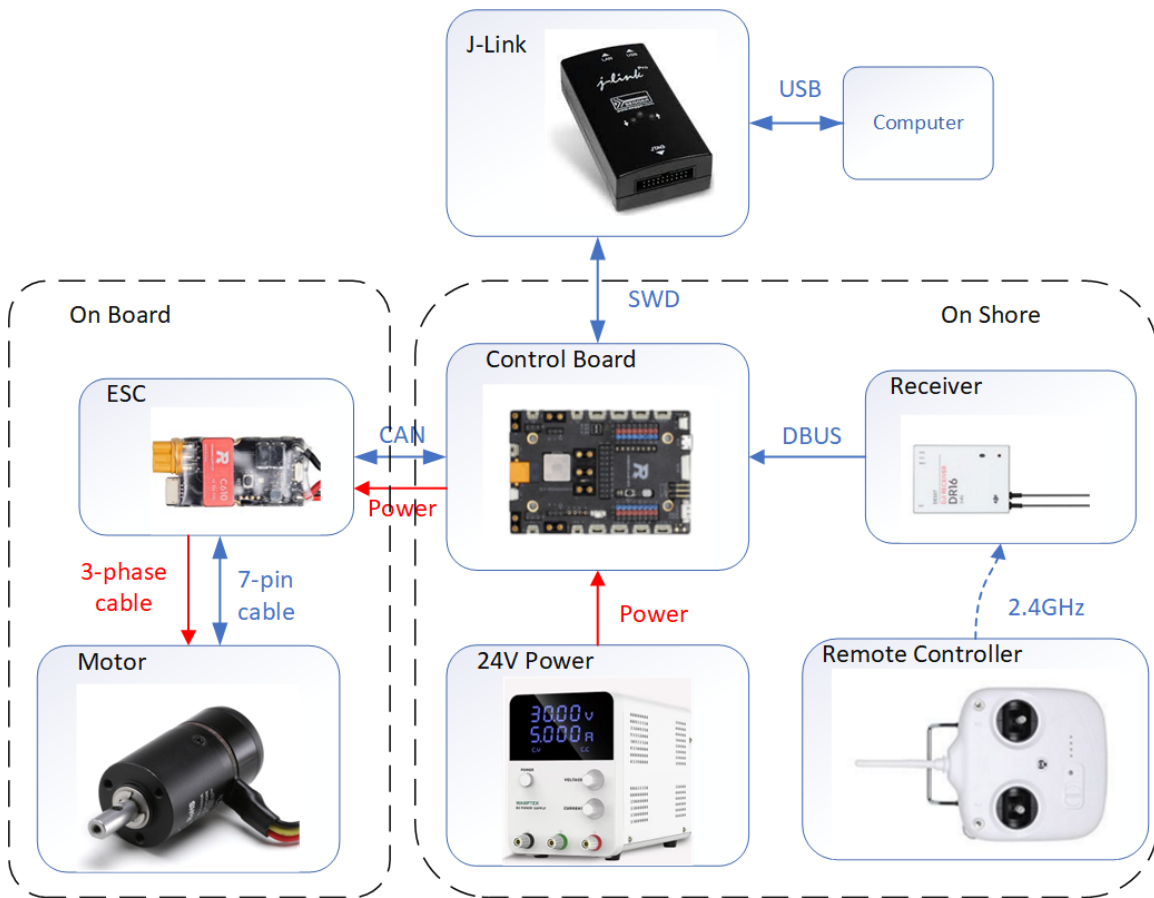


Figure 2-21: The Circuit of Robot Fish

Below are the introduction of electronic parts in the circuit.

RoboMaster Development Board Type A is an open source master controller for robot DIY. The main control chip of the development board is STM32F427IIH6. The development board has a wealth of expansion interfaces and communication interfaces, and an on-board IMU. The peripherals we use are:

1. A SWD debug interface is used for downloading and debugging the microcontroller program.
2. A 24V power supply port to supply power to the development board.
3. A 24V output power port to supply power to the ESC.
4. A CAN1 signal output port, used to communicate with the ESC.
5. A SMD buzzer to prompt the development board to start up.
6. 2 user-defined LEDs to display the working status of the development board.
7. 1 DBUS interface, used to connect the remote control receiver.

The M2006 P36 motor adopts a three-phase permanent magnet DC brushless structure, which has the characteristics of high output speed, small size, and high power density. The motor has a built-in position sensor, i.e., the encoder, which provides accurate position feedback, allowing the motor to generate continuous torque in a FOC vector control manner. The reduction ratio of the gear box is 36:1. The motor-rated rotational speed is $416RPM$, and rated torque is $1N \cdot M$.

The C610 ESC adopts a 32-bit custom motor driver chip and uses Field Oriented Control (FOC) technology to achieve precise control of the motor torque. It is matched with the M2006 DC brushless gear motor to form a power kit.

The DT7 remote control is a radio communication device operating in the 2.4 GHz frequency band, which is used with the DR16 receiver. The DR16 receiver is a 16-channel receiver with an operating frequency of 2.4 GHz. The remote control has a maximum control range of 1000 m in the open air. The DR16 receiver uses the characteristic 2.4 GHz D-BUS protocol.

We use J-Link to download the code to the development board and debug the code. J-Link is a JTAG-based emulator launched by German SEGGER Company. It supports both JTAG and Serial Wire Debug(SWD) protocol. The PC-side application sends the data in a certain protocol format to the J-Link through the USB interface. The J-Link processes the received USB data, and then sends it to the STM32F427 chip through the SWD interface. The SWD interface circuit on the STM32F427 chip operates through The register is directly accessed to the flash to realize reading and writing to the flash. In order to use J-Link, the J-Link driver must be installed on the computer.

2.5 Software

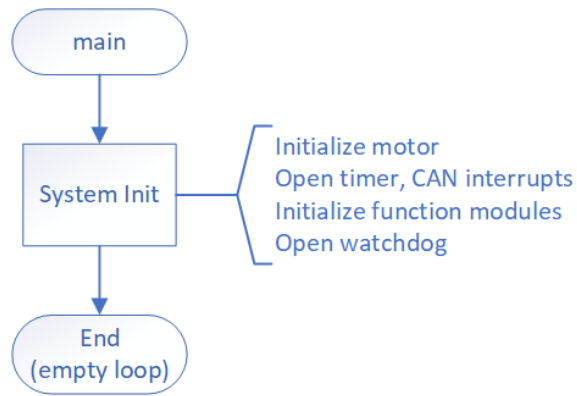
2.5.1 Development Environment

First of all, we can use STM32CubeMx to configure a template project since the chip is one of the STM32 series. Configurations such as clock and pins are set. Then STM32CubeMx can generate a template Keil project containing all drivers needed to run the STM32 chip. The project is in C language. We can develop based on this project.

The integrated development environment (IDE) we used is Keil5(*μVision* V5.34.0.0). After writing the code, we compile the project and download it to the chip through J-Link. To debug the project, the J-Link must stay connected between computer and the development board.

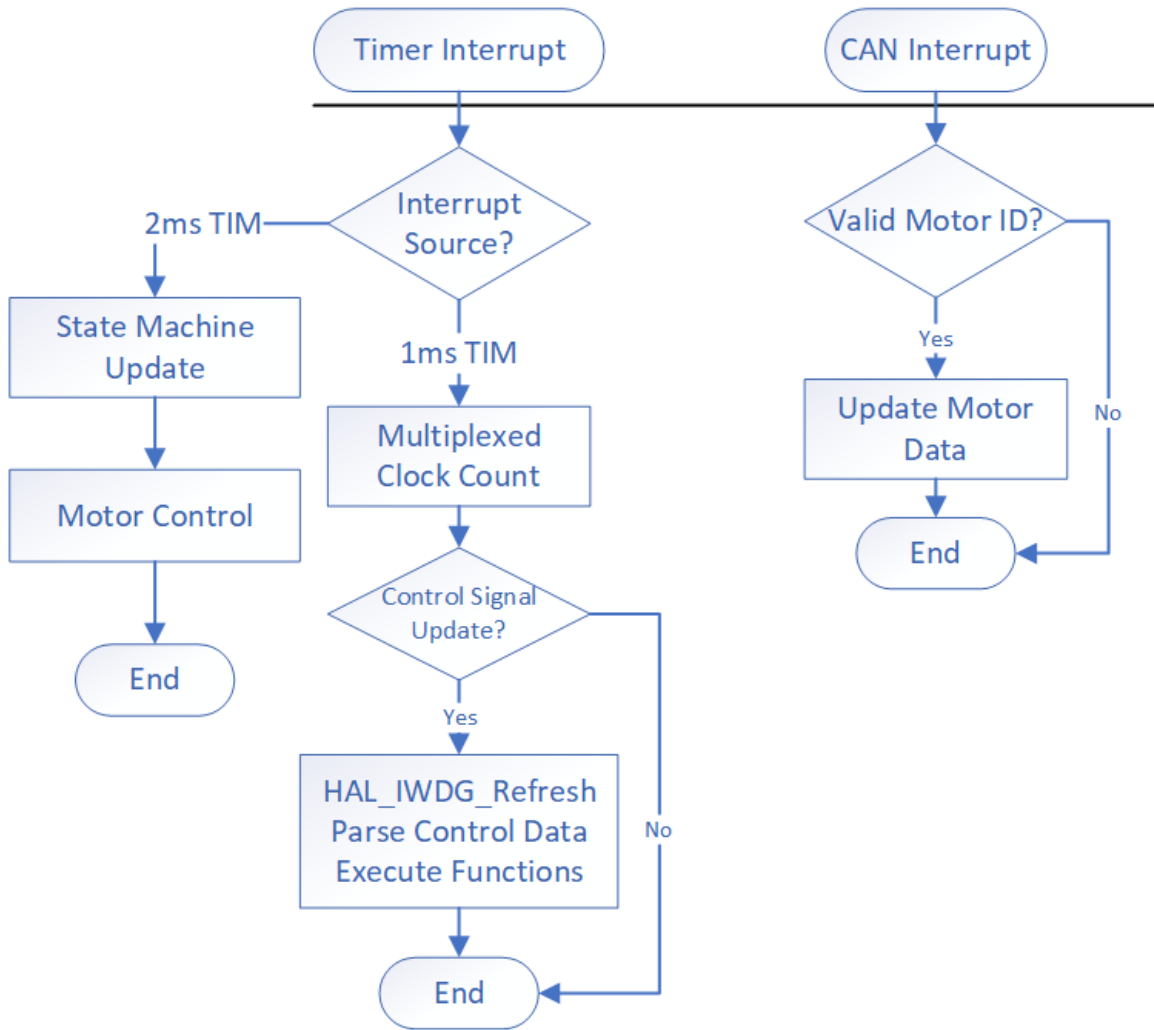
By installing J-Link's supporting software J-Scope in the computer, the data can be analyzed in real time and displayed graphically when the chip is running. This software can assist in parameter tuning. For example, the target value and actual value can be displayed graphically in real time when you fine-tun the PID parameters.

The architecture of the program is shown in Fig. 2-22. Since there is plenty of code, the code won't be attached. The project is uploaded to the public GitHub repository [84].



(a) main function

Code Running



(b) Interrupt Logic

Figure 2-22: The Project Logical Schematic Diagram

2.5.2 Motor Angle Calculation

An encoder is a sensor used to measure mechanical rotation. It can measure the displacement position information of mechanical parts as they rotate and convert it into a series of electrical signals. Due to the existence of the reduction gearbox, the readings of the motor encoder don't represent the actual position of the motor output shaft. Specifically, the reduction ratio is 36 : 1. Thus a particular encoder reading can correspond to 36 positions of the output shaft, making it impossible to get the actual position of the tail.

Since the absolute position cannot be calculated, let's switch our thinking to see if we can use the relative position and think about how to calculate it.

The motor we used has an encoder that divides the 360 degrees into 8192 pieces. The ESC can return the rotor mechanical angle from 0 to 8191. Every time the robot fish is turned on, we use the remote controller to fine-tune the motor to make the tail straight. At this time, we get an initial angle of the motor, which we record as *start* in Fig. 2-23. The positive rotational direction is assumed to be clockwise. For any measurement, assume the last position is *last*, and the current position is *this*. Due to the existence of the zero boundary, we need to judge whether *this* position crosses the zero boundary or not, and process the reading respectively. Using *this* and *last*, the incremental angle can be calculated. Thus, by summing up all incremental angles, we can calculate the angle relative to the initial position. In this way, the tail angle can be accessed.

Note that in order to ensure the above analysis is correct, there is a presumption that must be established: detecting frequency is fast enough. Specifically, the time interval between two readings of the encoder angle should be strictly less than the time required for the motor rotor to make a half-turn. In other words, the encoder is read at least once for each half-turn of the motor rotor. *this* position should be in the range of $(last, last - 4095)$ as Fig. 2-23 (a) shows. Let's check if this presumption holds or not.

The rated output rotational speed of the motor is 416 revolutions per minute(RPM),

and the reduction ratio is 36 : 1. Thus, the rated rotational speed of the rotor is calculated as follows.

$$\frac{416 \times 36}{60} = 249.6 < 250RPS \quad (2.1)$$

Hence, the detecting frequency should be larger than 500 Hz.

The clock in the control board chip STM32F427 can be set as fast as 1 ms. Hence, the maximum detecting frequency we can use in the embedded project is 1000 Hz. In conclusion, this presumption holds.

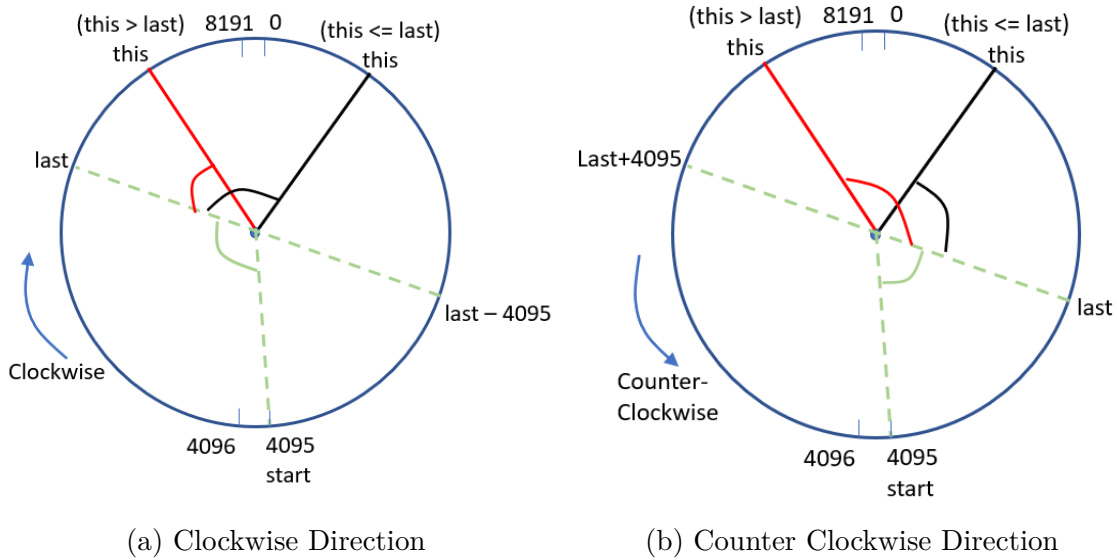


Figure 2-23: The Encoder Schematic Diagram

Depending on *this* position, there are two cases. The incremental angles are calculated differently.

1. $this < last - 4095$: $delta = \frac{this - 0 + 8192 - last}{8192} \times 360$ [degree]
2. $this > last$: $delta = \frac{this - last}{8192} \times 360$ [degree]

If motor rotates in counter-clockwise direction as Fig. 2-23 (b) shows, which means the direction is negative, the incremental angles are calculated as follows:

1. $this < last - 4095$: $delta = -\frac{last - this}{8192} \times 360$ [degree]

$$2. \text{ this } > \text{ last:delta} = -\frac{\text{last} - 0 + 8192 - \text{this}}{8192} \times 360 \text{ [degree]}$$

The corresponding code is attached in Appendix C.1.

2.5.3 Controller

The control method adopts proportional-integral-derivative (PID) control. PID control is the first controller used in Unmanned Surface Vehicle (USV) control. It has simple structure, fast response and certain robustness, and has been widely used in the control field. It calculates an error using target value and real value. The formula of PID is as follows:

$$e = \theta_{target} - \theta_{real}$$

$$I_{PID} = k_p e + k_i \int_0^t e + k_d \dot{e}$$

θ_{target} is the target value of the variable interested, θ_{real} is the real value of the variable interested. The second equation uses the difference to calculate proportional term, integral term and derivative term, and sum them up. The output is the motor's control intensity. k_p, k_i, k_d are parameters that need to fine-tune to get.

In our case, it is the tail angle we want to control. However, the ESC's input control variable is the intensity. The intensity directly controls the motor's rotational speed rather than the motor's angle. Hence, we use the dual loop PID controller, as Fig. 2-24 shows. The position loop can maintain the position. Even after being changed by an external force, it can be restored. The input to the position loop is the target angle of the motor, and the feedback is the real angle of the motor. The speed loop can make the motor rotate to the target angle faster. The input of the speed loop is the output of the position loop, the feedback is the real rotational speed of the motor, and the output is the current value passed to the ESC. The dual loop design allows the motor to respond quickly and maintain a preset angle position, fast and stable.

In order to avoid frequent adjustment of the motor when the PID output is small, the concept of the dead band is introduced. When the output is less than a certain

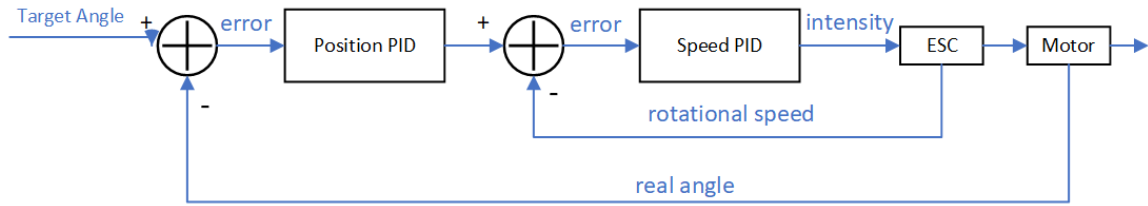


Figure 2-24: The Schematic Diagram of the Dual-loop PID Controller

value, the output is set to 0.

The C code of this dual-loop PID controller is attached in Appendix C.2.

Chapter 3

Prototyping

There are 77 parts in the robot fish. The way to manufacture and assemble these parts is summed up from many trials. From a process point of view, 3D printing, silicone injection molding, and laser cutting are used. In addition, some standard parts are used, such as nuts and screws. The standard parts are listed in Table A.2. After making all parts, we assemble them following specific procedures.

3.1 3D Printed Parts

Most parts are 3D printed. 3D printing is a rapid prototyping technology, which is a process of layer-by-layer slicing and paving materials to finally obtain a real object. It is very suitable for printing irregular objects. All parts that need to be 3D printed are listed in Table A.3.

The material of most 3D printed parts is Polylactic Acid(PLA), which has good mechanical and processing properties. The most important thing is that its water-resistance can ensure that the robot fish can swim stably underwater without draining water. Bevel gears are printed using nylon. Nylon can withstand a temperature range of 175°C, can withstand pressures up to 48 MPa, and has high wear resistance, which is stronger than PLA.

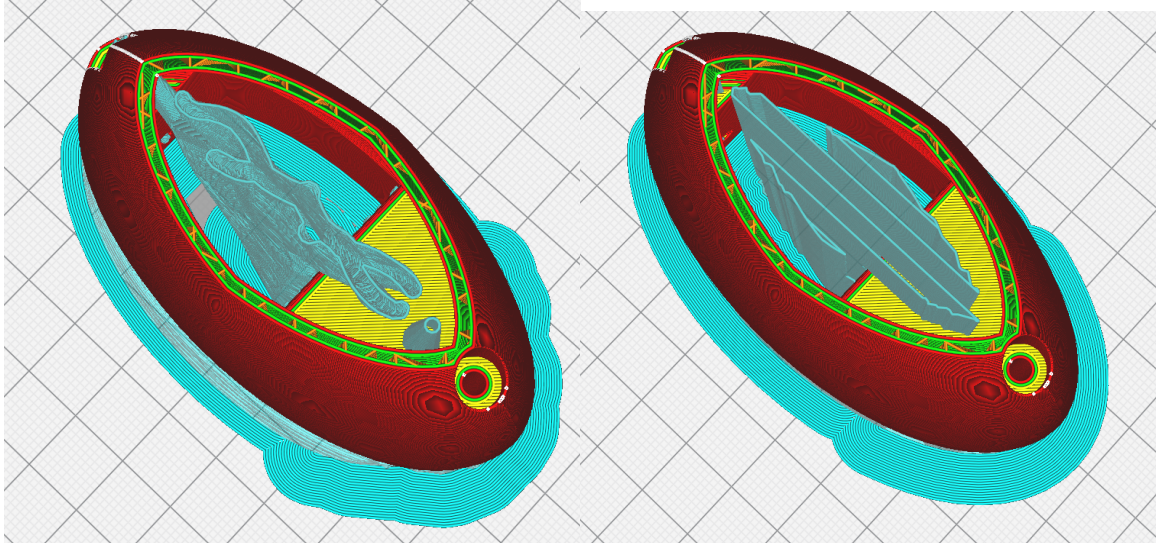
The 3D printer we used is Anet ET4 in Fig. 3-1, which is cheap but has good precision. To print a part, we follow the procedures below:

1. save the SolidWorks model as .STL format file.
2. open the .STL file using the software Ultimaker Cura. Of course, we should configure the printer settings in Cura before using it.
3. configure printing settings for each part following Table A.3. Note that the infill setting is a case-by-case parameter. It's related to the material type, material quality, and the usage of the part. For example, the 100% filled head has no water leakage, but 20% filled head might leak water depending on the quality of the PLA material.
4. slice the part and export the generated gcode into a micro SD card.
5. insert the SD card into the Anet ET4, adjust the printing bed level, and start to print.



Figure 3-1: The 3D Printer Anet ET4

When printing some 3D models with suspended parts, support building materials will be required. For all 3D printing parts, we recommend using the tree support structure rather than the normal structure. The advantages of tree support are that it uses less material than normal support, it is easier to remove from the model, and



(a) Tree Support

(b) Normal Support

Figure 3-2: Two Support Structures

it leaves much fewer marks on the model after removal. Fig. 3-2 shows two support structures when slicing the fish head.

A 10mm wide brim is recommended for the adhesion between part and build plate. In addition, to avoid the effect of thermal expansion and contraction increases part accuracy error, the printer should be placed in a constant $25 \text{ } ^\circ\text{C}$ environment.

3.2 Silicone Molding

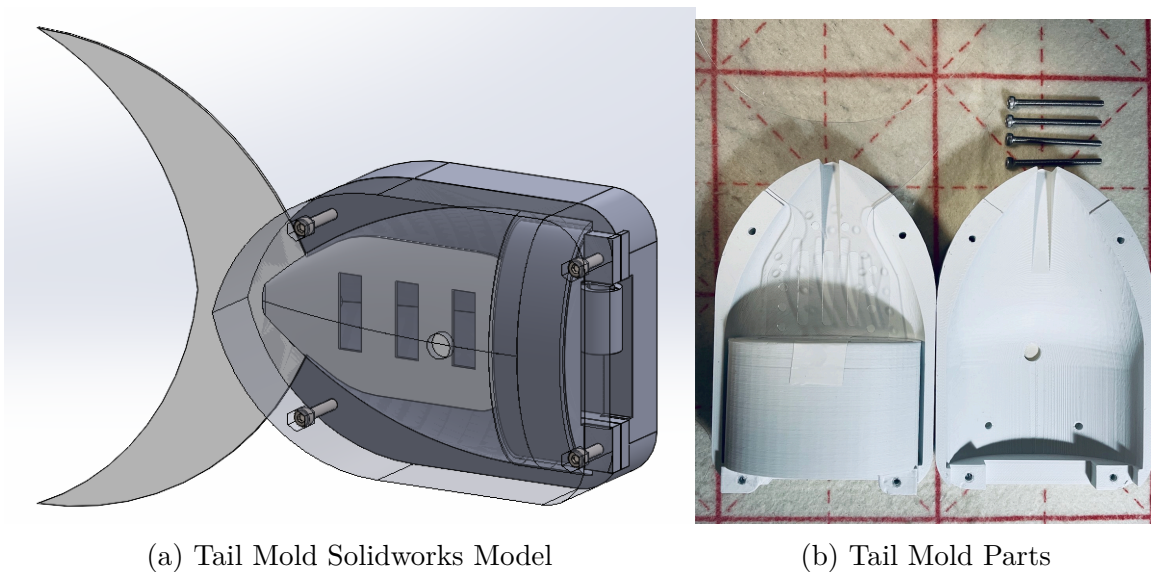
The soft tail is made of low-hardness liquid silicone with a Shore hardness of 10, which is colorless and translucent. It has excellent ductility and tear resistance and can be used for a long time in the temperature range of $-30\text{-}200^\circ\text{C}$ without changing its soft and elastic properties. It is environmentally friendly, pollution-free, and water-resistant.

To make the soft tail, we need to manufacture the central constraining layer first. The central constraining layer is made of 1.0mm thick PVC via laser cutting method. Fig. 3-3 shows the central constraining layer after laser cutting, without off the protective film. The holes on the layer allow the silicone to bond more tightly to the layer.



Figure 3-3: All Parts of Robot Fish

The next step is to make the mold. The mold is 3D printed. The Solidworks mold is shown in Fig. 3-4 (a), and Fig. 3-4 is the assembly of the mold. The “Cavity” feature in SolidWorks is mainly used when we build the mold CAD model.



(a) Tail Mold Solidworks Model

(b) Tail Mold Parts

Figure 3-4: The Mold of Making Tail

Then we start to make the tail:

1. Mix components A and B of the liquid silica gel in a ratio of 1:1. Using a scale can make this step easier, as Fig. 3-5(a) shows.
2. Stir it for two minutes and put it into a vacuum chamber to remove the air bubbles in the silica gel.

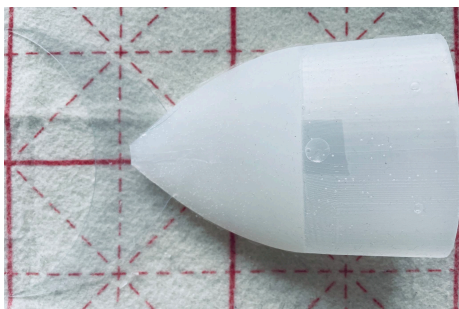
3. Injected it into the mold, and wait five hours to solidify at room temperature as Fig. 3-5(b) shows.
4. Carefully de-mold the tail. The final product is shown in Fig. 3-5(c).
5. Extra silicone can be used to make the silicone seal ring and silicone gaskets.



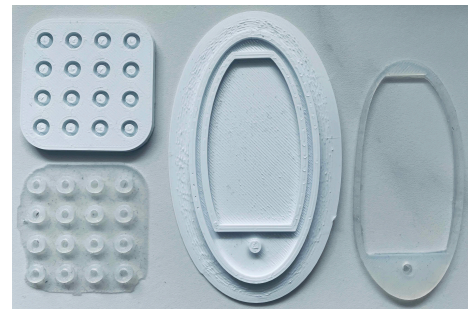
(a) Scale Usage



(b) Injection



(c) Tail



(d) Sear Ring and Gaskets

Figure 3-5: Procedures While Making the Tail

3.3 Assembly

Fig. 3-6 shows all the parts.

The assemble sequence is as follows:

1. Connect the horizontal bevel gear with the tail.



(a) Step 1



(b) Step 2



(c) Step 3



(d) Step 4



(e) Step 5



(f) Step 6

Figure 3-7: Procedures to Assemble the Robot Fish

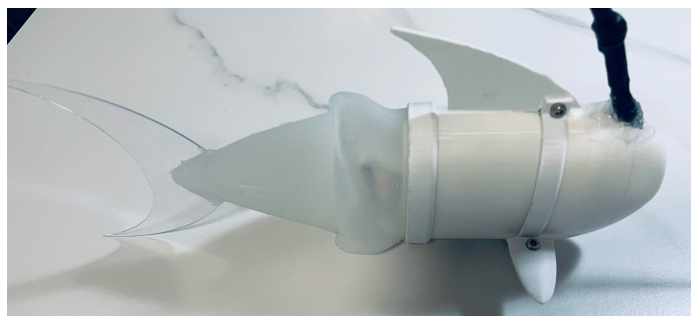


Figure 3-8: Final Assembly

Chapter 4

Prototype Experiment

4.1 Experiment Set-up

The robot fish is test in a water tank. As Fig. 4-1 shows, the water tank is $100\text{cm} \times 60\text{cm}$, and the water is 30cm deep. Above the water tank, a tripod is placed to hang the camera. The bottom of the pool is marked with a scale to measure the robot fish performance.

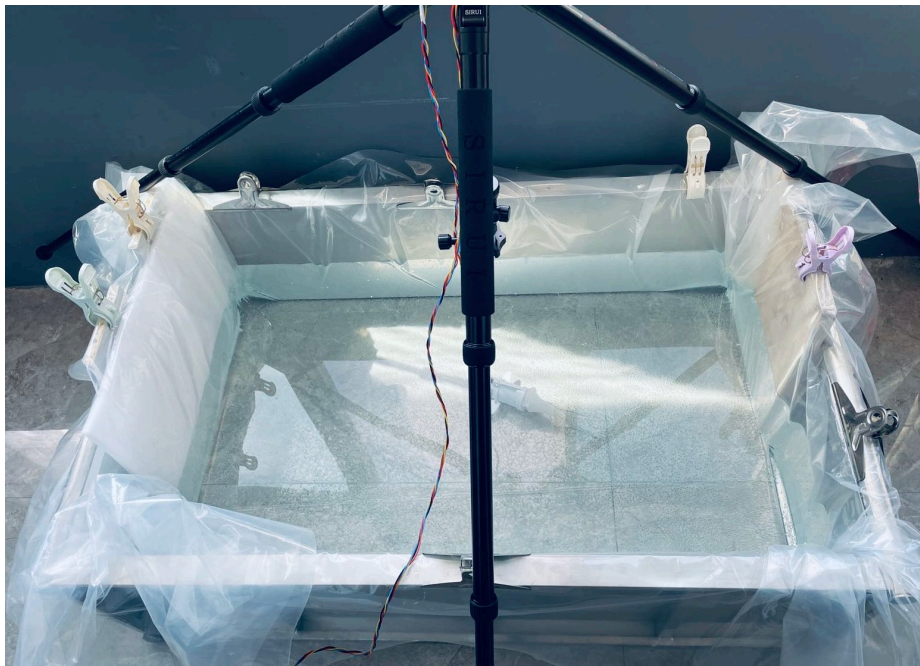


Figure 4-1: Water Tank

During the experiment, the circuit is connected as shown in Fig. 4-2. The development board and the robot fish are connected to the 24V power source. The CAN signal wires connect the robot fish and the development board. The PC is connected to the development board via J-Link, which can monitor the status of the robot fish in real-time and change parameters directly. The J-Scope window is on the left side of the PC's screen, showing the motor's response curve. The Keil Debug window is on the right side of the PC's screen, which can modify the parameters in the development board's memory. The remote controller can take over at any time.

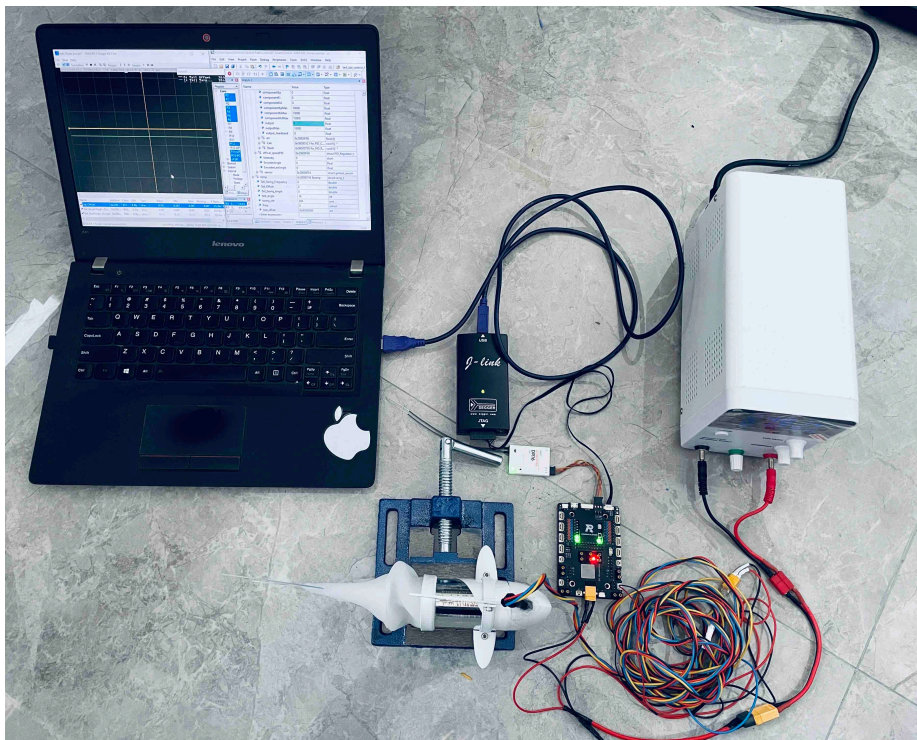


Figure 4-2: Experiment Electronics

4.2 Test Results

4.2.1 Tail Experiment

The theoretical maximal swing amplitude of the tail is 65° as stated in Section 2.3.4. The body was fixed in a bench vise. We rotated the tail to the limit position as shown in Fig. 4-3. It was about 60° , which is slightly smaller than the theoretical value.

This is mainly due to the constraint of the tail firm part of the fish body. Meanwhile, 60° is enough to drive the whole fish body to swing with high amplitude.



Figure 4-3: Tail Maximal Angle

We connected the PC with the development board using J-Link. In this way, the real-time status of the motor can be monitored.

First, we did trials and errors to fine-tune the PID parameters. Fig. 4-4 shows the result. The tail swings between 30° and -30° at 1Hz frequency. The x - axis represents the time; the y - axis represents the angle value. The blue line is the target angle, and the green line is the real angle. The response time is around 0.2s; the overshoot is around 10%.

Second, we test the swing angle between -40° and 40° , and its performance under different swing frequencies. The frequency range is 2--6 Hz. Fig.4-5(a) shows the tail swings at 2Hz, and (b) shows the tail swings at 6Hz. Overshoot decreases compared with 30° case.

As stated in Section 2.3.4, an offset for the center plane can make the robot fish turn. Taking swing range 40° as an example, the robot fish moves forward if the tail swings between $[-40^\circ, 40^\circ]$, which is the normal case. Given the center plane a 30° offset, the tail swings between $[-60^\circ, 10^\circ]$. In this situation, the robot fish will turn.

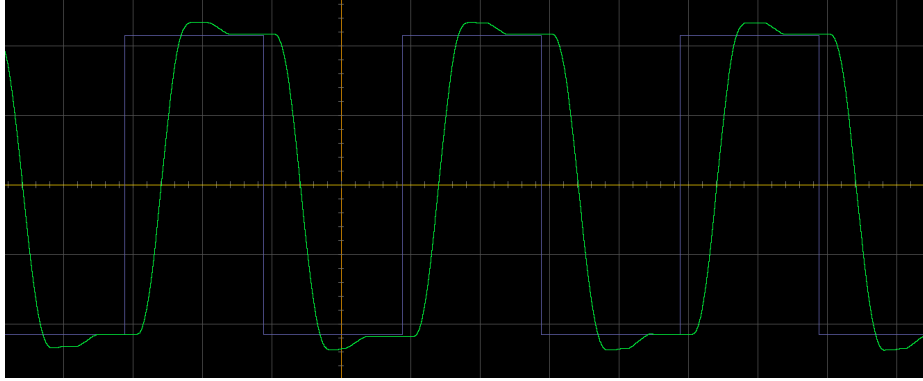
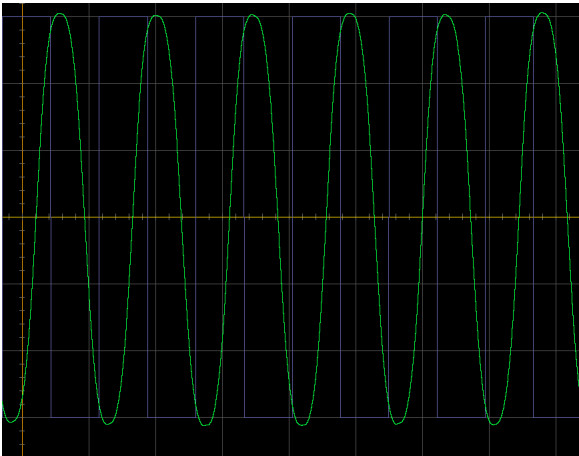
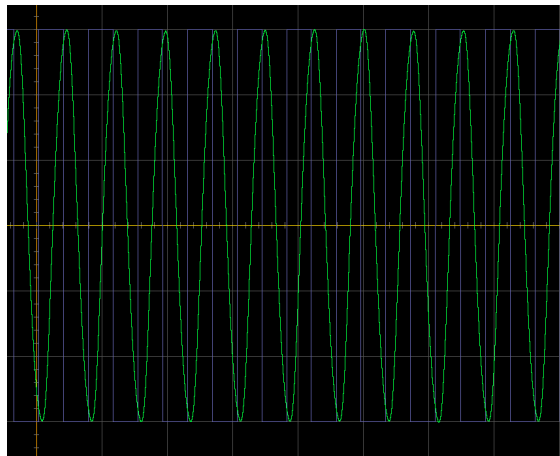


Figure 4-4: Motor Response curve (30°)



(a) 2Hz



(b) 6Hz

Figure 4-5: Tail Swings Between $[-40^\circ, 40^\circ]$

Note that the tail can not swing between $[-70^\circ, 10^\circ]$ since the limitation is 60° . Fig. 4-6 shows the response curve for the example above.

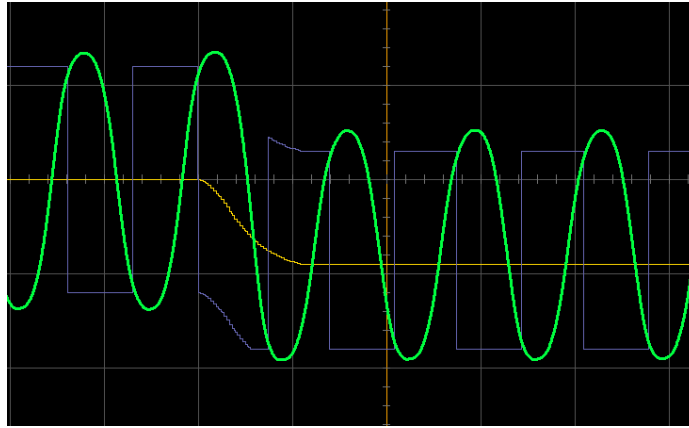


Figure 4-6: Tail Swings Between $[-60^\circ, 10^\circ]$

By operating the joysticks of the remote control, the target angle and swing frequency can be changed continuously. Fig. 4-7 (a) shows the continuous change of the swing amplitude from 0° to 60° . Fig. 4-7 (b) shows the continuous change of the swing frequency from 2Hz to 6Hz.



(a) Amplitude

(b) Frequency

Figure 4-7: Continuously Change Variables

4.2.2 Static Experiment

The robot fish is sealed in the water tank for the static experiment, which is designed aiming to:

1. Check the balance of the fish, i.e., whether the center of mass(COM) is aligned with the center of buoyancy(COB).

2. Check if there is water leakage.

The ideal experimental result is that the robot fish can be suspended in the water. In such a situation, the robot fish body will be parallel to the water surface, and no water will be entered inside. This result can be achieved after many trials.

Through the static experiment, we found that the weight of the cable affects the robot fish balance. This can be solved by replacing the wire to the soft silicone wire, whose density is close to the water density. In addition, the soft silicone wire wouldn't cause stress to the robot fish.

4.2.3 Dynamic Experiment

A linear swimming experiment is conducted first. When the tail swings evenly, the robot fish can swim in a straight line at a constant speed. The robot fish is placed in the start side, and it will swim following the marked scaled line in the bottom of the water tank. The experiment is recorded on a 60 frame per second(FPS) video. Then we used video editing software, such as the Final Cut Pro, to find the time that the fish takes from the start side to the end side. In this way, the speed can be calculated, and the accuracy is acceptable.

As Fig. 4-8 shows, the robot fish can move forward in a straight line. The reason that the fish can swing forward in a straight line is introduced in Section 2.3.4. The tail swing amplitude is 30° , and the tail swing frequency is 4Hz. The speed in Fig. 4-8 is around 13.19cm/s.

We tested different swing amplitudes, namely, 10° , 20° , 30° , 40° , 50° , 60° . For each swing angle, we tested different swing frequencies, namely, 1, 2, 3, 4, 5, 6 Hz. For each set of experiments, we tested at least three times and then took the median speed. Fig. 4-9 shows the speed under different swing amplitudes and swing frequencies. The data of the swing amplitude 10° is abandoned due to measurement results fluctuating widely. This is because that 10° swing amplitude produces a small thrust. As Fig. 4-9 shows, both the amplitude and the frequency can affect the speed. The speed increases as the swing amplitude increases. Under a certain swing amplitude, the speed is

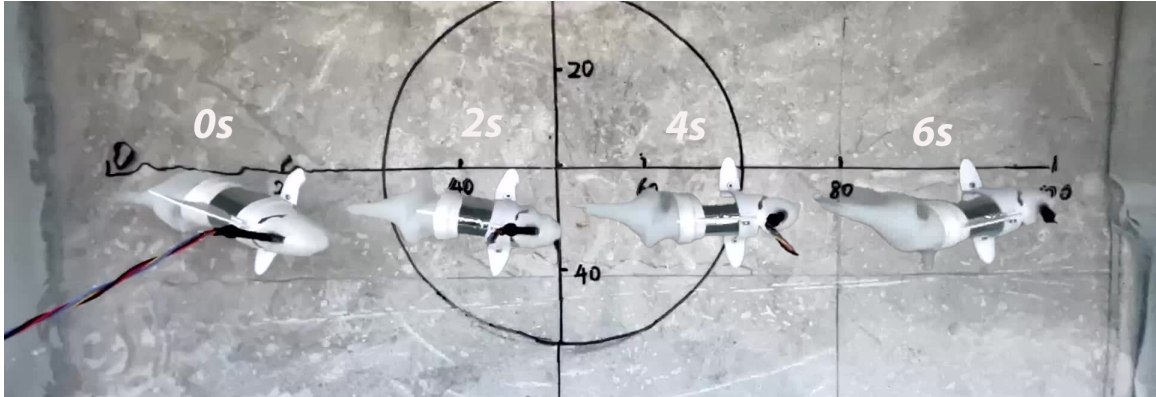


Figure 4-8: Straight Line Experiment (swing amplitude 30° , frequency 4 Hz)

almost linear to the frequency. The top speed 32cm/s occurs at swing amplitude 60° and swing frequency 6 Hz. The straight line experiment videos can be checked online [85].

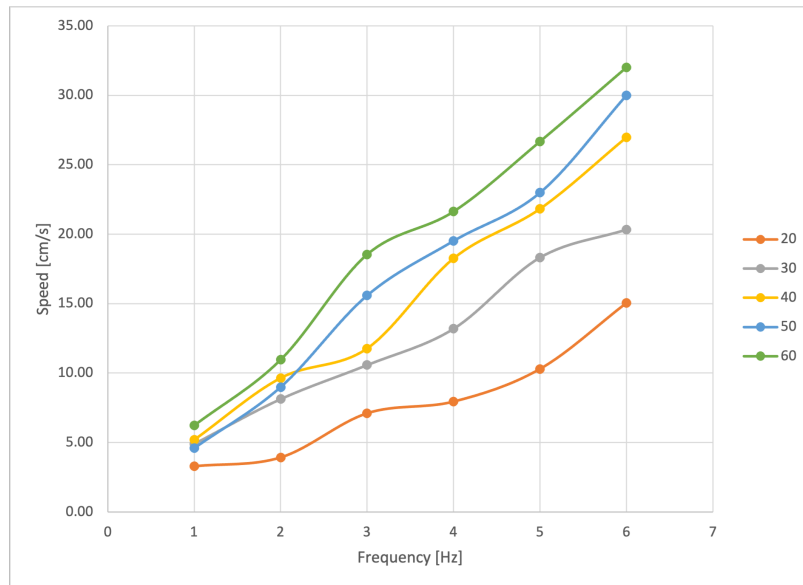


Figure 4-9: Speed Under Different Swing Amplitudes and Frequencies

Fig. 4-10 shows the screenshot of the edited video.

Steering experiment is conducted in swing frequency 5Hz, but in different offset angles, namely, 10° , 20° , 30° . For each offset, we tested different swing angles as Table 4.1 shows.

We extract a frame from the steering experiment video every 1s or 2s. Then we use image processing software, such as Adobe Photoshop, to superimpose these frame

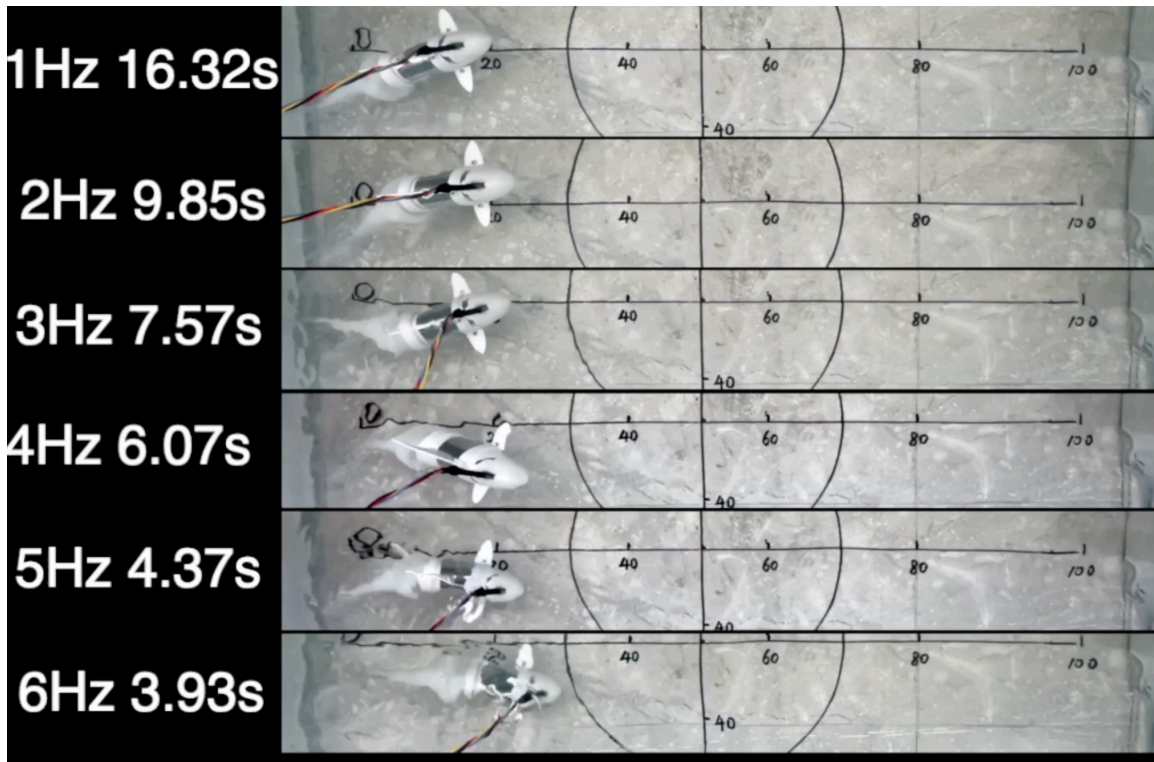
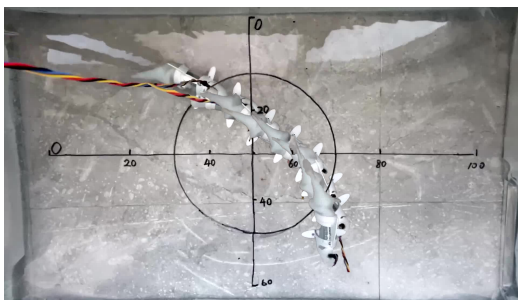


Figure 4-10: Straight Line Experiment (swing amplitude 30°)

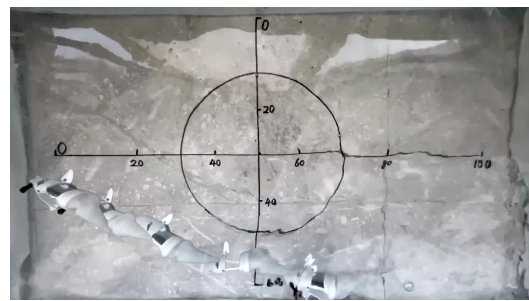
Table 4.1: Steering Experiment Test Sets and Result

Offset Angle	Swing Amplitudes	Radius
10°	$20^\circ, 30^\circ, 40^\circ, 50^\circ$	> 60 cm
20°	$20^\circ, 30^\circ, 40^\circ$	50 – 55 cm
30°	$10^\circ, 20^\circ, 30^\circ$	20 – 25 cm

photos together and combine them into one picture. In this way, we can estimate the turning radius from the composite images. Fig. 4-11, 4-12, and 4-13 show the composite images for each test set in clockwise direction. Other than the clockwise direction, the counter-clockwise direction turning experiment is also conducted as Fig. 4-13 (d) shows. According to the steering experiment, we found that the larger the offset angle, the smaller the turning radius. However, the swing amplitude doesn't affect the turning radius. It only makes the fish speed faster. The steering experiment videos can be checked online [86]



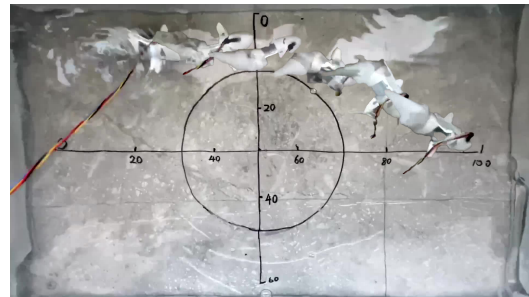
(a) Swing Amplitude 20°



(b) Swing Amplitude 30°

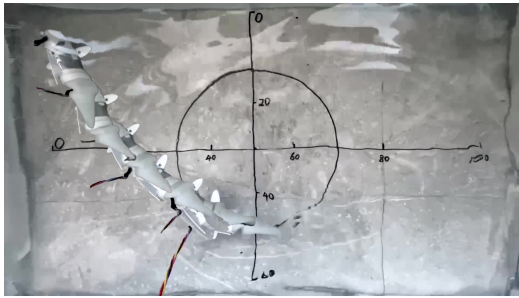


(c) Swing Amplitude 40°

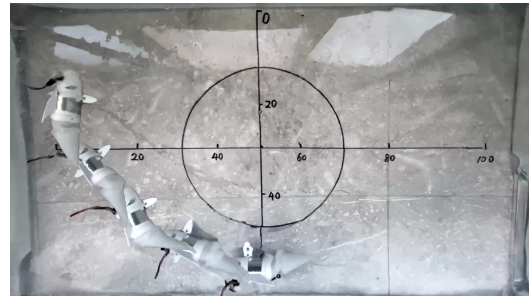


(d) Swing Amplitude 50°

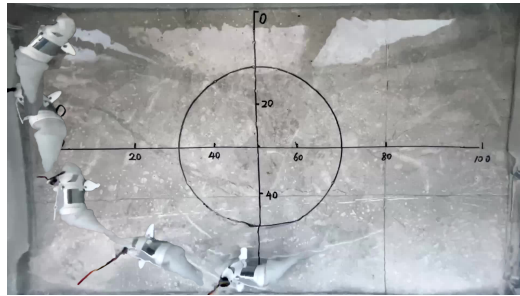
Figure 4-11: Steering Experiment (Offset Angle 10°)



(a) Swing Amplitude 20°



(b) Swing Amplitude 30°

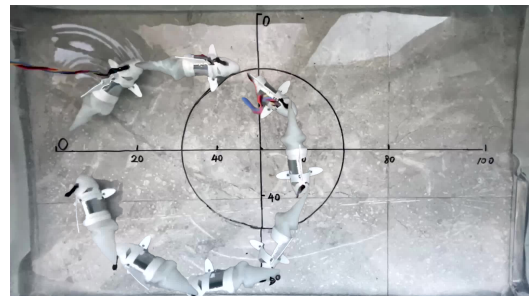


(c) Swing Amplitude 40°

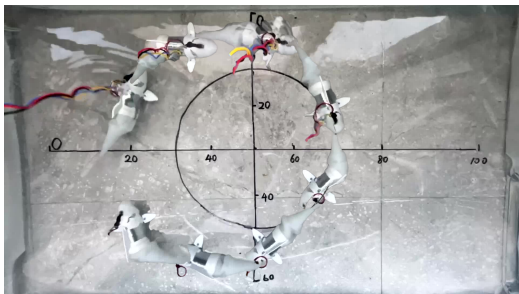
Figure 4-12: Steering Experiment (Offset Angle 20°)



(a) Swing Amplitude 10°



(b) Swing Amplitude 20°



(c) Swing Amplitude 30°



(d) Swing Amplitude 30° , counter-clockwise

Figure 4-13: Steering Experiment (Offset Angle 30°)

Chapter 5

Conclusions

The development of biomimetic robot fish is a complex research topic that involves interdisciplinary research in many disciplines, including biology, automatic control, and mechanism design, fluid dynamics, manufacturing, material science, to name a few. Difficulties can arise in each of these fields, not to mention the integration of different research realms. At present, most robot fish are rigidly driven. The corresponding mechanical structures are usually complex. For rigid design, the better flexibility it requires, the less robustness it is. This research proposes a new type of PVC central constraining layer-driven soft robot fish designs, manufactures, and tests of the prototype.

5.1 Result Analysis

The main research contents and results can be summarized as follows:

1. A comprehensive review of locomotion principles, actuator types, and control, along with two case studies demonstrating the implementation of a robot fish is presented.
2. The design methodology and design process used in this project are introduced.
3. Starting from a rough idea, a motor actuated layer-silicon soft tail mechanism is designed. To verify the feasibility of this actuation, a whole robot fish is

designed. Detailed engineering considerations during the mechanical design process is discussed.

4. Electronic design and software design are also presented.
5. The process of making parts and assembling the robot fish is listed later.
6. Three types of experiments are conducted:
 - (a) Solo tail swing experiment.
 - (b) Static experiment: the robot fish is placed underwater to test tightness and balance.
 - (c) Dynamic experiment: the robot fish swims following a straight line and turns.

A suitable material is selected to make the soft tail, and the swing of the soft tail is controlled by the single-chip microcomputer. The soft tail is made of low-hardness liquid silica gel, which is poured into the 3D printed tool to be cured and formed. The operator issues command via the remote control. The single-chip microcomputer accepts and processes the commands, and controls the motor to drive the center layer to swing. The soft tail swing can be realized through the cantilever beam effect. Experiments show that the soft tail control system can swing in different amplitudes and frequencies. This design is simple to implement, fast in response, and able to complete underwater forward and steering movement. The effectiveness of the design of the soft robot fish has been verified. In addition, the design methodology for an engineering prototype is proven to be valid.

5.2 Future Work

The research of bionic robotic fish involves a series of fields such as control, communication, fluid dynamics, mechanical, etc. It is a complex system engineering. The

robot fish designed in this project still has a lot of room to improve. The shortcomings of this research work and the work that can be further developed in the future are listed as follows:

1. Since the main purpose of this thesis is to verify the feasibility of the proposed soft tail design, the tether design for the whole fish is adopted. The external power supply and the main control board are connected to the robot fish body through cables. This cable makes the experiment inconvenient, and may also affect the swimming gesture of the robot fish. In the future, the robot fish needs to be redesigned to carry the battery and the main control board to get rid of the limitation of cables.
2. This experiment is conducted at home. Due to the limited experimental conditions and the small water tank, the collected data includes an acceleration phase, resulting in a slightly lower calculation speed than the real value. Furthermore, without a high-speed camera and underwater videography markers, it is impossible to precisely analyze the posture of the tail when it swings underwater. Therefore, the experimental conditions need to be improved in the future, and more valuable data can be collected.
3. Due to the limitation of time and energy, the robot fish designed in this thesis cannot achieve the function of diving, and can only swim in a horizontal plane. This greatly limits the applicability of the prototype. In the future, a diving device similar to the swim bladder can be added, and the control of the two pectoral fins can be implemented, so that the robot fish can achieve 3D swimming.
4. At present, the shape design of the entire fish body is relatively rough. Due to the limited domain knowledge, we didn't optimize its shape using fluid dynamics. Subsequent analysis of the fluid dynamics can be performed to improve its hydrodynamic properties.
5. Improve the startup procedure to have an auto centering method at startup of

the device. Hence, the manual centering can be avoided.

Appendix A

Mechanics

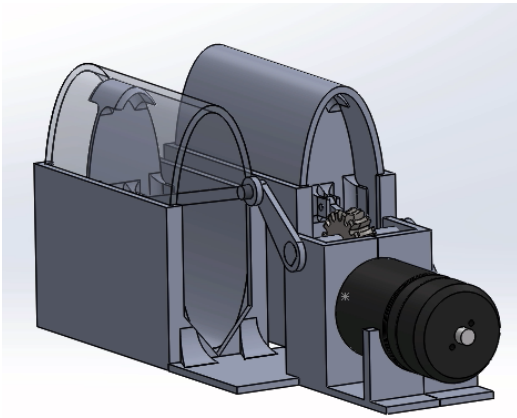
A.1 Preliminary Actuator Designs

A.1.1 The First Version

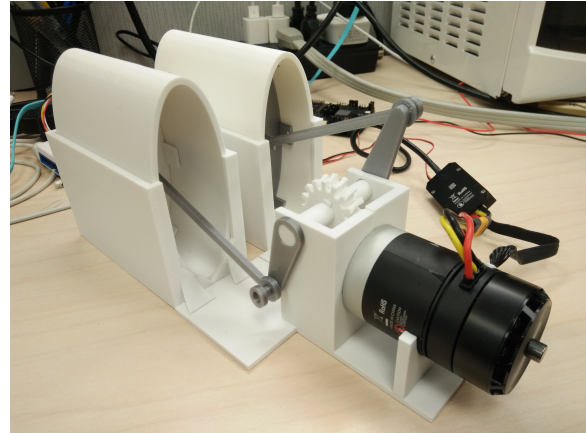
The first actuation mechanism can transmit the motor power to the continuous oscillation of soft robot fish. Specifically, as Fig. A-1 (a) shows, an electric motor is linked to a rotating double crank-slider via a transmission mechanism, which converts the motor rotation into the non-synchronous sliding motion of the pistons at two identical elliptical tubes. As Fig. A-1 (c) shows, the elliptical tube is connected with a hollow chamber of the soft tail and filled with tiny granular balls. Force will be transformed from the piston to the tail chamber wall via granular jamming media. The non-synchronous motion of the pistons will thus result in the oscillatory bending motion of the tail by stressing the granular balls on one side while unstressing them on the other side. With proper design of the chamber wall structure, the tail will undulate following biological fishtail swing patterns.

The soft tail consists of two parts: the main body of the tail, and the middle constraint layer, which splits the main body evenly. The soft tail is fabricated by a lost-wax fabrication process. The wax cores are made to form the cavities in the main body of the tail. The tail can be fabricated in the following steps:

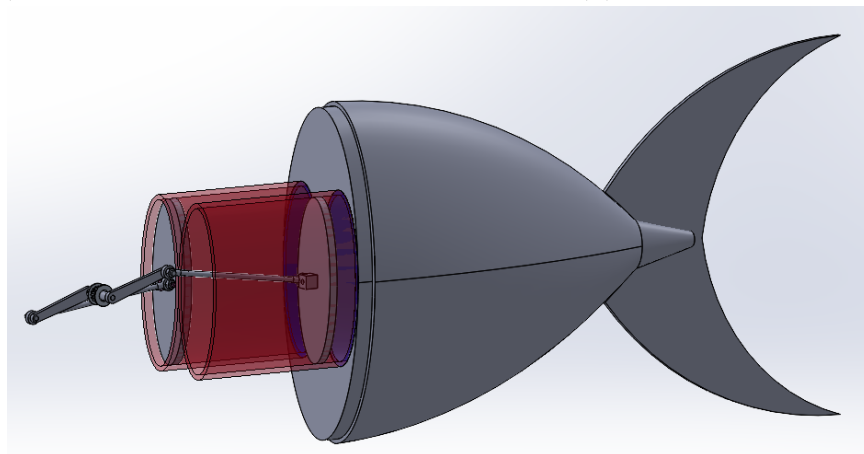
1. Make two wax cores.



(a) SolidWorks Model



(b) Actuator Prototype



(c) Crank Connected with Tail

Figure A-1: The First Version Actuator

- (a) 3D print the outer mold and the model core. Put the model core inside the outer mold.
 - (b) Pour the silicone gel into the outer mold. Wait for the silicone to solidify. Remove the model core and outer mold.
 - (c) Heat the wax. Pour the liquid hot wax onto the silicone rubber mold. Wait for the wax to cool down and release the wax.
2. Make the middle constraint layer via laser cut.
 3. 3D print the outer tail mold. Assemble the outer mold, the middle constraint layer, and wax cores.
 4. Pour silicone gel into the assembled mold. Wait for the silicone to solidify. Release the cured tail.
 5. Heat the tail to melt out the wax core. Then remove the remaining wax through a water bath.

However, after building a prototype and testing it, we found that this idea doesn't work. The small silicone rubber balls are used as the granular jamming media. The expected tail bending did not occur when the piston squeezed these pellets. This is because the pellets undergo a large elastic deformation when they are squeezed and do not transmit the pressure to the raised ribs in the inner cavity of the tail as expected. So the tail doesn't bend but expands as the pellets deform.

A.1.2 The Second Version

The second design is shown in Fig. [A-2](#). This design can convert the circular motion of the motor shaft into reciprocating swing motion continuously without changing the rotational direction of the motor. Therefore, it can provide a higher tail swing frequency. However, after building a prototype and testing it, we found it has a fatal flaw: it's impossible to limit the tail swing around the central plane. The tail itself has large inertia. The movement of the tail is uncontrolled between the two-sector

gears alternating. Thus, this design is abandoned. Nevertheless, this design helped us come up with the final design used in the robot fish.

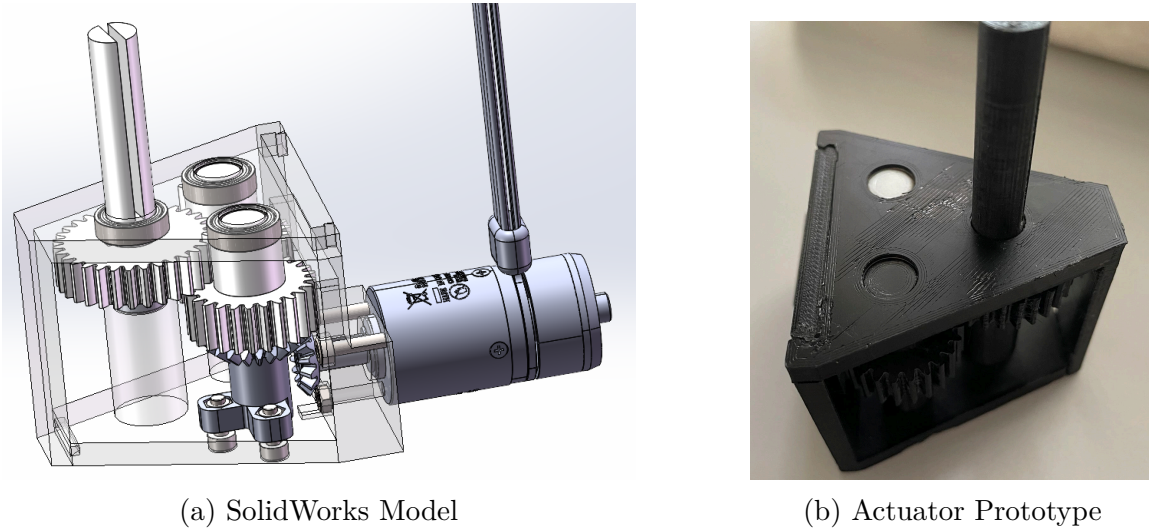


Figure A-2: The Second Version Actuator

A.2 Gear Parameters

Table A.1: Spur Gears Parameters

Item	Unit	Horizontal Gear	Vertical Gear
Modulus	mn	1	1
Number of teeth	z	20	14
Tooth angle	a	20	20
Addendum height factor	h	1	1
Helix angle	B	0	0
Spiral direction		spur	spur
Radial displacement coefficient	xn	0	0
Common normal length	W	6.84	4.79
Number of teeth across	k	2.72	2.06
Axis angle	Σ	90	90

A.3 Calculate the COB in SolidWorks

By following these operation steps in SolidWorks, you may calculate the center of buoyancy(COB) of the robot fish CAD model. First, we need to extract the outer surface of the robot fish.

1. Open the robot fish assembly and insert a new part.
2. Edit this new part.
3. Click “offset surfaces”, and select all the outer surfaces of the robot fish to create a zero offset surface [87].

Now we get a “surface-offset1” under the new part in the “Feature Manager Tree”. Then we need to edit this new part following the steps below.

1. edit this new part.
2. fill two holes on the head surface using “Filled Surfaces”.
3. knit head surface with two new filled surfaces (turn on “create solid”).
4. trim the tail central layer.
5. extend the tail(body part) to the head.
6. knit tail surface with the knitted head surface.
7. fill the tail surface central gap caused by trimming as Fig. A-3 shows.
8. heal all surfaces on the tail that need to heal
9. knit all the original surface with the newly filled tail surface (turn on “create solid”)

Now we can get a solid fish body and calculate its center of mass(COM).

1. Configure the material to water.
2. Check “Mass Properties” in “Evaluate”. The mass is the buoyancy of robot fish.
3. Show the COM. The COM is the COB we want.

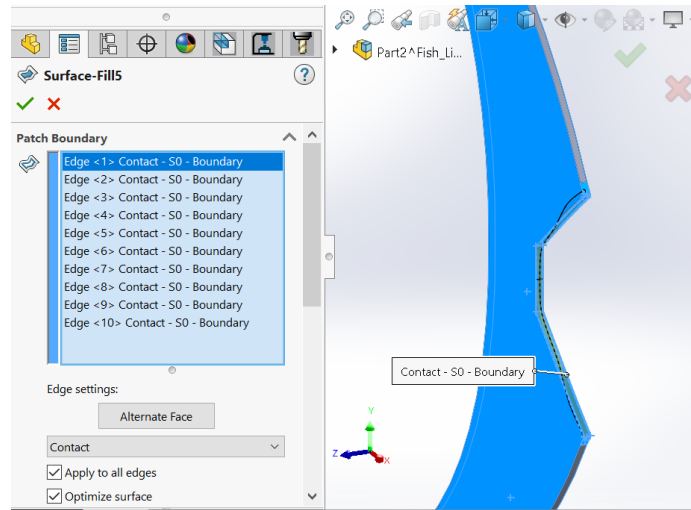


Figure A-3: Fill Tail Surface

A.4 Prototyping Parts

All standard parts used in the robot fish are listed in Table A.2. All parts needed to be 3D printed are listed in Table A.3.

Table A.2: Standard Parts

Part	Quantity
M3 Nut	21
M3x6 Screw	2
M3x8 Screw	12
M3x16 Screw	4
M3x40 Screw	5
Ball Bearing 15x10x4	1
Ball Bearing 4x8x3	1

Table A.3: 3D Printed Parts

Part	Material	Infill	Profile[mm]
Gear - Base	PLA	20%	0.15
Gear - Lid	PLA	20%	0.15
Gear - Main_Rod_Station	PLA	100%	0.15
Gear - Rod	PLA	100%	0.15
Gear - Rod_Claw	PLA	100%	0.15
Gear - Motor_Claw	PLA	20%	0.15
Gear - Horizontal Bevel Gear	Nylon	100%	0.1
Gear - Vertical Bevel Gear	Nylon	100%	0.1
Body	PLA	100%	0.15
Tail_Body_Connector	PLA	100%	0.15
Pectroal_Fin x 2	PLA	100%	0.15
Dorsal_Fin	PLA	20%	0.15
Fin_Body_Connector	PLA	100%	0.15
Head	PLA	100%	0.15
Silicon Tail Female Mold	PLA	20%	0.2
Silicon Tail Male Mold	PLA	20%	0.2
Silicon Seal Ring Mold	PLA	20%	0.2
Silicon Gasket Mold	PLA	20%	0.2

Appendix B

Electronics

All electronic parts and corresponding online store links are listed in Table B.1.

Table B.1: Hardware Purchase Link

Control Board	https://store.dji.com/product/rm-development-board-type-a
C610 ESC	https://store.dji.com/product/rm-c610-brushless-dc-motor-speed-control
M2006 Motor	https://store.dji.com/product/rm-m2006-p36-brushless-motor
Remote Controller and Receiver	https://www.robomaster.com/zh-CN/products/components/detail/122
J-Link Debug Probes	https://www.segger.com/products/debug-probes/j-link/

Appendix C

Software

C.1 Motor Control Function

The function to calculate the motor angle using incremental method is given below. Note that, struct definitions, such as “ramp_t”, “MotorINFO”, are not given below. Please refer to the complete project code [84] for details. This piece of code is in the file “MotorTask.c” and “MotorTask.h”.

```
0 uint32_t swing_cnt = 0;
1 uint8_t swing = 0;
2 ramp_t ramp = RAMP_GEN_DAFUALT_T;
3 int32_t ramp_scale = 500;
4 void ControlTAIL(MotorINFO *id) {
5     static float encoder2degree_ratio;
6     encoder2degree_ratio = 360 / 8192.0 / id->ReductionRate;
7     if(id==0) return;
8     // id->s_count is used to reduce the execution frequency
9     if(id->s_count == 1) {
10        // Manuel speed control
11        if (WorkState == NORMAL_STATE) {
12            id->TargetAngle = M2006_Target_Speed;
13            id->Intensity = PID_PROCESS_Single(&(id->speedPID), id->TargetAngle, id->RxMsgC6x0.RotateSpeed);
14            id->FirstEnter = 1; // reset the position
15        }
16        // Auto swing
17        else if (WorkState == ADDITIONAL_STATE_ONE) {
18            uint16_t thisEncoder = id->RxMsgC6x0.angle;
19            // initialize
20            if(id->FirstEnter==1) {
21                id->lastRead = thisEncoder;
22                id->FirstEnter = 0;
23                id->RealAngle = 0;
24                // function ControlTAIL's execution frequency is 500Hz
25                ramp.init(&ramp, 500);
26                return;
27            }
28        }
29    }
```

```

28
30 if(thisEncoder <= id->lastRead) {
31     // the motor rotates from encoder 0 to encoder 8191 (positive direction)
32     if((id->lastRead - thisEncoder) > 4095)
33         id->RealAngle = id->RealAngle + (thisEncoder + 8192 - id->lastRead) * encoder2degree_ratio;
34     // the motor rotates from encoder 8191 to encoder 0 (negative direction)
35     else
36         id->RealAngle = id->RealAngle - (id->lastRead - thisEncoder) * encoder2degree_ratio;
37 }
38 else {
39     // the motor rotates from encoder 8191 to encoder 0 (negative direction)
40     if((thisEncoder - id->lastRead) > 4095)
41         id->RealAngle = id->RealAngle - (id->lastRead + 8192 - thisEncoder) * encoder2degree_ratio;
42     // the motor rotates from encoder 0 to encoder 8191 (positive direction)
43     else
44         id->RealAngle = id->RealAngle + (thisEncoder - id->lastRead) * encoder2degree_ratio;
45 }
46
47 int diff = id->TargetAngle - id->RealAngle;
48 // change direction when it arrives the target
49 if(abs(diff) < 3) {
50     swing = swing<1? swing+1:0;
51     swing_cnt = 0;
52     ramp.reset(&ramp);
53 }
54 // change direction anyway after a while, in case the motor is blocked
55 else {
56     swing_cnt++;
57     if((swing_cnt/400)%2){swing = swing<1? swing+1:0;}
58 }
59
60 if (swing == 1){ // positive direction
61     id->TargetAngle = Tail_Swing_Angle + Tail_Offset;
62 }
63 if (swing == 0){
64     id->TargetAngle = -Tail_Swing_Angle + Tail_Offset;
65 }
66 if (fabs(id->TargetAngle) > TAIL_MAX_ANGLE) {
67     if (id->TargetAngle < 0) {id->TargetAngle = -TAIL_MAX_ANGLE;}
68     else {id->TargetAngle = TAIL_MAX_ANGLE;}
69 }
70
71 // Angle control
72 id->Intensity = PID_PROCESS_Double(&(id->positionPID), &(id->speedPID), id->TargetAngle, id->RealAngle, id->RxC6x0.
73 RotateSpeed);
74 // Control speed by using ramp function
75 id->Intensity *= ramp.calc(&ramp);
76 id->lastRead = thisEncoder;
77 }
78 test_tail_control_Freq++;
79
80 MINMAX(id->Intensity, -10000, 10000);
81 id->s_count = 1;
82 }
83 else {
84     id->s_count++;
85 }
86 }

```

C.2 Dual Loop PID Controller

The dual loop PID controller in C is given below. This code is in the project file “pid_regulator.h” and “pid_regulator.c”.

```
0 #define PID_I_CNT 4
1 #define MINMAX(value, min, max) value = ((value) < (min)) ? (min) : ((value) > (max) ? (max) : (value))
2 #define fw_PID_INIT(Kp, Ki, Kd, KpMax, KiMax, KdMax, OutputMax, Output_DeadBand) { \
3     0.0, 0.0, 0.0, 0.0, 0.0, 0.0, \
4     Kp, Ki, Kd, 0.0, 0.0, 0.0, \
5     KpMax, KiMax, KdMax, 0.0, \
6     OutputMax, Output_DeadBand, \
7     {0.0}, \
8     &fw_PID_Calc, &fw_PID_Reset \
9 }
10 typedef __packed struct fw_PID_Regulator_t
11 {
12     float target;
13     float feedback;
14     float errorCurr;
15     float errorSum;
16     uint16_t SumCount;
17     float errorLast;
18     float kp;
19     float ki;
20     float kd;
21     float componentKp;
22     float componentKi;
23     float componentKd;
24     float componentKpMax;
25     float componentKiMax;
26     float componentKdMax;
27     float output;
28     float outputMax;
29     float output_deadband;
30     float err[PID_I_CNT];
31
32     void (*Calc)(struct fw_PID_Regulator_t *pid);
33     void (*Reset)(struct fw_PID_Regulator_t *pid);
34 }fw_PID_Regulator_t;
35
36 void fw_PID_Reset(fw_PID_Regulator_t *pid);
37 void fw_PID_Calc(fw_PID_Regulator_t *pid);
38
39 void fw_PID_Reset(fw_PID_Regulator_t *pid){
40     pid->errorCurr = 0;
41     pid->componentKd = 0;
42     pid->componentKi = 0;
43     pid->componentKp = 0;
44     pid->errorLast = 0;
45     pid->errorSum = 0;
46     pid->feedback = 0;
47     pid->output = 0;
48     pid->SumCount = 0;
49     pid->target = 0;
50     for(int i=0;i<PID_I_CNT;i++) pid->err[i] = 0;
51 }
52
53 void fw_PID_Calc(fw_PID_Regulator_t *pid){
54     pid->errorCurr = pid->target - pid->feedback;
```

```

pid->errorSum += pid->errorCurr - pid->err [pid->SumCount];
56 pid->err [pid->SumCount] = pid->errorCurr;
pid->SumCount = (pid->SumCount + 1) % PID_I_CNT;
58
pid->componentKp = pid->kp * pid->errorCurr;
60 MNMAX(pid->componentKp, -pid->componentKpMax, pid->componentKpMax);
pid->componentKi = pid->ki * pid->errorSum;
62 MNMAX(pid->componentKi, -pid->componentKiMax, pid->componentKiMax);
pid->componentKd = pid->kd * (pid->errorCurr - pid->errorLast);
64 MNMAX(pid->componentKd, -pid->componentKdMax, pid->componentKdMax);

66 pid->errorLast = pid->errorCurr;

68 pid->output = pid->componentKp + pid->componentKi + pid->componentKd;
MNMAX(pid->output, -pid->outputMax, pid->outputMax);
70 if ((pid->output_deadband != 0) && (fabs(pid->output) < pid->output_deadband))
    pid->output = 0;
72 }

74 int16_t PID_PROCESS_Single(fw_PID_Regulator_t* pid, float target, float feedback)
{
76     pid->target = target;
    pid->feedback = feedback;
78     pid->Calc(pid);
    return pid->output;
80 }

int16_t PID_PROCESS_Double(fw_PID_Regulator_t* pid_position, fw_PID_Regulator_t* pid_speed, float target, float
    position_feedback, float velocity_feedback)
82 {
    //position
84     pid_position->target = target;
    pid_position->feedback = position_feedback;
86     pid_position->Calc(pid_position);
    //speed
88     pid_speed->target = pid_position->output;
    pid_speed->feedback = velocity_feedback;
90     pid_speed->Calc(pid_speed);
    return pid_speed->output;
92 }

```

Bibliography

- [1] J. Yu and M. Tan. *Motion Control of Biomimetic Swimming Robots*. Research on Intelligent Manufacturing. Springer Singapore, 2019.
- [2] Sayyed Masoomi, Stefanie Gutschmidt, Xiaoqi Chen, and Mathieu Sellier. The kinematics and dynamics of undulatory motion of a tuna-mimetic robot. *International Journal of Advanced Robotic Systems*, 12, 07 2015.
- [3] Robert K Katzschmann, Joseph DelPreto, Robert MacCurdy, and Daniela Rus. Exploration of underwater life with an acoustically controlled soft robotic fish. *Science Robotics*, 3(16), 2018.
- [4] D. N. Beal, F. S. Hover, M. S. Triantafyllou, J.C. Liao, and G.V. Lauder. Passive propulsion in vortex wakes. *Journal of Fluid Mechanics*, 549:385–402, 2006.
- [5] RW Blake. Fish functional design and swimming performance. *Journal of fish biology*, 65(5):1193–1222, 2004.
- [6] J. Liu and Hu. H. Biological inspiration: From carangiform fish to multi-joint robotic fish. *Journal of Bionic Engineering*, 7:35–48, 2010.
- [7] M. S. Triantafyllou and G. S. Triantafyllou. An efficient swimming machine. *Scientific American*, 272(3):40–48, 1995.
- [8] Yoseph Bar-Cohen and Cynthia Breazeal. Biologically inspired intelligent robots. In *Smart Structures and Materials 2003: Electroactive Polymer Actuators and Devices (EAPAD)*, volume 5051, pages 14–20. International Society for Optics and Photonics, 2003.
- [9] Vladislav Kopman and Maurizio Porfiri. Design, modeling, and characterization of a miniature robotic fish for research and education in biomimetics and bioinspiration. *IEEE/ASME Transactions on mechatronics*, 18(2):471–483, 2012.
- [10] Huosheng Hu. Biologically inspired design of autonomous robotic fish at essex. In *IEEE SMC UK-RI Chapter Conference on Advances in Cybernetic Systems*, pages 3–8, Sheffield, United Kingdom, 2006.
- [11] Li Wen, Jianhong Liang, Guan hao Wu, Jinlan Li, et al. Hydrodynamic experimental investigation on efficient swimming of robotic fish using self-propelled

- method. In *The Twentieth International Offshore and Polar Engineering Conference*. International Society of Offshore and Polar Engineers, 2010.
- [12] Frank E Fish. Limits of nature and advances of technology: What does biomimetics have to offer to aquatic robots? *Applied Bionics and Biomechanics*, 3(1):49–60, 2006.
- [13] Promode R Bandyopadhyay. Trends in biorobotic autonomous undersea vehicles. *IEEE Journal of Oceanic Engineering*, 30(1):109–139, 2005.
- [14] Ruxu Du, Zheng Li, Kamal Youcef-Toumi, and Pablo Valdivia y Alvarado. *Robot fish: bio-inspired fishlike underwater robots*. Springer Berlin, Heidelberg, 2015.
- [15] David Scaradozzi, Giacomo Palmieri, Daniele Costa, and Antonio Pinelli. Bcf swimming locomotion for autonomous underwater robots: a review and a novel solution to improve control and efficiency. *Ocean Engineering*, 130:437 – 453, 2017.
- [16] C. M. Breder. The locomotion of fishes. *Zoologica: scientific contributions of the New York Zoological Society*, 4:159–297, 1926.
- [17] C. C. Lindsey. Form, function, and locomotory habits in fish (volume 7). In W.S. Hoar and D.J. Randall, editors, *Fish Physiology*, chapter 1, pages 1–100. Academic Press, New York, 1978.
- [18] Paul W. Webb. The biology of fish swimming. In L. Maddock, Q. Bone, and J. M. V. Rayner, editors, *The Mechanics and Physiology of Animal Swimming*, chapter 4, pages 45–62. Cambridge University Press, Cambridge, UK, 1994.
- [19] Michael Sfakiotakis, David Lane, and John Davies. Review of fish swimming modes for aquatic locomotion. *Oceanic Engineering, IEEE Journal of*, 24:237 – 252, 05 1999.
- [20] John J Videler. *Fish swimming*, volume 10. Springer Dordrecht, London, 1993.
- [21] Aditi Raj and Atul Thakur. Fish-inspired robots: design, sensing, actuation, and autonomy—a review of research. *Bioinspiration and Biomimetics*, 11:031001, 04 2016.
- [22] Fengran Xie, Qiyang Zuo, Qinglong Chen, Haitao Fang, Kai He, Ruxu Du, Yong Zhong, and Zheng Li. Designs of the biomimetic robotic fishes performing body and/or caudal fin (bcf) swimming locomotion: A review. *Journal of Intelligent & Robotic Systems*, 102, 05 2021.
- [23] Aditi Raj and Atul Thakur. Hydrodynamic parameter estimation for an anguilliform-inspired robot. *Journal of Intelligent & Robotic Systems*, 99(3):837–857, 2020.

- [24] Daniele Costa. *Development of biomimetic propulsiv systems in a multiphysics environment*. PhD thesis, Università Politecnica delle Marche, 2019.
- [25] Daniele Costa, Giacomo Palmieri, Matteo-Claudio Palpacelli, Luca Panebianco, and David Scaradozzi. Design of a bio-inspired autonomous underwater robot. *Journal of Intelligent & Robotic Systems*, 91(2):181–192, 2018.
- [26] Farah Abbas Naser and Mofeed Turkey Rashid. Labriform swimming robot with steering and diving capabilities. *Journal of Intelligent & Robotic Systems*, 103(1):14, 2021.
- [27] D.S. Barrett. *The Design of a Flexible Hull Undersea Vehicle Propelled by an Oscillating Foil*. Massachusetts Institute of Technology, Department of Ocean Engineering, 1994.
- [28] G. I. Taylor. Electrically driven jets. *Proceedings of the Royal Society of London. A. Mathematical and Physical Sciences*, 313:453 – 475, 1969.
- [29] M. J. Lighthill. Note on the swimming of slender fish. *Journal of Fluid Mechanics*, 9(2):305–317, 1960.
- [30] Theodore Wu. Mathematical biofluidynamics and mechanophysiology of fish locomotion. *Mathematical Methods in the Applied Sciences*, 24:1541, 11 2001.
- [31] Pablo Valdivia y Alvarado. *Design of biomimetic compliant devices for locomotion in liquid environments*. PhD thesis, Massachusetts Institute of Technology, 2007.
- [32] T. Yao-Tsu Wu. Swimming of a waving plate. *Journal of Fluid Mechanics*, 10(3):321–344, 1961.
- [33] Jian-Yu Cheng, Li-Xian Zhuang, and Bing-Gang Tong. Analysis of swimming three-dimensional waving plates. *Journal of Fluid Mechanics*, 232:341–355, 1991.
- [34] A Peter Schaffarczyk and John T Conway. Comparison of a nonlinear actuator disk theory with numerical integration including viscous effects. *Canadian Aeronautics and Space Journal*, 46(4):209, 2000.
- [35] M. K. Habib. Mechatronics - a unifying interdisciplinary and intelligent engineering science paradigm. *IEEE Industrial Electronics Magazine*, 1(2):12–24, 2007.
- [36] Sayyed Farideddin Masoomi, Stefanie Gutschmidt, and Xiaoqi Chen. State of the art in biomimetic swimming robots: Design principles and case study. In *Handbook of Research on Advancements in Robotics and Mechatronics*, pages 118–152. IGI Global, Pennsylvania, USA, 2015.

- [37] David Barrett, Mark Grosenbaugh, and Michael Triantafyllou. The optimal control of a flexible hull robotic undersea vehicle propelled by an oscillating foil. In *Proceedings of Symposium on Autonomous Underwater Vehicle Technology*, pages 1–9. IEEE, 1996.
- [38] Sayyed Masoomi, Stefanie Gutschmidt, Nicolas Gaume, Thomas Guillaume, Connor Eatwel, Xiaoqi Chen, and Mathieu Sellier. Design and construction of a specialised biomimetic robot in multiple swimming gaits. *International Journal of Advanced Robotic Systems*, 12:1, 11 2015.
- [39] Andrew D Marchese, Cagdas D Onal, and Daniela Rus. Autonomous soft robotic fish capable of escape maneuvers using fluidic elastomer actuators. *Soft Robotics*, 1(1):75–87, 2014.
- [40] Robert K Katzschmann, Austin de Maille, David L Dorhout, and Daniela Rus. Cyclic hydraulic actuation for soft robotic devices. In *2016 IEEE/RSJ International Conference on Intelligent Robots and Systems (IROS)*, pages 3048–3055. IEEE, 2016.
- [41] Wikipedia. Occam’s razor. https://en.wikipedia.org/wiki/Occam's_razor, 2022. [Online; accessed 8-May-2022].
- [42] Michael Sachinis. *The design and testing of a biologically inspired underwater robotic mechanism*. PhD thesis, Massachusetts Institute of Technology, 2000.
- [43] John Muir Kumph. *Maneuvering of a robotic pike*. PhD thesis, Massachusetts Institute of Technology, 2000.
- [44] Liang Jianhong Zou Dan Wang Song and Wang Ye. Trial voyage of spe-ii fish robot [j]. *Journal of Beijing University of Aeronautics and Astronautics*, 7, 2005.
- [45] Koichi Hirata. *Prototype PPF-01*, 2003 (accessed Sept., 2020). <https://www.nmri.go.jp/oldpages/eng/khirata/fish/model/ppf01/ppf01e.htm>.
- [46] Sander van den Berg. Design of a high speed soft robotic fish. Master’s thesis, Delft University of Technology, 2019.
- [47] Richard James Clapham and Huosheng Hu. iSplash-OPTIMIZE: Optimized linear carangiform swimming motion. In E. Menegatti, N. Michael, K. Berns, and H. Yamaguchi, editors, *Intelligent Autonomous Systems 13*, volume 302 of *Advances in Intelligent Systems and Computing*, pages 1257–1270. Springer, Cham, 2016.
- [48] D. Lachat, A. Crespi, and Auke Jan Ijspeert. Boxybot: a swimming and crawling fish robot controlled by a central pattern generator. In *The First IEEE/RAS-EMBS International Conference on Biomedical Robotics and Biomechanics, 2006. BioRob 2006.*, pages 643–648, 2006.

- [49] N. Kato. Control performance in the horizontal plane of a fish robot with mechanical pectoral fins. *IEEE Journal of Oceanic Engineering*, 25(1):121–129, 2000.
- [50] T. Wang, Y. Hao, X. Yang, and L. Wen. Soft robotics: Structure, actuation, sensing and control. *Journal of Mechanical Engineering*, 53(13), 2017.
- [51] Robert K. Katzschmann, Andrew D. Marchese, and Daniela Rus. *Hydraulic Autonomous Soft Robotic Fish for 3D Swimming*, pages 405–420. Springer International Publishing, Cham, 2016.
- [52] Brower T.P.L. Design of a manta ray inspired underwater propulsive mechanism for long range, low power operation. Master’s thesis, Tufts University, 2006.
- [53] K. Suzumori, S. Endo, T. Kanda, N. Kato, and H. Suzuki. A bending pneumatic rubber actuator realizing soft-bodied manta swimming robot. In *Proceedings 2007 IEEE International Conference on Robotics and Automation*, pages 4975–4980, 2007.
- [54] New Scientist. Manta ray robot can loop-the-loop. *New Scientist*, 195(2622):27, 2007.
- [55] Festo. rives and control. artificial rays take to the water, 2022.
- [56] Jamie Lee Cho. *Electronic subsystems of a free-swimming robotic fish*. PhD thesis, Massachusetts Institute of Technology, 1997.
- [57] Andrew D. Marchese, Cagdas D. Onal, and Daniela Rus. Autonomous soft robotic fish capable of escape maneuvers using fluidic elastomer actuators. *Soft robotics*, 1 1:75–87, 2014.
- [58] Kyu-Jin Cho, E. Hawkes, C. Quinn, and R. J. Wood. Design, fabrication and analysis of a body-caudal fin propulsion system for a microrobotic fish. In *2008 IEEE International Conference on Robotics and Automation*, pages 706–711, 2008.
- [59] Won-Shik Chu, Kyung-Tae Lee, Sung-Hyuk Song, Min-Woo Han, Jang-Yeob Lee, Hyung-Soo Kim, Min-Soo Kim, Yong Jai Park, Kyu-Jin Cho, and Sung-Hoon Ahn. Review of biomimetic underwater robots using smart actuators (vol 13, pg 1281, 2012). *International Journal of Precision Engineering and Manufacturing*, 13, 07 2012.
- [60] Kyu-Jin Cho, Je-Sung Koh, Sangwoo Kim, Won-Shik Chu, Yongtaek Hong, and Sung-Hoon Ahn. Review of manufacturing processes for soft biomimetic robots. *International Journal of Precision Engineering and Manufacturing*, 10:171–181, 07 2009.

- [61] Mohsen Shahinpoor, Yoseph Bar-Cohen, J.O. Simpson, and J. Smith. Ionic polymer-metal composites (ipmcs) as biomimetic sensors, actuators and artificial muscles: A review. *Smart Materials and Structures*, 7, 02 1998.
- [62] Palmani Duraisamy, Rakesh Kumar Sidharthan, and Manigandan Nagarajan Santhanakrishnan. Design, modeling, and control of biomimetic fish robot: A review. *Journal of Bionic Engineering*, 2019.
- [63] W. Huang and Z. Ding. Shape memory materials. *Materials Today*, 13(7):54–61, 2010.
- [64] Claudio Rossi, Julian Colorado, William Coral, and Antonio Barrientos. Bending continuous structures with SMAs: A novel robotic fish design. *Bioinspiration and Biomimetics*, 6(4):045005, 12 2011.
- [65] Z. Chen, S. Shatara, and X. Tan. Modeling of biomimetic robotic fish propelled by an ionic polymer–metal composite caudal fin. *IEEE/ASME Transactions on Mechatronics*, 15(3):448–459, 2010.
- [66] Seok Heo, Tedy Wiguna, Hoon Cheol Park, and Nam Seo Goo. Effect of an artificial caudal fin on the performance of a biomimetic fish robot propelled by piezoelectric actuators. *Journal of Bionic Engineering*, 4(3):151 – 158, 2007.
- [67] Sung-Hoon Ahn, Kyung-Tae Lee, Hyungjung Kim, Renzhe Wu, Ji-Soo Kim, and Sung-Hyuk Song. Smart soft composite: An integrated 3d soft morphing structure using bend-twist coupling of anisotropic materials. *International Journal of Precision Engineering and Manufacturing*, 13, 04 2012.
- [68] C. Rossi, W. Coral, J. Colorado, and A. Barrientos. A motor-less and gear-less bio-mimetic robotic fish design. In *2011 IEEE International Conference on Robotics and Automation*, pages 3646–3651, 2011.
- [69] Zhenlong Wang, Guanrong Hang, Yangwei Wang, Jian Li, and Wei Du. Embedded sma wire actuated biomimetic fin: A module for biomimetic underwater propulsion. *Smart Materials and Structures*, 17:025039, 03 2008.
- [70] Z. Wang, Y. Wang, J. Li, and G. Hang. A micro biomimetic manta ray robot fish actuated by sma. In *2009 IEEE International Conference on Robotics and Biomimetics (ROBIO)*, pages 1809–1813, 2009.
- [71] K. H. Low, J. Yang, A. P. Pattathil, and Y. Zhang. Initial prototype design and investigation of an undulating body by sma. In *2006 IEEE International Conference on Automation Science and Engineering*, pages 472–477, 2006.
- [72] Joseph Ayers, Joel. L. Davis, and Alan Rudolph. *Neurotechnology for Biomimetic Robots*. MIT press, Cambridge, MA, 2002.

- [73] M. Aureli, V. Kopman, and M. Porfiri. Free-locomotion of underwater vehicles actuated by ionic polymer metal composites. *IEEE/ASME Transactions on Mechatronics*, 15(4):603–614, 2010.
- [74] Xiufen Ye, Yudong Su, Shuxiang Guo, and Liquan Wang. Design and realization of a remote control centimeter-scale robotic fish. In *2008 IEEE/ASME International Conference on Advanced Intelligent Mechatronics*, pages 25–30. IEEE, 2008.
- [75] Zheng Chen, Tae Um, Jianzhong Zhu, and Hilary Bart-Smith. Bio-inspired robotic cownose ray propelled by electroactive polymer pectoral fin. *ASME 2011 International Mechanical Engineering Congress and Exposition, IMECE 2011*, 2, 01 2011.
- [76] Jamie Anderson and Narendra Chhabra. Maneuvering and stability performance of a robotic tuna. *Integrative and comparative biology*, 42:118–26, 02 2002.
- [77] Pan Liao, Shiwu Zhang, and Dong Sun. A dual caudal-fin miniature robotic fish with an integrated oscillation and jet propulsive mechanism. *Bioinspiration and Biomimetics*, 13, 01 2018.
- [78] Cameron Aubin, Snehashis Choudhury, Rhiannon Jerch, Lynden Archer, James Pikul, and Robert Shepherd. Electrolytic vascular systems for energy-dense robots. *Nature*, 571, 07 2019.
- [79] Guorui Li, Xiangping Chen, Fanghao Zhou, and etc. Self-powered soft robot in the mariana trench. *Nature*, 591:66–71, 03 2021.
- [80] Filip Ilievski, Aaron Mazzeo, Robert Shepherd, Xin Chen, and George Whitesides. Soft robotics for chemists. *Angewandte Chemie (International ed. in English)*, 50:1890–5, 02 2011.
- [81] S. Neppalli, B. Jones, W. McMahan, V. Chitrakaran, I. Walker, M. Pritts, M. Csencsits, C. Rahn, and M. Grissom. Octarm - a soft robotic manipulator. In *2007 IEEE/RSJ International Conference on Intelligent Robots and Systems*, pages 2569–2569, 2007.
- [82] Xinyu Jian. Robot Fish SolidWorks Model. <https://github.com/JianXinyu/Robot-Fish/tree/main/SolidWorks>, 2022. [Online; accessed 8-May-2022].
- [83] etc Zhang Y.S., Li H. Biomimetic swimming principle of a micro robot fish using giant magnetostrictive thin film as caudal fin. *Chinese Journal of Mechanical Engineering*, 42(2):37–42, 2006.
- [84] Xinyu Jian. Robot Fish Embedded Projectl. https://github.com/JianXinyu/Robot-Fish/tree/main/Code/RM_Infantry, 2022. [Online; accessed 8-May-2022].

- [85] Xinyu Jian. Robot Fish Straight Line Experiment. <https://youtu.be/Y4nbsXTZy-w>, 2022. [Online; accessed 9-Aug-2022].
- [86] Xinyu Jian. Robot Fish Steering Experiment. <https://youtu.be/HtfJKcQQRSY>, 2022. [Online; accessed 9-Aug-2022].
- [87] GoEngineer. Find Assembly Volumes Using Surfaces. <https://www.youtube.com/watch?v=bT5ru4oq33A>, 2022. [Online; accessed 8-May-2022].